High Throughput Microfluidic Labyrinth for the Label Free Isolation of CTCs for Single Cell Gene Expression Profiling

by

Eric Lin

A dissertation submitted in partial fulfillment
of the requirements for the degree of
Doctorate of Philosophy
(Chemical Engineering)
in the University of Michigan
2017

Doctoral Committee:

Associate Professor Sunitha Nagrath, Chair
Professor Ronald G. Larson
Assistant Professor Ariella Shikanov
Assistant Professor Fei Wen
Professor Max S. Wicha

Eric Lin

gogodidi@umich.edu

ORCID ID: 0000-0001-7571-1657

DEDICATION

I dedicate this thesis to my mother, who gave me unconditional love and support through my life; to my father, whose suffering to disease became my strength and belief; to my mentor Dr. Sunitha Nagrath, who guided and shaped me with her wisdom and patience.

ACKNOWLEDGEMENTS

I would like to thank all the people who made this dissertation possible. First and foremost, my advisor Dr. Sunitha Nagrath, who is the best mentor one could have ever dreamed of. Her passion in research and compassion for cancer patients has greatly motivated me to continue my study. She is always supporting us both in professional and in personal lives. I am far away from my family, but she made our lab a cozy family. I also want to thank all my lab mates, for all the hard work that made our lab such a wonderful place, and for being helpful to each other. I would like to acknowledge our former post-doctoral fellow Dr. Hyeun Joong Yoon, who guided me and inspired me into the field of microfluidics. I am grateful to all my undergraduate assistants, especially Stephanie Guthrie and Jacob Wieger, who dedicated so much to this research and made it successful. I am greatly thankful to my committee members Dr. Max Wicha, Dr. Ronald Larson, Dr. Ariella Shikanov and Dr. Fei Wen for their valuable feedback and guidance throughout my research.

I am especially grateful to Dr. Max Wicha for being a wonderful collaborator and mentor, and for making this research possible. I would also like to express my gratitude to the entire CTC project team – Dr. Ebrahim Azizi, Dr. Monika Burness, Dr. Ramdane Harouaka, Dr. Yadwinder Deol, Shamileh Fouladdel, Jill Hayden, Shraddha Pardesi, and Anoop Gill for being a wonderful team and for providing samples, feedback, and more. I would like to acknowledge Dr. Lisa Larkin and Dr. Brian Syevrud for their useful insights and hard works on the Muscle Satellite Cells project. I would like to thank Dr. Euisik Yoon, Yu-Heng Cheng, and Dr. Yu-Chih Chen for their help with

the Hydro-Seq collaboration. I appreciate the help from Susan Hamlin and Mary Beth Westin for handling all of my random questions and requests. I would also like to thank all the faculties, staffs and fellows in Microfluidics in Biomedical Sciences Training Program (MBSTP) for the inspiration and collaboration. Additionally, I am grateful to Rackham Merit Fellowship, Rackham Conference grants and MBSTP fellowship which supported me through my study. I would also like to acknowledge the Lurie Nanofabrication Facility (LNF), the Microscopy and Image Analysis Lab (MIL) at University of Michigan, and the Takayama lab. And most importantly, I am very grateful to all the patients who participated in our study, and kindly provided blood for our research.

TABLE OF CONTENTS

LIST OF FIGURES

LIST OF TABLES

ABSTRACT

Circulating tumor cells (CTCs) present in the blood are the seeds of metastasis and are of high biological and clinical relevance. Single-cell technologies are playing an increasing role in profiling CTCs in the peripheral blood for detection and real time monitoring of cancer metastasis. CTCs also help in identifying distinct drivers of metastasis. However, current approaches are limited to subjective selection of CTCs based on biomarkers, which hinders the unbiased comprehensive study of CTCs on a single cell level. We present a unique label-free microfluidic "Labyrinth" device to isolate CTCs at a high throughput of 2.5mL mL of blood per minute, offering the first biomarker independent single cell isolation and genomic characterization platform to study heterogeneous CTC subpopulations in cancer patients. The Labyrinth takes advantage of inertial forces on the microscale in curved geometries to differentially focus cells based on the size difference between CTCs (15-25 μm) and blood cells (2-12 μm). This novel strategy of multi-course path traversing across inner loops to outer loops yielding highest hydrodynamic path length enabling focusing of both CTCs and white blood cells (WBCs) differentially, leading to high recoveries (> 90%) and efficient separation of WBCs from CTCs, resulting in high purity of CTCs in the final product (~ 600 contaminating WBCs per mL remained), even in whole blood samples without any pre-processing. CTCs were successfully isolated from 56 breast cancer (9.1 CTCs/mL average, range 2-31/mL) and 20 pancreatic cancer (51.6 CTCs/mL average, range 11-115/mL) patients. We detected not only CTCs typically defined by epithelial markers, but also significant numbers of CTCs (> 50%) lacking epithelial markers but expressing mesenchymal and cancer

stem cell (CSC) markers. Patient samples were then analyzed using single cell multiplex gene expression. Seventy single cells were successfully recovered and used to identify different subpopulations of CTCs based on their genetic signature, unlike other methods where a positive or negative selection based on protein expression is used. Interestingly, both inter- and intra-patient molecular heterogeneity at the single cell level in CTCs were observed with cells expressing genes uniquely related to epithelial, mesenchymal-epithelial transition (MET), and epithelial-mesenchymal transition (EMT) phenotypes. The Labyrinth platform allows a thorough molecular understanding of the heterogeneity among CTCs. This platform also shows CTCs potential as a biomarker to non-invasively evaluate tumor progression and response to treatment in cancer patients.

As a truly biomarker free isolation platform, Labyrinth is also adopted for the isolation of CTCs from various types of cancers, including but not limited to adenoid cystic carcinoma (ACC), hepatocellular carcinoma (HCC), and lung cancer. Besides enumeration, the isolated CTCs were used in a wide range of studies, such as ex vivo culture of live CTCs from pancreatic patients and generating xenograft tumor model in mice. Beyond CTC isolation, Labyrinth was applied in the study of skeletal muscle satellite cells in collaboration with Dr. Brian C. Syverud and Prof. Lisa M. Larkin.

All in all, Labyrinth device offers a microfluidic technology to address the need for efficient isolation of rare cells and enables downstream studies on the target cells.

CHAPTER 1 Design and Development of the High Throughput Label-Free Labyrinth Platform for the Separation of Rare Cells

1.1 Abstract

CTCs are seeds of metastasis and are the key players in understanding the biological process of metastasis and could serve as potential non-invasive biomarker to evaluate tumor progression and response to treatment. However the unbiased isolation of CTCs remains challenging due to the rarity and heterogeneity that hinders further studies on these cells. In an attempt to overcome the limitations in current isolation approaches, we developed a high throughput, label-free, and inertial-based Labyrinth device for the size-based separation of CTCs. The cell separation in Labyrinth is based on the inertial focusing and Dean forces that focus and isolate sized cells into different streamlines. Cell line experiments were performed in order to understand the physics of cells in microfluidic environment, and to optimize the design for a separation of WBCs and CTCs. The finalized design of Labyrinth consists of 11 loops and 56 corners with 4 outlet at the end. The optimized flow condition is at 2.5 mL/min, in which over 95% of cancer cells are recovered and over 98% of WBCs are removed. Compared to other published label-free technologies, Labyrinth offers the highest throughput, equal or higher

performance, the capability to preserve cell viability, and the potential for further downstream analysis.

1.2 Introduction

Breast cancer is the most frequently diagnosed cancer and the leading cause of cancer-related death in women in developed countries [1]. In 2016, breast cancer is estimated to have accounted for 23% of all cancer diagnoses among women in the US; around 226,870 new cases of invasive breast cancer are expected to occur in 2017. Based on the cases diagnosed from 2001 to 2007, the overall five-year survival rate of breast cancer in females is 89%. However the survival rate drops to 23% if the breast cancer has spread to parts of the body remote from the primary tumor, while the rate rises to 99% if the cancer is detected early while in local or regional stages [1].

Non-aggressive treatments are as effective as other treatments if breast cancer is detected in early stages. Depending on the size and extent of tumor, the surgical treatment of breast cancer usually involves lumpectomy (removal of the tumor and surrounding tissue) or mastectomy (removal of the breast) [2]. For women with localized or regional breast cancer, studies have shown the long-term survival after lumpectomy plus radiation therapy is similar to that for mastectomy. The removal of underarm lymph nodes is recommended during surgery to determine the spread of breast cancer. Sentinel lymph node biopsy, removal of the first lymph nodes on the path of cancer dissemination, is as effective as and less damaging than full axillary node dissection for women with early stage breast cancer [2].

Early detection of breast cancer mostly relies on mammography due to the lack of symptoms in early stage breast cancer when the primary tumor is small and treatment is more efficient. On average, mammography can detect 80-90% of breast cancers at an early stage in

women without symptoms, and has reduced risk of death by 15% in all women screened. Mammography is a rather accurate screening tool, but the chance for false negatives remains around 20% and that for false positive is over 30% [2]. Mammography also detects indolent localized cancers that may not require treatment [3].

The metastasis of cancer is preceded by the dissemination of cancer cells from the primary tumor site to remote sites via the blood circulation. Circulating tumor cells (CTCs) were first discovered in 1869 by Ashworth, T. R. during an autopsy of a metastatic cancer patient [4]. It was observed that the cancer cells in a site distant from the tumor resembled the originating tumor. The observation implied that the cancer cells would have been carried by the blood circulation in order for them to be located in the distant site. Since then CTCs have been believed to be an important factor in metastasis, a major reason of deaths due to cancer.

The presence of occult metastatic tumor cells in the peripheral blood (Figure 1.1) of patients with primary breast cancer represents a strong and independent prognostic factor for decreased disease-free and overall survival [5-7]. Studies have shown that even a small amount of these CTCs found in blood (i.e. <5 per 7.5 mL of blood) could indicate poor prognosis or no response to therapy. Cristofanilli et. al. reported that overall survival in metastatic breast cancer patients can be predicted through CTCs [8]. Furthermore, the molecular characteristics of CTCs might support individualized therapy to cancer and the monitoring of treatment [9].

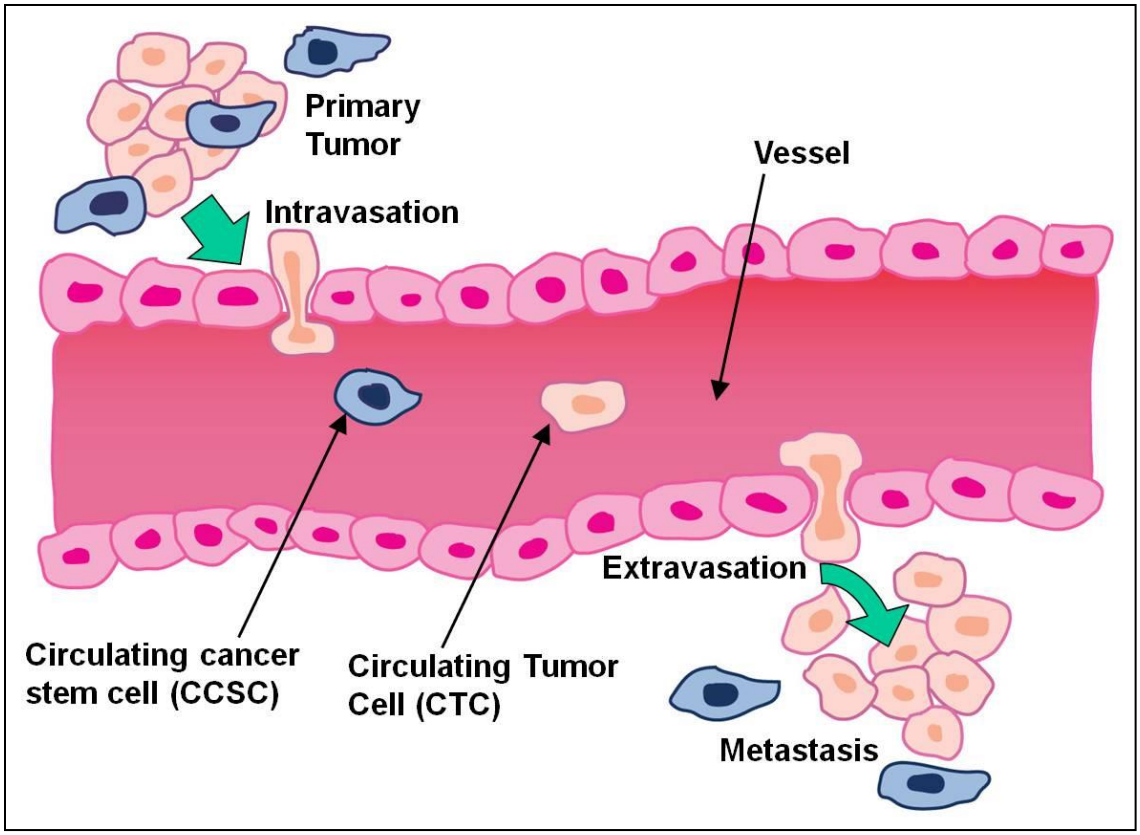

Figure 1.1 Role of Circulating Cancer stem cells (CCSCs) and circulating tumor cells (CTCs) in metastasis.

Unfortunately, early spread of tumor cells (Figure 1.1) usually remains undetected in breast cancer patients even by conventional histopathological analysis and high-resolution imaging technologies. The rarity of CTCs in peripheral blood from patients (1 per 10^9 blood cells) hinders the collection of CTCs [10-14]. The plasticity and phenotypic alterations of CTCs further hamper the detection and isolation of these cells.

1.3 CTC Isolation Technologies

1.3.1 Affinity-based Isolation of CTCs

The clinical and biological relevance of CTCs makes their isolation an active area of research, bolstered by several technological developments over the past two decades [15]. Technologies taking advantage of microfluidic principles to manipulate cells are establishing their niche and are an active area of research [16]. These approaches are mainly categorized by their exploitation of either CTCs' distinctive biological or physical properties. The most widely used microfluidic approach for isolation of CTCs is immune-affinity capture using distinct antibodies targeting molecules that are expressed exclusively on tumor cells and are absent in blood cells. The most commonly used antibody for isolation of CTCs is against the epithelial cell adhesion molecule (EpCAM). This strategy has been successfully validated for use in prognosis, therapeutic monitoring and molecular diagnosis [17-21].

The CTC-chip is the first immuno-capture microfluidic technology developed in 2007 by Nagrath et. al [18]. The PDMS-based device consists of thousands of microposts coated with antibodies against EpCAM, which allows the capturing of CTCs expressing the antigen using a one step process without requisite pre-labeling or processing of whole blood samples. The advantage and novelty of this technology is its high sensitivity and cell viability that enables downstream analysis such as immunostaining or DNA/RNA extraction of the captured cells [18]. Various technologies applying similar concept yet different designs emerged following the CTC-chip. Stott et al. developed the transparent PDMS-based herringbone chip that provides passive mixing through the generation of microvortices for enhancing the capture efficiency [19]. Adams et al. combined a polymer-based microfluidic device to capture CTCs and an integrated conductivity sensor to count CTCs after they are released from the capture chamber [22]. Wang et al. introduced a microfluidic chaotic mixing chip with a patterned silicon nanopillar (SiNP) substrate [23]. Several commercialized devices also adopted the immuno-capture technology, such

as NanoVelcro CTC chip which applied nano-sized structures coated with EpCAM for CTC capture [24], and GEDI chip which applied an antibody against prostate specific membrane antigen (PSMA) for CTC isolation [25].

Immuno-magnetic capture is another similar approach of the immune-affinity based isolation which applies antibody-coated magnetic beads to bind the targeted cells. The bonded cells/magnetic beads duplet are further captured by applying magnetic fields to separate CTCs from unbounded blood cells [26]. CellSearch™ is the first and by far the only FDA approved CTC isolation technology for clinical application [27]. It made use of aforementioned magnetic beads to capture EpCAM-positive CTCs and followed with immunostaining to quantify CTC numbers. In 2010, Saliba et al. proposed a cell-sorting device by immobilizing specific capture molecules on magnetic beads [28].

Affinity-based technologies offer high specificity and purity of the recovered CTCs due to the nature of antibody-antigen interaction [25], and therefore enable various downstream analysis on the purified population of these recovered CTCs. However, these technologies suffer from two major limitations: low throughput for sample processing and the inability to capture whole CTC populations due to the heterogeneity of these cells. Most affinity-based devices, such as the CTC-chip [18] and the herringbone chip [29], have an operating flow rate of 1 to 3 mL hr^{-1}. Increasing the flow rate in affinity-based devices would significantly decrease the capture efficiency due to the higher shear disrupting the antibody-antigen binding [18]. This limits the volume of blood sample that can be processed and constraints the overall CTCs that can be recovered.

Cell plasticity refers to the ability of some cells, e.g. stem cells, to acquire the characteristics of other cells. Epithelial–mesenchymal transition (EMT), a complex process leading to a phenotypic alteration, transforms cancer cells into a more aggressive phenotype – the

mesenchymal phenotype. CTCs with mesenchymal phenotype, also called circulating cancer stem cells (CCSCs), have the potential for dedifferentiation and the rearrangement of cellular contact junctions. For the cells undergoing EMT, the expression of biomarkers, specifically the epithelial markers often used for immune-affinity based isolation, could decrease or become non-existent, and these cells may be missed by EpCAM targeted approaches [30, 31]. The biomarkers of the mesenchymal phenotype CTCs have not yet been well recognized, and the lack of information regarding these biomarkers continues to make the isolation of this aggressive phenotype challenging.

1.3.2 Physical Properties-based Isolation of CTCs

In order to overcome the limitations of biased cell selection using immune-affinity based isolation techniques, researchers have proposed various label-free methods utilizing the physical properties of CTCs to achieve the enrichment. The size differences among CTCs and other blood components make size-based separation an appealing strategy (Figure 1.2). More in specific, the sizes of CTCs are generally within the range of 13 to 25 μm in diameter [32], larger than other blood cells such as leukocytes within the range of 8 to 11 μm in diameter [33] and red blood cells (RBCs) within the range of 5-9 μm in diameter [34]. Major approaches utilizing the physical properties of CTCs are filtration, dielectrophoresis (DEP), and hydrodynamic separation.

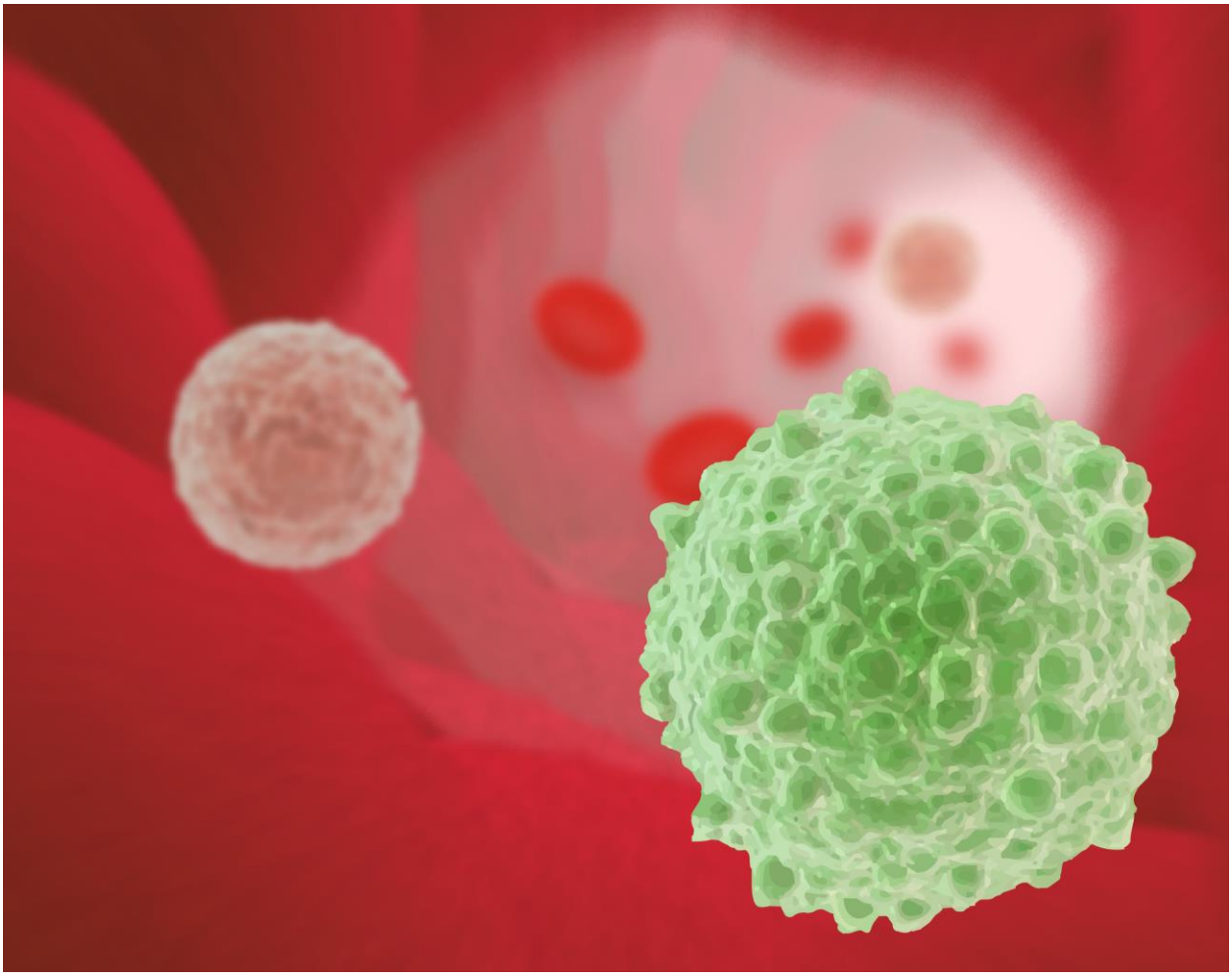

Figure 1.2 Illustration of the size difference among CTCs (green cell), leukocytes (brown cells), and RBCs (red cells) circulating in blood vessel.

Filtration based approaches typically apply membranes with pore sizes around 7-8 μm that allows smaller blood cells to flow through while trapping larger CTCs [35]. Mohamed et al. reported the first size-based separation device with micro-filters (pores etched on membrane) to physically trap the larger cells [36]. Vona et al. developed ISET (Isolation by Size of Epithelial Tumor Cells) that uses polycarbonate to form 8 μm cylindrical pores as membrane-filter to capture CTCs [37]. Lin et al. proposed a parylene membrane microfilter that had higher sensitivities than the CellSearch system from 57 cancer patients [38]. Nonetheless, filtration approaches generally

suffer from low purity and efficiency resulted from cell clogging on membrane when processing larger sample volume [39].

DEP is used in CTC isolation as an electric method that manipulate cells relying on their dielectric properties in accordance with their phenotype and membrane capacitance [40]. CTCs and other cells can therefore be separated depending on their responses to electrical fields [41]. Peter et al. studied the separation of cultured tumor cells from peripheral blood using dielectrophoretic field-flow fractionation (depFFF) method [40]. Shim et al. reported an integrated microfluidic platform using DEP, sedimentation and hydrodynamic lift forces to isolate CTCs from clinical samples [42]. Although DEP methods can be used to identify CTCs with different phenotypes, they are limited by the low throughput (<1mL hr^{-1}) [35].

Hydrodynamic based approaches are one of the most promising CTC isolation methods due to its highest throughput capability [43]. Di Carlo introduced the inertial migration of particles to achieve high throughput cell separation in microfluidic channels [44]. In short, particles flowing through microfluidic channels can be focused into certain designated streamlines due to the equilibrium of two inertial lift forces- shear gradient and wall lift forces [44]. Hur et al. developed a microfluidic device using microscale laminar vortices to retain large CTCs in assigned areas based on the inertial migration of particles [45]. Other technologies further incorporate a secondary flow termed Dean flow that occurs in the flow of curved channels to separate cells by size difference [46]. Dean flow-based technologies generally adopt spiral design as the basis for cell focusing as well as sized separation [46]. Sun et al. proposed a double spiral design to separate spiked tumor cells from peripheral blood [47]. Warkiani et al. reported a stacked design with three layers of spiral channel for ultra-high-throughput processing [48]. Although hydrodynamic based

approaches having the advantage of higher throughput, they typically compromise for either low CTC recovery or low blood cell removal as the smaller cells are not efficiently focused [46].

1.4 Design and Principle of Labyrinth

1.4.1 Motivation

The design of the Labyrinth device (Figure 1.3) is inspired by the Labyrinth in Greek mythology, an elaborate structure with numerous turns and corners built to hold the Minotaur. We applied a similar structure for the size-based enrichment of CTCs by bulk depletion of hematopoietic cells using inertial microfluidics based separation. More in specific, we incorporated both inertial focusing and Dean flow for sized separation in the design of Labyrinth, enabling continuous focusing of all cells while separating CTCs from smaller blood cells at the outlet (Figure 1.4).

Figure 1.3 Illustration of a Labyrinth device with whole blood flowing through.

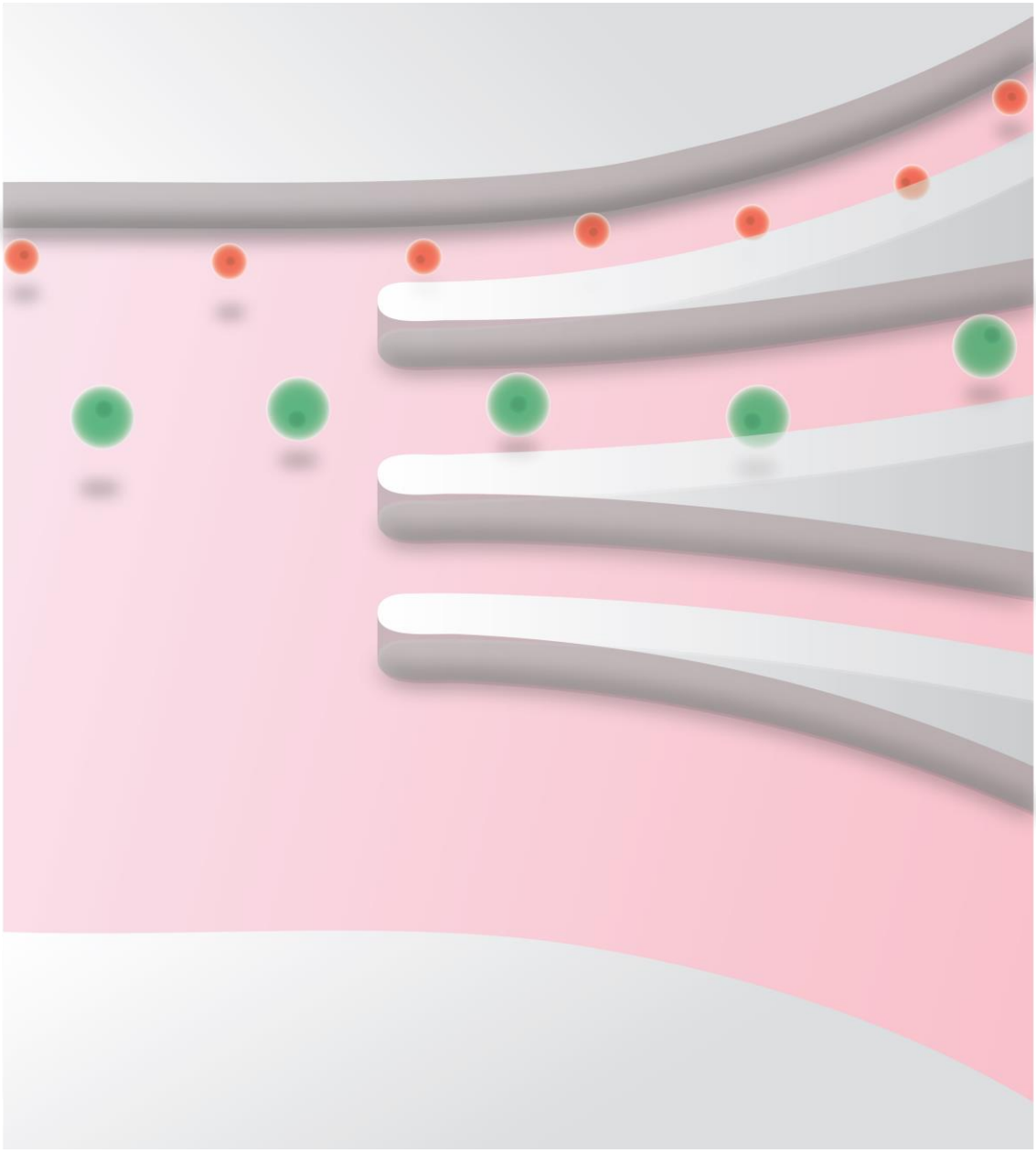

Figure 1.4 Illustration of the separation of blood cells (red spheres at top channel) and cancer cells (green spheres at the second channel from top).

1.4.2 Inertial Focusing of Particles in Microfluidic Channels

The inertial migration based particle separation relies on the equilibrium between inertial lift forces and Dean flow that results in the migration of particles during laminar flow in microfluidic devices with curved channels. Particles in a straight channel experience stresses that

act over the entire channel surface, including shear stress that yields drag forces and normal stress that yields lift forces perpendicular to the direction of flow. The migration of particles due to lift forces was first observed by Segré and Silberberg in the 1960s [49, 50]. Di Carlo reported that particles would be maintained at specific positions due to the combination of inertial lift forces where shear gradient lift pushes the particles toward the wall and the wall lift effect pushes the particles toward the center (Figure 1.5A). These forces will confine the particles in a straight channel to several equilibrium positions, where the number of equilibrium positions is related to the geometry of the channel (Figure 1.5B-C).

A relation describing the magnitude of lift force (Fz) was reported by Asmolov [51]:

$$F_z = \frac{\mu^2}{\rho} {Re_p}^2 f_c(\mathrm{Re}_c, x_c) \tag{1.1}$$

Here Re_c is the channel Reynolds number, Re_p is the particle Reynolds number $Re_p = \mathrm{Re}_c \frac{a^2}{D_h^2}$, D_h is the hydraulic diameter defined as $2\mathrm{wh}/(\mathrm{w}+\mathrm{h})$, and x_c is the position of the particle within the channel. $f_c(\mathrm{Re}_c, x_c)$ can be considered a lift coefficient and is a function that is dependent on the position of the particle within the cross-section of the channel x_c and the channel Reynolds number, but independent of particle geometry. At the equilibrium position, where the wall effect and shear-gradient lift balance, $f_c = 0$ [44].

1.4.3 Dean Flow in Curvilinear Microfluidic Channels

The Dean flow, on the other hand, occurs in the flow of curved channels. Dean flow is the secondary flow due to the centrifugal effects that will affect the particle equilibrium positions. Dean flow is characterized by counter-rotating vortices where the flow at the midline of the channel is directed outward around a curve, while the flow at top and bottom of the channel is directed inward (Figure 1.6). The drag force due to Dean flow is correlated with the particle size

and curvature of the channel, and this drag force will also affect the equilibrium position of the particles. Therefore, the equilibrium between inertial lift forces and drag force from Dean flow can be utilized for size-based sorting. Assuming Stokes drag, the attributable to Dean flow (Dean drag, F_D) scales as [44]

$$F_D \sim \rho U_m^2 a D_h^2 r^{-1} \tag{1.2}$$

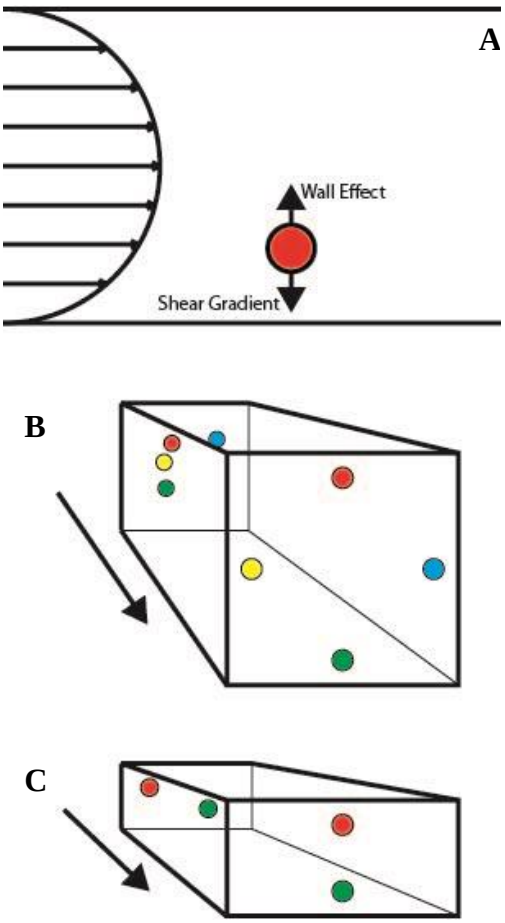

Figure 1.5 Inertial lift force in straight channels (A) forces on particles (B) 4 equilibrium positions; (C) 2 equilibrium positions.

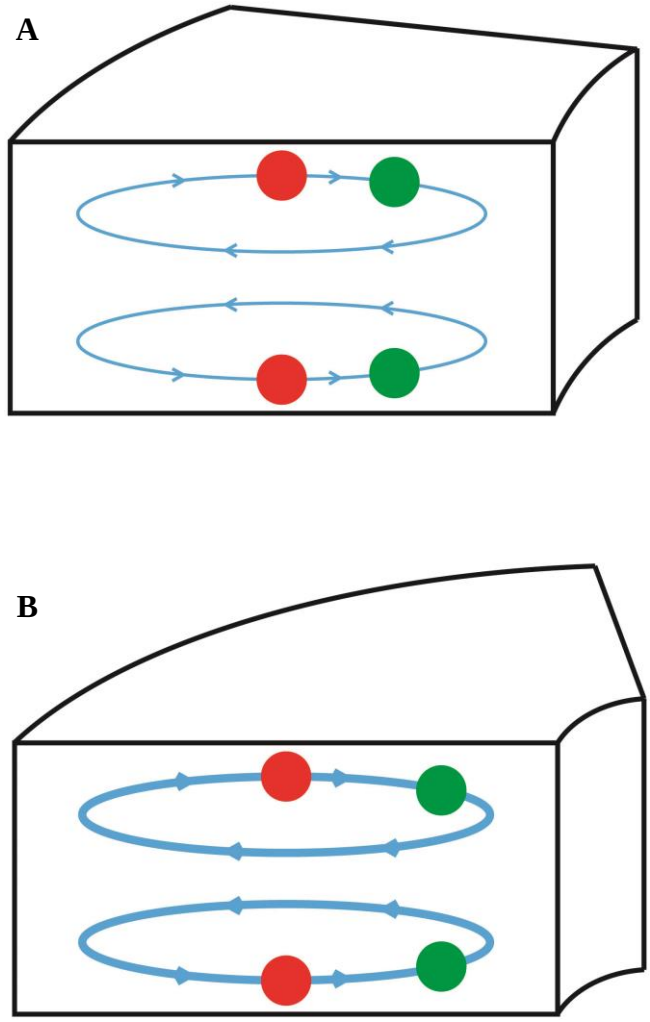

Figure 1.6 Migration of particles in curved channel from original equilibrium positions (red) to new positions (green) in (A) small curvature, (B) large curvature.

The lift forces stabilize particles at positions located along the centerline of a channel cross section, while Dean flow drag forces cause particles to circulate in the cross section (Fig. 4). A new equilibrium position can be estimated from the ratio of F_z to F_D which scales as [44]:

$$\frac{F_z}{F_D} \sim \frac{1}{\delta}\left(\frac{a}{D_h}\right)^3 \mathrm{Re}_c{}^n, \ (n < 0) \tag{1.3}$$

Here δ is the curvature ratio, $\delta = \frac{D_h}{2r}$.

Equation 3 implied that CTCs can be isolated from smaller blood cells in curved microfluidic devices by specifying an appropriate flow rate and radius of curvature. The inertial

force can be considered as the driving force that focuses the particles, while the drag force from Dean flow is the force that moves the particles away from the center of the channel, leading to size-based separation. For the situation where F_D dominates, either no focusing would be observed due to the strong mixing force F_D compared to focusing force F_z, or all the particles with different sizes could be pushed to the same equilibrium position. For the case when F_z dominates, particles with different sizes remain at the same equilibrium positions as that in a straight channel due to the dearth of mixing force. A proper control of flow rate and good design of microfluidic structure would lead to an adequate ratio of F_z to F_D that will cause cells to be well separated by size.

1.4.4 Sharp corners in Labyrinth

The major difference between Labyrinth and all other spiral designs is the numerous "corners" (Figure 1.7) placed across the flow pattern. It is proposed by Sun and Li that the sharp change in flow direction can increase the focusing of smaller particles [47]. Smaller particles (e.g. RBCs, WBCs) are more difficult to be focused due to the weaker lift force F_z (Equation 1.1). A possible explanation of the enhanced focusing of small particles at sharp turns is the strong Dean vortices generated at the turns and therefore the particles are passively migrated along the vortices. This passive migration transports the particles to their equilibrium positions. Once the particles are focused, the change in flow direction will not disperse the focused stream, hence the turns can only benefit but not harm the focusing of particles.

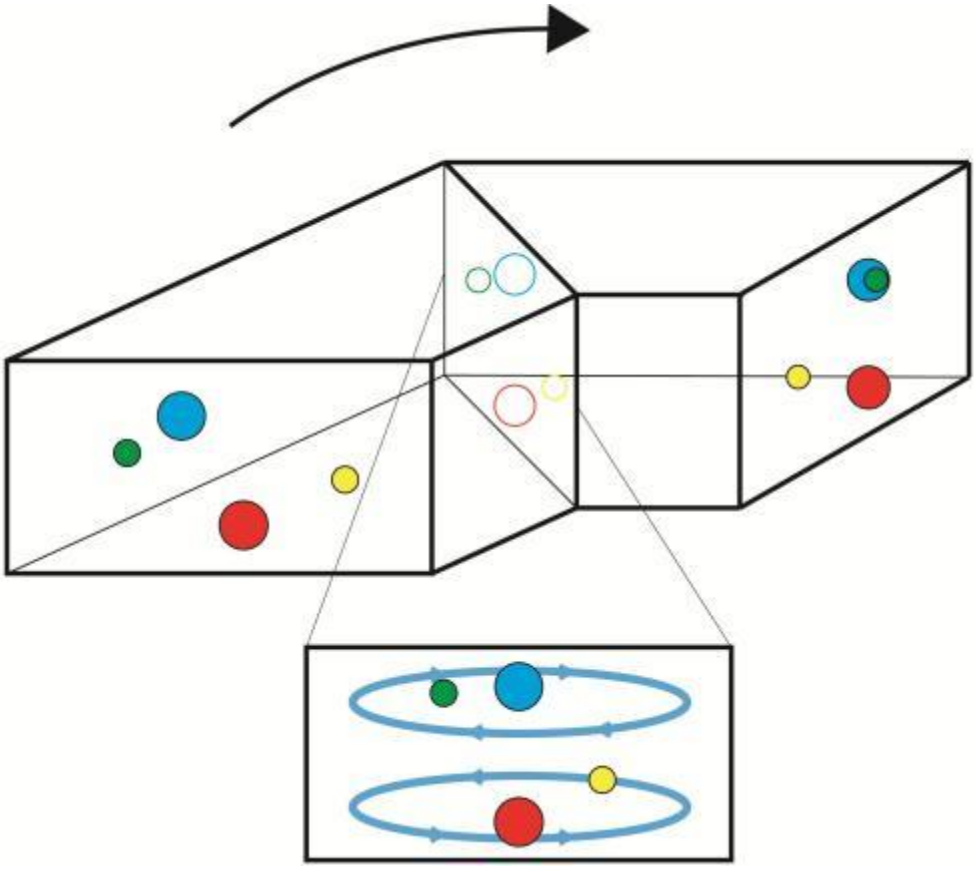

Figure 1.7 Illustration of a corner in Labyrinth that enhances the focusing of small particles or cells (green and yellow spheres).

1.5 Materials and Methods

1.5.1 Device Fabrication

The fabrication of Labyrinth devices includes the design of film mask, the fabrication of SU-8 mold in clean room, and the fabrication of PDMS (Ellsworth Adhesives) device in laboratory. The film mask was designed in laboratory using L-Edit software. The design was converted to a photomask (FineLine Imaging) and used to prepare a mold by traditional photolithography. In short, a negative photoresist SU-8 100 was utilized to form the mold for the PDMS device by applying soft lithography. Using a spin-coater, the negative photoresist layer, SU-8 100, was deposited onto silicon wafer with 2450 rpm rotating for 1 minute. The wafer was

then soft-baked for 10 minutes at 65 °C and 70 minutes at 95°C. The mask was aligned to the wafer and is exposed to UV light for 20 seconds. Post-exposure-baking was applied for 3 minutes at 65 °C and 10 minutes at 95°C. Then, the wafer was developed by soaking in developer for 6 minutes and in IPA for 1 minute to remove the inactivated photoresist. It was hard baked for 3 to 5 minutes at 150-180 °C. The height of the mold built on silicon wafer was ideally 100 μm, and the width of the channel was 500 μm (Figure 1.8).

To prepare the PDMS device from fabricated mold, 30 mL Sylgard polymer base and 3 mL curing agent were well-mixed and poured onto silicon mold. The mixture was left in desiccator for 2 hours to remove trapped air within the mixture. It was then heated at 65 °C overnight to harden the polymer. The polymer was cut into desired shape, e.g. rectangular for Labyrinth, and punched with needle for tubing later. The PDMS device as then bonded to standard sized glass slides via plasma surface activation of oxygen. The bonded device was tubed with 0.66 mm diameter tubes.

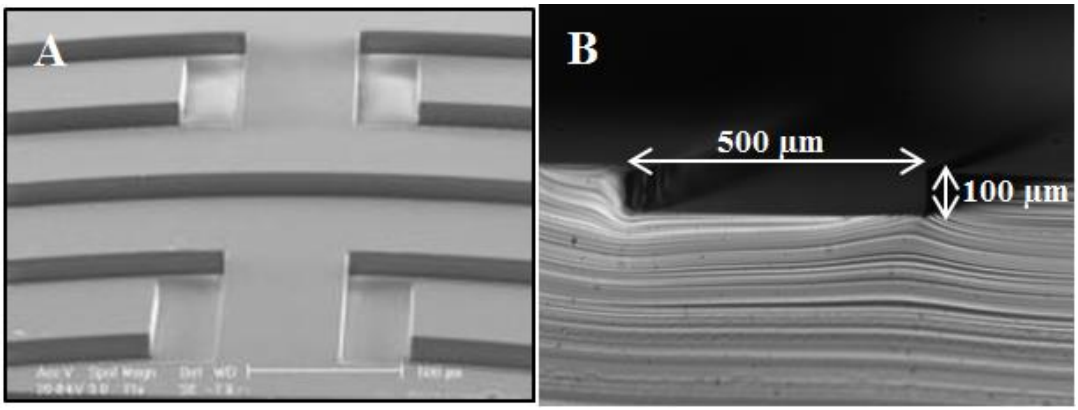

Figure 1.8 (A) SEM image of the channel in labyrinth; (B) Cross-sectional image of labyrinth taken with microscope

1.5.2 Cell Culture

Human breast cancer cell line MCF7 and human pancreatic cancer cell line PANC-1 were maintained in in DMEM (Invitrogen - LifeTechnologies, Inc.) supplemented with 10% fetal

bovine serum and 1% Antibiotic-Antimycotic (100X) at 37°C in a humidified atmosphere at 5% CO2. Human prostate cancer cell line PC-3 and human lung cancer cell line H1650 were maintained in RPMI-1640 (Invitrogen - LifeTechnologies, Inc.) supplemented with 10% fetal bovine serum and 1% Antibiotic-Antimycotic (100X) at 37°C in a humidified atmosphere at 5% CO2. Medium were renewed every 3-4 days and passaged with Trypsin - 0.53 mM EDTA (Invitrogen - LifeTechnologies, Inc.).

1.5.3 Preparation of Spiked Samples with Cancer Cell Lines

Labyrinth was optimized with the experiments of spiked samples. Cancer cell lines were spiked in buffer solution (PBS), diluted whole blood, or RBC removed whole blood. For buffer samples, cancer cell lines were stained with Green Cell Tracker (Life Technologies) and mixed with white blood cells (stained with DAPI) into PBS). For diluted blood samples, cancer cell lines were stained with Green Cell Tracker and spiked into diluted blood. For RBC removed blood samples, RBCs were first removed from whole blood using density separation with dextran solution (6 m/v% dextran and 0.87 m/v% sodium chloride in DNase/RNase-Free Distilled Water). Cancer cell lines stained with Green Cell Tracker were then spiked into the RBC removed blood. Typical numbers of cells spiked into the samples were 50,000 cells/mL for the observation under microscope, or 10-100 cells/mL for the simulation of patient sample.

1.5.4 Experimental Protocol for Optimization and Characterization

The device was pre-flowed with 1% Pluronic acid solution (diluted in 1X PBS) at 100 μL/min for 10 minutes and then incubated for 10 minutes to prevent cell clotting on channel walls. Cell sample suspended in buffer was flowed through the labyrinth at different flow rates (500-3000 μL/min) and was observed under a microscope. After 1 minute duration of flow stabilization,

outputs from all outlets were collected for cell counting to calculate the percentage recovery. Cells collected from outlets were quantified using hemocytometer. To observe the isolation of cancer cells from other blood components, images and movies were taken using both a high-speed camera and a fluorescence microscope under brightfield, FITC, and DAPI filters at 10X and 20X magnification.

1.6 Results

The design of Labyrinth was modified and optimized for numerous times. Figure 1.9 A-F depicts the evolution of the design from earliest (Figure 1.9 A) to the latest version (Figure 1.9 F). The white pattern in Figure 1.9 represents the flow channel, while the black pattern represents the PDMS wall. Outlet design of each version is highlighted at the zoomed-in images in Figure 1.9 A-F.

In the first model of Labyrinth (Figure 1.9 A), the channel was separated into three outlets at the center of Labyrinth. These outlet channels were directed to the outer part of labyrinth to facillitate the collection of cell outputs. A partial separation of cancer cells was observed in the experiment with PC3 cell line spiked into diluted blood sample at the flow rate of 2000 μL min^{-1} (Figure 1.10). Both PC3 cells and WBCs were focused into separated steamlines. PC3 cells were focused into the middle channel, while WBCs were directed into the bottom channel. However, the outlet channels were blocked by the aggregation of huge clots soon after the experiment began. Possible reasons for the cell clotting at the outlet were the narrow width of the outlets, the interaction among cells and PDMS wall, and contamination in sample preparation. This cell aggregation at the outlets hindered further collection of separated products and the diminished the application of this device.

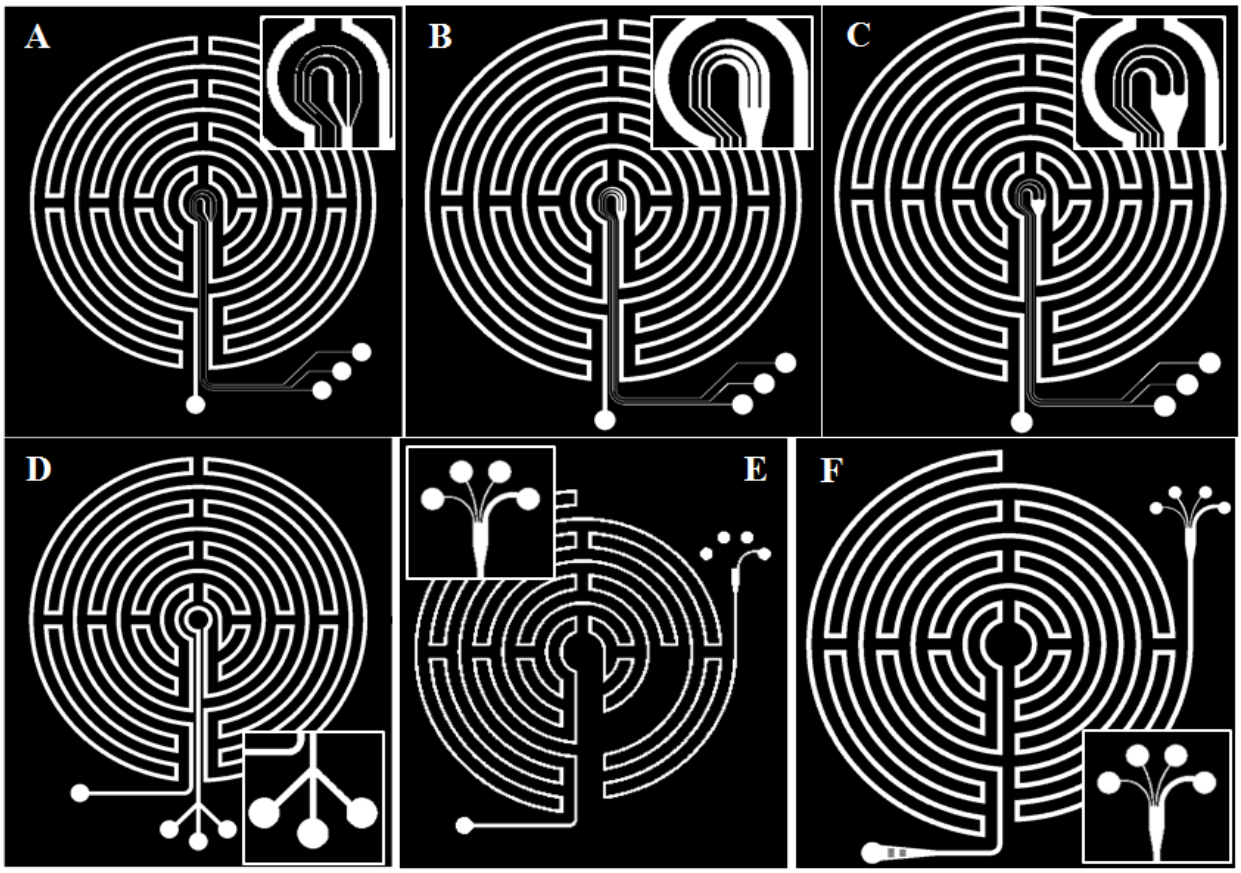

Figure 1.9 Different versions of Labyrinth design.
(A) Original design (B) and (C) Expanded outlet designs (D) Revised versions (E) Four outlets model (F) Four outlets model (revised).

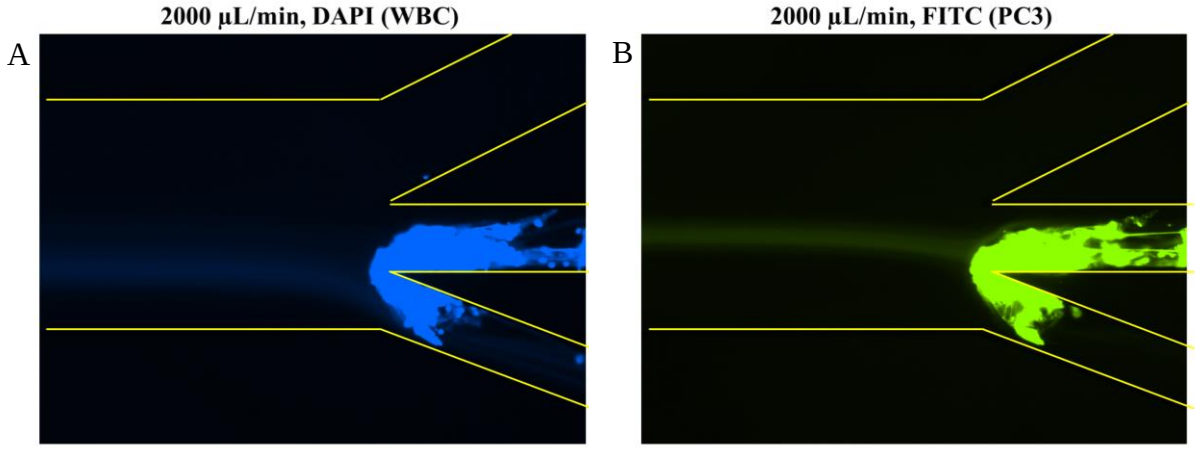

Figure 1.10 WBC and cancer cell partial separation in original design of Labyrinth.
(A) WBCs (blue stream, imaged in DAPI channel) focusing into bottom outlet (B) PC3 cells (green stream, imaged in FITC channel) focusing into middle outlet. Yellow lines depict the channel wall of the device. Flow velocity was at 2000 µL min^{-1} with direction from left to right.

To reduce the cell aggregation, various outlet configurations were designed and tested (Figure 1.9B and C). In these designs, the channel was first expanded before being separated into three outlets at the center of Labyrinth. Although the aggregation was reduced in several models, cells were not well separated in all of them. By observing the outlet design, we found that the narrow duct of each of the three outlets may cause a huge pressure drop that dramatically lowers the flow rate at the outlets and thus results in the aggregation and poor separation.

To avoid the narrow ducts, the outlet channels were relocated to the outer part of Labyrinth, where the less crowded area enabled the placement of three equal-width outlet channels (Figure 1.9D). A different separation profile was observed in these models however: WBCs were partially focused into the top and bottom channels, while cancer cells were focused into the middle channel (Figure 1.11A). However, the streams of both WBCs and CTCs were not tightly focused as multiple streams were spreading through in Figure 1.11A, indicating that the purity and recovery were not consistent and varied in each individual samples. Therefore, a new experiment was designed for a better understanding of the separation within the whole device.

From the previous experiments, it was observed that particle separation in Labyrinth was greatly related to the position where the single channel was separated into multi-outlet channels. In order to characterize the best position for outlet placement, Labyrinth was scanned under fluorescent microscope while processing the cell mixture of pre-labeled cancer cells and WBCs. Through these experiments, we were able to observe the positions where cancer cells or WBCs start to focus, and to measure the gap between these two focused streamlines at different locations (Figure 1.11B).

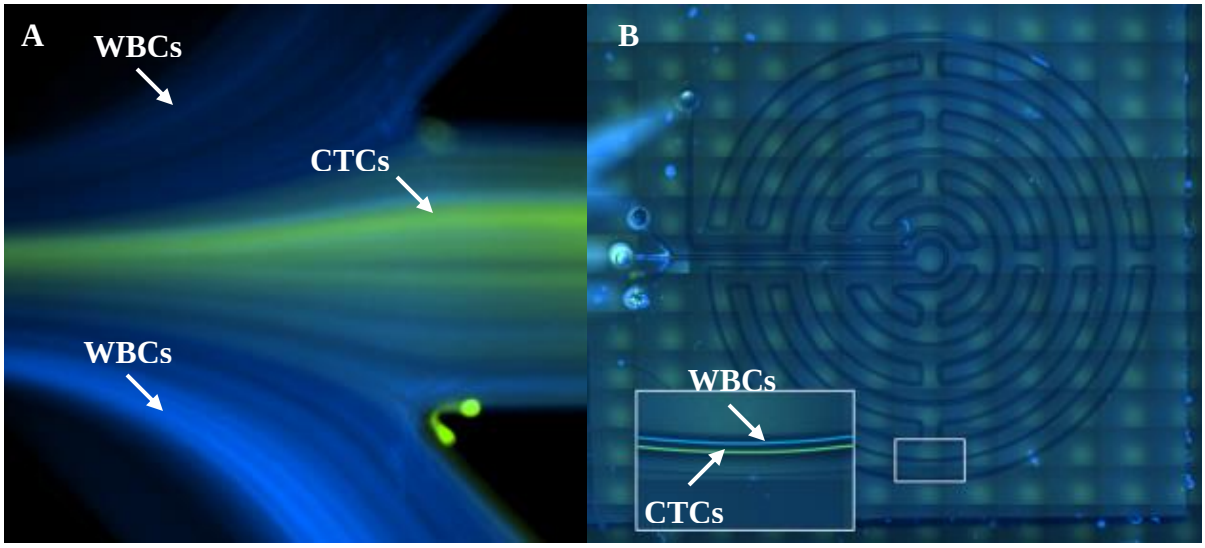

Figure 1.11 WBC and cancer cell distribution in the revised design of Labyrinth.
(A) Outlet image shows WBCs (blue streams, imaged in DAPI channel) were partially focused at top and bottom outlets, and cancer cells (green streams) were focused at the middle outlet (B) Whole Labyrinth was scanned under fluorescent microscope while processing the cell mixture in order to observe the cell distribution through the flow pattern. The enlarged area showed highly focused and separated streams of WBCs (blue) and CTCs (green).

The optimization of the configuration in Labyrinth was based on both calculations and observations from experiments. As shown in following Table 1.1, the ratio between the inertial force (Fz) and Dean force (Fd) were calculated in each loop of both WBCs and CTCs (Equation 1.3). The Fz over Fd ratio dominates the equilibrium position of sized particles. From the calculation, we observed that the magnitude of the ratio becomes higher as the radius are larger, or the loops are farther away from the center of Labyrinth. Dean force is dominant in the inner loops (smaller r and Fz/Fd ratio), causing particles/cells focused closed to the inner wall or defocused as the dominant Dean flow mixes particles. Lift forces becomes more dominant in the outer loops (larger r and Fz/Fd ratio), resulting in a narrower gap between the streamlines of small and large particles as the condition is similar to a straight channel.

It is to be noted that the Fz/Fd ratio of CTCs are 1 to 2 orders greater than the ratio of WBCs (e.g. 0.93 to 0.04 at the loop where r = 0.01725 m). This relation suggests that CTCs focus

quicker, while WBCs require longer distance to be focused. This also suggested that the focused WBC streamline are farther superpositioned by the Dean flow as the drag force are relatively greater on WBCs than on CTCs.

The purpose of this calculation was to find a loop which has the best curvature to separate CTCs from WBCs while maintaining their focusing. We observed that it takes 5 corners and 50 mm in length for CTCs to focus, and 47 corners and 480 mm in length for WBCs to focus. The design must incorporate a channel longer than 480 mm to enable the focusing of WBCs. Combining experimental observations, theoretical calculations, and numerous revisions in device design, we were able to fine tune and optimize the configuration of Labyrinth (Figure 1.9F and 1.12).

Table 1.1 Ratio between the inertial force (Fz) and Dean force (Fd) in each loop of both WBCs and CTCs.

r (m)	Fz/Fd (WBCs, 10um)	Fz/Fd (CTCs, 20um)
0.00225	0.01	0.12
0.00375	0.01	0.20
0.00525	0.01	0.28
0.00675	0.02	0.36
0.00825	0.02	0.44
0.00975	0.03	0.52
0.01125	0.03	0.60
0.01275	0.03	0.69
0.01425	0.04	0.77
0.01575	0.04	0.85
0.01725	0.04	0.93
0.01875	0.05	1.01

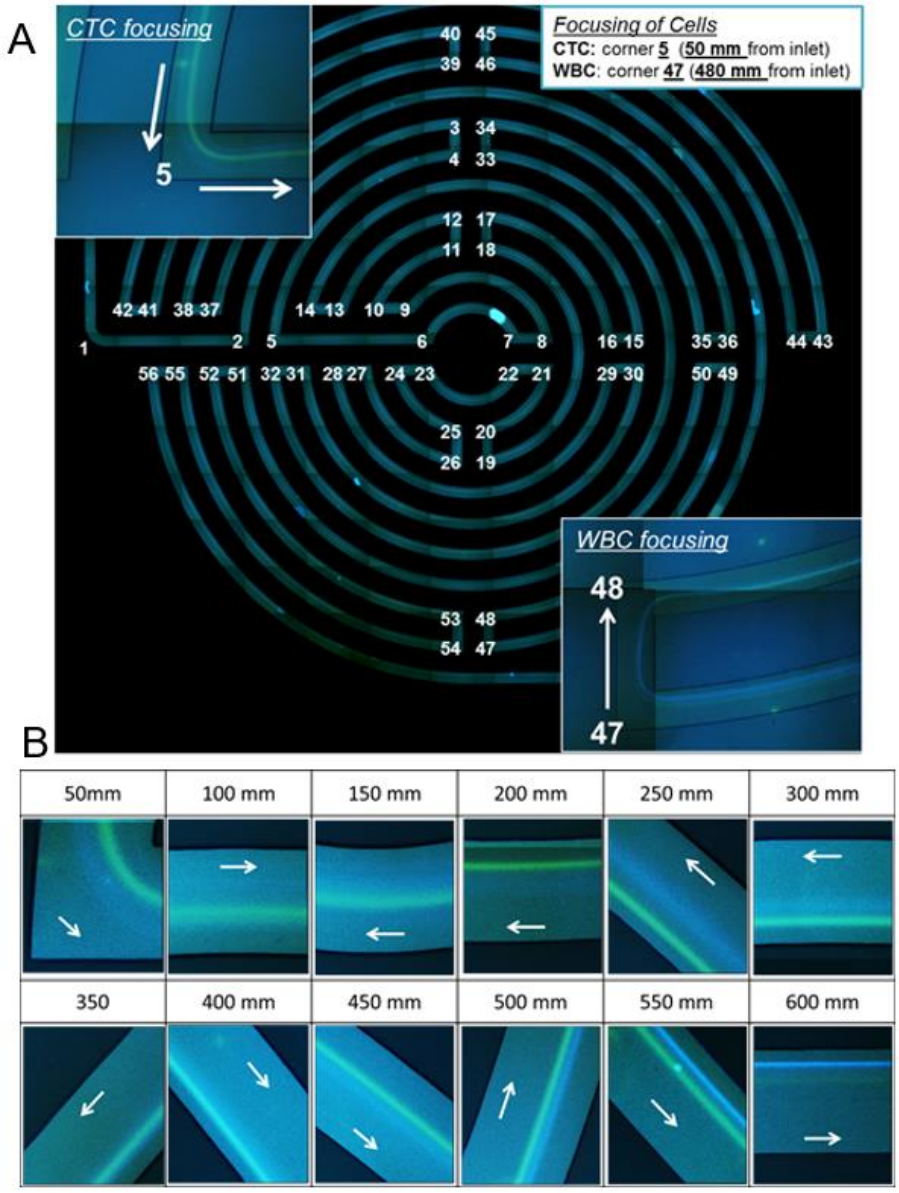

Figure 1.12 WBC and cancer cell distribution in the optimized design of Labyrinth.
(A) Scanned image shows all corners labeled from the first to the last. WBCs (blue stream, imaged in DAPI channel) were focused at 48th corner and bottom, and cancer cells were focused at the 5th corner (B) Flow distribution in Labyrinth at different distance from inlet.

The final design of Labyrinth has a total channel length of 637 mm, 500 μm in width, and around 100 μm in height. The channel height was later optimized after the Labyrinth model was finalized. It consists of 11 loops and 56 corners. The loops (Figure 1.13A), which have a small curvature ratio δ range from 5.29×10^{-3} to 3.70×10^{-2} m^{-1}, and were incorporated into the Labyrinth

to provide enough length of channel to achieve total focusing of cells and to have the proper curvature for the separation between CTCs and blood cells. The 56 sharp right-angle corners (Figure 1.13B), which have high curvature ratio, further enhance the focusing of smaller cells without the need for positive or negative selection. The channel width expands to 1000 μm from 500 μm before the streams are diverted into the outlets (Figure 1.13C). The outlets were designed such that the focused individual streams could be collected separately (Figure 1.13D).

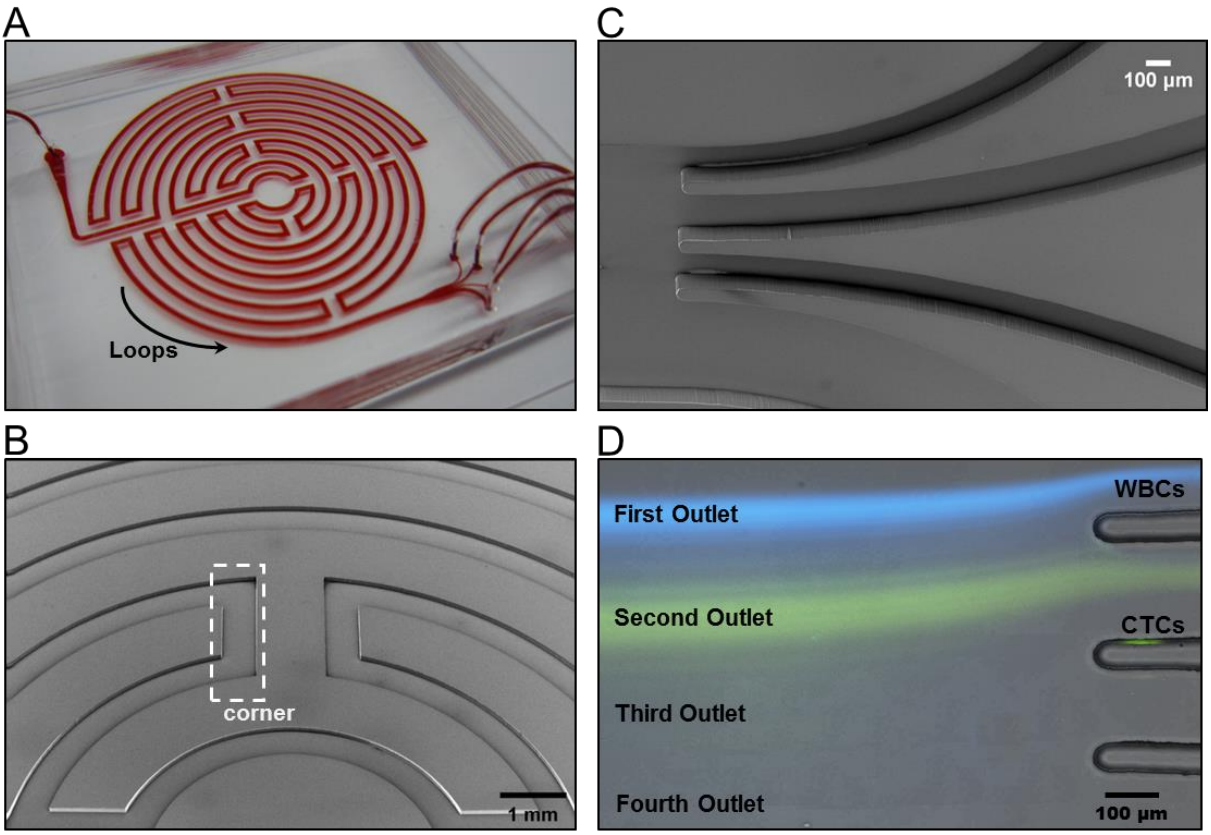

Figure 1.13 Specifications in the final design of Labyrinth.
(A) Labyrinth filled with red color food dye to indicate the flow pattern and the definition of "loops" (B) and (C) SEM images of channel and outlets in Labyrinth (D) Separation of pre-labeled WBCs and cancer cells at the outlet of Labyrinth

In order to determine the best channel height for CTC separation, Labyrinth with different height of microfluidic channels (range: 90-110 μm) were tested with spiked buffer sample at

various sample flow rate (range: 500-3000 µL/min). In all models of Labyrinth, no streamline focusing or cell separation was observed at low flow rate (500-1000 µL/min), and cell focusing occurred at flow rate above 1500 µL/min.

Labyrinth with 95 µm channel height was selected as the finalized model due to its widest separation distance among all models. The separation is optimized at 2500 µL/min, where the two streamlines of cells are apart for 238 µm with a minimum gap distance of 150 µm (Figure 1.14).

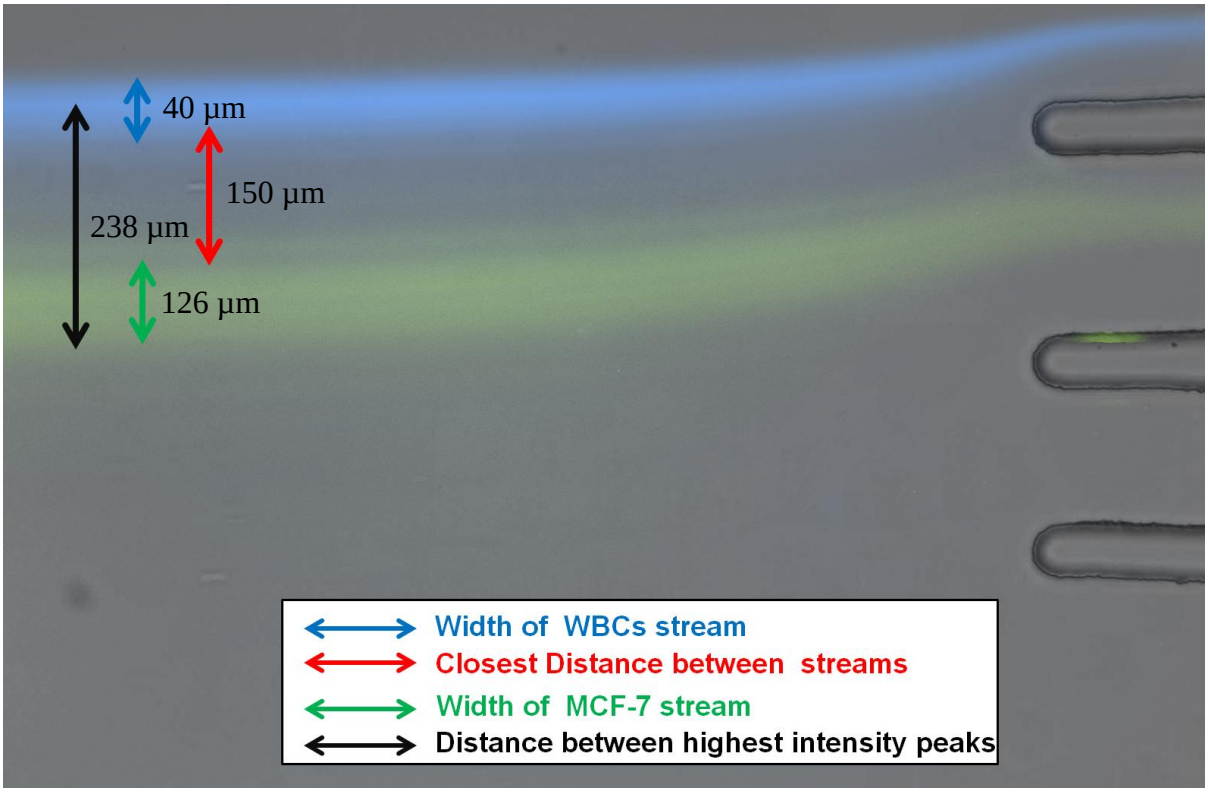

Figure 1.14 Streamline separation measurements for the Labyrinth of height 95 µm at 2500 µL/min.

The Labyrinth was optimized and tested for inertial separation of cancer cells using human breast (MCF-7), pancreatic (PANC-1), prostate (PC-3) and lung (H1650) cancer cell lines. It was determined that the optimal flow rate for maximized recovery and purity was 2.5 mL/min and also that it takes 60sec for the flow to stabilize in the device for optimal collection. Pre-labeled (Cell

Tracker) cancer cells and WBCs were spiked at a high concentration (~100,000/mL and ~500,000/mL, respectively) into buffer and separated using the Labyrinth. Using MCF-7 cells, 91.5 ± 0.9% of cancer cells were recovered from the second outlet while 91.4 ± 3.3% of WBCs were removed through the first outlet (Figure 1.15A). With GFP-labeled PANC-1 cells, a similar separation was achieved, with 92.4 ± 3.2% recovery of cancer cells with 89.0 ± 1.1% of WBCs removed in the first outlet (Figure 1.15A). Labyrinth recovery was further tested with other solid tumor cell type such as lung and prostate and found the yields to be similar (Figure 1.15A). MCF-7 and PC-3 cells were spiked into whole blood and run through Labyrinth without any pre-processing. The recoveries even from whole blood are higher than 90% (Figure 1.15A). Separation of cancer cells from other blood cells was visualized using a high speed camera and, as shown in Figure 1.15B, the cell streams were physically separate. To further characterize the ability of the Labyrinth to isolate lower concentrations of CTCs (100/mL), MCF-7/GFP cells were spiked into buffer and into healthy donor blood samples, and then processed through the Labyrinth. In this set of experiments, blood was treated with Dextran following the spike to remove excess RBCs and see its effect on recovery. The average recovery in buffer solution was 94.4 ± 3.8%, while in RBC depleted blood a 95.3 ± 0.7% recovery was obtained (Figure 1.15C). Importantly, an MTT assay demonstrated that the shear stress experienced by cells processed through the Labyrinth did not affect the cell viability or the proliferation ability (Figure 1.15D-E).

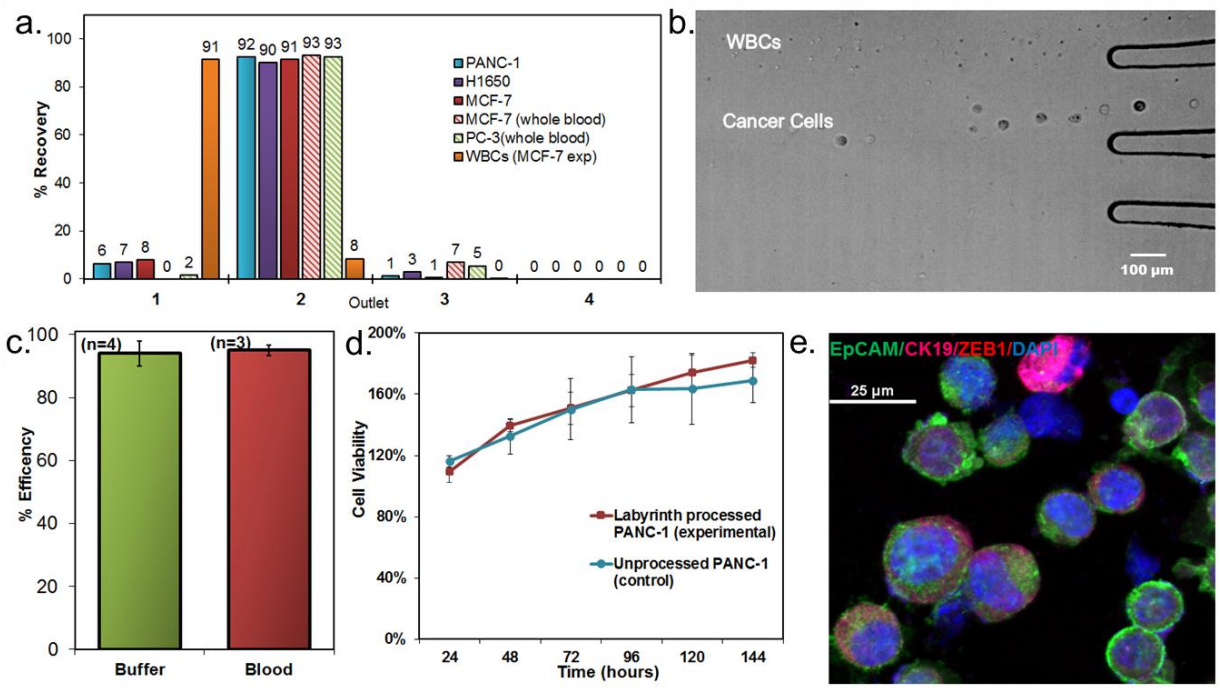

Figure 1.15 Characterization of Labyrinth with cell line experiments.
(A) Recovery results from each outlet of the Labyrinth for four different cancer cell lines: breast (MCF-7), pancreatic (PANC-1), prostate (PC-3) and lung (H1650) cancer along with white blood cells (WBCs). PANC-1 (n=3), H1650 (n=1), and MCF-7 (n=3) were spiked into RBC-removed blood, whereas MCF-7 (n=3) and PC-3 (n=1) were spiked into whole blood (B) High speed camera image showing Labyrinth's ability to separate WBCs from cancer cells through first and second outlet (C) Recovery results from second outlet using 100 MCF-7 cells for both buffer experiments (n=4) and spiked cells in whole blood (n=3) (D) MTT assay results for Labyrinth-processed PANC-1 cells and cultured over a period of 7 days (E) Fluorescence image showing morphology preservation of PANC-1 cells processed at 2.5 mL/min

1.7 Conclusion

CTCs are seeds of metastasis and are the key players in understanding the biological process of metastasis and could serve as potential non-invasive biomarker to evaluate tumor progression and response to treatment. There is a substantial evidence that CTCs released from the primary tumor travel through the blood to distant anatomic sites and contribute to the development of lethal metastases. However the unbiased isolation of CTCs remains challenging due to the rarity and heterogeneity that hinders further studies on these cells. The most commonly used approach

is antibody-based isolation of CTCs against the epithelial cell adhesion molecule (EpCAM). This strategy has been successfully validated for use in prognosis, therapeutic monitoring and molecular diagnosis. However, it is now widely accepted that CTCs can have heterogeneous expression of cell surface markers. In an attempt to move away from affinity based isolation approaches, researchers have turned toward size based technologies, such as filtration, DEP, and hydrodynamic separation. One of the common limitations among these techniques is the limited flow rate or yet to successfully isolate CTCs from clinical specimens.

A high throughput, label-free, and inertial-based Labyrinth device for the size-based separation of CTCs was developed and optimized. The cell separation in Labyrinth is based on the inertial focusing and Dean forces that focus and isolate sized cells into different streamlines. Cell line experiments were performed in order to understand the physics of cells in microfluidic environment, and to optimize the design for a separation of WBCs and CTCs. The finalized design of Labyrinth consists of 11 loops and 56 corners with 4 outlet at the end. The optimized flow condition is at 2.5 mL/min, in which over 95% of cancer cells are recovered and over 98% of WBCs are removed. Compared to other published label-free technologies, Labyrinth offers the highest throughput, equal or higher performance, the capability to preserve cell viability, and the potential for further downstream analysis (Table 1.2).

Table 1.2 Comparison of Labyrinth to published label-free CTC isolation technologies

Technology	Approach	Flow Rate	Recovery Cell Lines	Purity or WBCs/mL	Whole Blood	Live Cells	Genomic Analysis	Biomarker Independent
CTC iChip	Size based separation with negative selection with magnetic beads	160 µL/min	> 95%	>10,000	Y	Y	Y, single cell RNA expression	N
ISET	Size based filtration	NA	One CTC per 1ml of blood	NA	N	N	Y, FISH	Y

Inertial Spiral Devices	Inertial size based separation	500 µL/min	>80%	>10,000	N	Y	N	Y
tilted-angle standing surface acoustic waves	Acoustic waves	20 µL/min	>83% with MCF-7, HeLa, UACC903M-GFP, LNCaP	≈90% removal	N	Y	N	Y
p-MOFF	Hydrodynamic	0.6 mL/min	93.75% with MCF-7 91.60% with MDA-MB-231	NA	N	NA	N	Y
Deterministic lateral displacement (DLD)	Hydrodynamic	200µL/min	99% for MCF-7 80% for MDAMB231	47%	Y	NA	N	Y
Microfluidic Labyrinth	**Inertial microfluidics size based separation**	**2.5 mL/min**	**> 95%**	**98% removal, 600/mL with double devices***	**Y**	**Y**	**Y, single cell RNA expression**	**Y**

CHAPTER 2 Detection of Circulating Tumor Cells from Breast Cancer Patients using Labyrinth

2.1 Abstract

Single-cell technologies are playing an increasing role in profiling CTCs for detection and real time monitoring of cancer metastasis. We previously presented a label-free microfluidic "Labyrinth" device to isolate CTCs taking advantage of inertial forces to focus cells based on their size at a high throughput of 2.5mL/min. The multi-course path enables high recoveries (> 90%) and high purity. We further optimized the protocol of Labyrinth for the isolation of CTCs from metastatic breast cancer patients. Optimized protocol includes the sample pre-processing to stabilize blood samples and to remove RBCs, the sample post-processing to maximize sample purity and recovery, and downstream analysis to characterize CTCs. CTCs were isolated from 56 breast cancer patients (9.1 CTCs/mL, range 2-31/mL) with an 80% sensitivity. We not only detected CTCs typically defined by epithelial markers, but also significant numbers of CTCs (> 50%) lacking epithelial but expressing mesenchymal and stem cell markers.

2.2 Motivation

Various CTC isolation technologies have emerged over the past two decades [15]. The performances of most reported technologies were characterized by the experiments with cultured cancer cells [52]. Typically, cultured cancer cell lines were spiked into buffer or blood and recovered through individual technologies. Recovery and purity as the performance of the technology could then be calculated through the enumeration of recovered cells. However, spiking experiments do not perfectly account for clinical samples. Blood is more viscous compared to buffer, and also exhibits non-Newtonian properties that has effect on fluidic dynamics in microfluidic devices [53]. Blood also contains higher concentration of cell suspension that the effect of particle collisions becomes greater [53]. Moreover, cancer patients' blood have different properties compared to healthy blood, where radiation treatment and chemotherapy may have effect on the production of blood cells and alter the fluid dynamics [54]. Compared to CTCs, cell lines are relatively uniform in both biological and physical properties, including size, phenotype, and selection antigen expression [52]. Therefore, cell line recoveries may not directly translate to performance for highly heterogeneous CTCs from clinical samples.

Affinity-based isolation approaches are widely adopted and validated for the use in prognosis, therapeutic monitoring and molecular diagnosis [17-21]. The performance of CTC-chip was reported to be over 60% recovery against different concentrations of lung cancer cell line NCI-H1650, 50% sample purity, and was tested with 116 patient samples (lung, prostate, pancreatic, breast and colon cancers) ranging 5-1281 CTCs per mL [18]. The Herringbone chip has 92% recovery against prostate cancer cell line PC3, 14% sample purity, and tested with 15 prostate cancer patient samples ranging 0.6-3168 CTCs per mL [19]. The GEDI chip has 85% recovery in blood against prostate cancer cell line LNCaP, 68% sample purity, and tested with 20 prostate cancer patient samples ranging 0-1200 (median = 54) CTCs per mL [25]. The NanoVelcro chip

has over 80% recovery against prostate cancer cell lines LNCaP, PC3, and C4-2, and was tested with 40 prostate cancer patient samples [24]. The Graphene Oxide chip has over 85% recovery with breast cancer cell line MCF7, and was tested with 20 patient samples (breast, pancreatic and lung cancer). Although being widely verified with clinical samples to have high specificity and purity in the isolation, affinity-based technologies are limited by their throughputs and the heterogeneity of CTCs [18, 30, 31]. Most affinity-based approaches have an operating flow rate of 1 to 3 mL hr^{-1}, limiting the blood volume to be processed and the overall CTCs to be recovered. The CTCs undergoing EMT would have reduced expression of epithelial markers, and may be missed by EpCAM targeted approaches [30, 31]. For instance, the CTC gold standard CellSearch™ system has a recovery of 12% against cell line with low EpCAM expression level (MDA-MB-231), 44% against cell line with moderate EpCAM expression level (BT20), and over 75% against cell lines with high EpCAM expression level (T47D and SKBR3) [55].

Label-free isolation technologies utilize the physical properties to separate CTCs in a relatively unbiased manner and have the potential of higher performance. One of the first label-free methods tested with clinical samples was reported by Lin et al. in 2010 [56]. The filter-based biochip has 80% recovery among different cell lines (AGS, N87, HepG2, Huh7, CAL27, and FADU), 89% mean purity, and was tested with 5 metastatic lung cancer patient samples [56]. The inertial-based Vortex chip was published in 2013, which has 15.9% to 18.2% recovery among different cell lines, 57%-94% sample purity, and was tested with 12 patient samples (breast and lung cancer) [53]. The Dean flow fractionation-based spiral devices, or later introduced slanted and multiplexed spiral devices, were published since 2013 with over 80% recover, 4 log depletion of WBCs, and were tested with at least 10 patient samples individually [48, 57, 58]. Despite being unbiased compared to affinity-based technologies in terms of CTC selection, label-free isolation

approaches suffer from various limitations. Filtration approaches generally have low capacity of sample volume resulted from cell clogging on membrane [39]. DEP methods are limited by the low throughput (<1mL hr^{-1}) [35]. Hydrodynamic based approaches typically compromise for either low CTC recovery or low blood cell removal as the smaller cells are not efficiently focused [46].

In the exploration for a label-free platform that ensures high throughput of sample processing, high purity of CTC for downstream analysis, and high specificity and sensitivity in clinical samples, we developed and optimized the protocol to apply Labyrinth device in clinical samples. Labyrinth has a throughput of 2.5mL hr^{-1}, the highest among current label-free approaches, and is capable of processing 5-20 mL of blood samples within 2 hours with the developed protocol. The sample purity was improved through the application of double device in series to achieve over 4 log depletion of WBCs. The protocol was successfully applied in over 56 metastatic breast cancer patient samples to isolate both epithelial and EMT like CTCs to demonstrate the potential of label-free isolation.

2.3 Methods

2.3.1 Blood Samples from Human Subjects

All human subjects in this study were consented by the study team or research nurse prior to the scheduled blood draw using standard procedures for clinical research employed in the University of Michigan Comprehensive Cancer Center (UMCCC). Whole blood sample as control group was obtained from volunteer healthy people as part of an Institutional Review Board approved protocol (HUM00070190). Whole blood from patients with pancreatic cancer was obtained as part of an Institutional Review Board approved protocol (HUM00025339). Whole

blood from patients with metastatic breast cancer was obtained as part of an Institutional Review Board approved protocol (HUM00070190). All participants were over 18 years of age.

To optimize the preservation of blood in terms of cell viability, cell morphology, and RNA integrity, three different vacutainer blood collection tubes along with various storage conditions were tested. EDTA (Ethylenediaminetetraacetic acid) or so called lavender top tubes (Invitrogen - LifeTechnologies, Inc.) are the most widely used in blood collection as EDTA is a strong anticoagulant for whole blood preservation. Other commercial available tubes such as AdnaGen RNA preservation tubes (Qiagen) or Cell-Free RNA Blood Collection Tube (Streck, Inc.) were also tested. Blood was drawn into the collection tubes and stored at room temperature or on ice.

2.3.2 Patient Sample Processing using Labyrinth

Labyrinth was pre-flowed with 1% Pluronic acid solution to prevent cell clotting on channel walls. Blood samples from metastatic breast cancer patients were collected in EDTA tubes and processed through the Labyrinth within 4 hours of collection. RBCs in blood samples were removed using density separation with dextran solution (6 m/v% dextran and 0.87 m/v% sodium chloride in DNase/RNase-Free Distilled Water) prior to the Labyrinth process. The blood sample with dextran solution was kept still in room temperature for 45 minutes to bring down the RBCs driven by density difference. The supernatant, which includes everything in whole blood except RBCs, was carefully taken out using pipettes, and was diluted with PBS. Blood samples were then processed through the device at a flow rate of 2.5mL/min using motorized syringe pump.

2.3.3 Immunostaining Protocol of Cytoslides

The Labyrinth output from outlet 2 were cytospun onto poly-lysine coated slides. Samples were permeabilized by applying 0.05% Triton X-100 (PBST) solution for 15 minutes. Slides were

then blocked using 20% donkey serum for 30 minutes at room temperature (RT). A cocktail of primary antibodies were added and left in a humidified chamber overnight. The next day, cytoslides were washed thrice with 0.05% PBST for 5 minutes. Samples were incubated in the dark with secondary antibodies for 45 minutes at RT. Finally, samples were washed thrice with 0.05% PBST for 5 minutes and mounted with Prolong Gold Antifade Mountant with DAPI.

2.3.4 CTC Identification from Cytoslides

The immunofluorescent stained slides were auto-scanned under a Nikon TI fluorescent microscope at 10X magnification for initial assessment. A typical WBC from the slide was selected as reference for its CD45 and CK fluorescent intensity levels. A cell was identified as a WBC if it had similar CD45 and CK expression compared to the reference cell. A cell was identified as a CTC if it had at least 50% lower CD45 and 50% higher CK expression compared to the reference cell. Cells with both significant CD45 and CK expression with respect to the reference cell would be considered as double positive cells. DAPI positive cell but lower expression of CD45 and CK when compared to the reference cell were considered to be double negative cells. A scatter plot of typical CK and CD45 fluorescent intensity levels for CTC identification from patient samples is presented in Figure 2.1. The potential CTCs (pan-CK+/DAPI+/CD45-) were re-imaged at 40X resolution to further confirm their morphology and fluorescent signals.

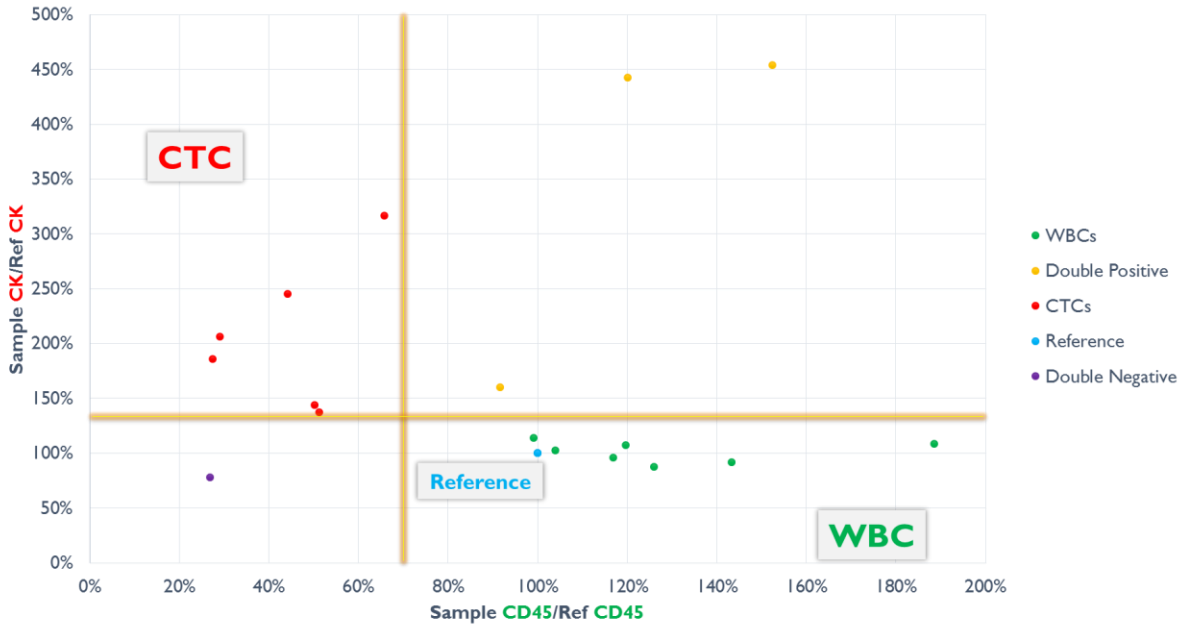

Figure 2.1 Scatter plot of CK and CD45 fluorescent intensity levels from patient samples for CTC identification.
The upper left quarter contains CTCs and the lower right quarter contains the WBCs. After a patient sample was processed through Labyrinth and fluorescently stained with DAPI, CD45, and CK, a typical WBC from the slide was selected as reference for its CD45 and CK fluorescent intensity levels. A cell could be identified as a WBC by having similar CD45 and CK expressions comparing to the reference cell. A cell could be identified as a CTC by having at least 50% lower CD45 and 50% higher CK expressions comparing to the reference cell. Cells with both CD45 and CK significant expressions with respect to the reference cell would be considered as double positive cells. Cells with DAPI positive but much lower expressions in CD45 and CK when compared to the reference cell would be considered as double negative cells.

2.4 Results

2.4.1 Pre-processing of Blood Samples

Previous data showed that Labyrinth is capable of processing diluted blood samples with a high performance comparable to RBC removed samples. However, in order to simplify the quantification of separated CTCs from patient samples and to enable downstream analysis on these cells without the RBC interference, multiple approaches were applied and optimized to remove RBCs prior to the sample processing in Labyrinth.

The most common approach for RBC removal is through RBC lysis buffer. Blood samples were treated with RBC lysis buffer (Qiagen) at a 2:1 ratio (buffer to sample) and incubated on ice for 3 minutes. Samples were then spun down and the pellet was resuspended in PBS. Although the minimal incubation time and moderate temperature for cell preservation were applied in this approach, loss and damage on targeted cell were still observed through the lysis process.

Density separation is another alternative for RBC removal as RBCs are much denser than the rest of blood components. Ficoll density gradient centrifugation is widely adopted in CTC isolation technologies as an approach of sample pre-processing [28, 59]. Briefly, blood sample incubated with Ficoll reagent was centrifuged to create a buffy coat which contains all nucleated cells. The buffy coat was then carefully removed through pipetting to recover the nucleated cells. Major drawback of Ficoll centrifugation is the cell loss ranging from 20-33% due to the centrifuge and pipetting process [60-62].

Here we applied a similar concept of density separation but different reagent called Dextran (Spectrum) to minimize the cell loss. The blood sample with dextran solution (6 m/v% dextran and 0.87 m/v% sodium chloride in DNase/RNase-Free Distilled Water) was kept still in room temperature for 45 minutes to bring down the RBCs driven by gravity. The supernatant, which includes everything in whole blood except RBCs, was carefully taken out using pipettes. Compared to Ficoll density gradient centrifugation, the approach using Dextran has the advantage of excluding centrifugation process, and the easiness of recovering cells from supernatant instead from the thin buffy coat. The optimized Dextran process was applied in this study when the blood samples were processed to ultimately undergo downstream analysis such as immunostaining and single cell analysis.

Multiple blood collection tubes and storage conditions were tested in an attempt to better preserve the cell integrity and to facilitate the overall sample processing. The blood samples in different tubes (EDTA, AdnaGen RNA preservation tubes, and Streck Cell-Free RNA Blood Collection Tubes) were treated with RBC removal processes (RBC lysis or Dextran density separation). We observed the damage in cell morphologies during the RBC lysis process not only in EDTA tubes, but also in the RNA preservation tubes that were claimed to keep the cell integrity. When Dextran was applied in the blood contained in the three different tubes, we found that the EDTA tubes have highest performance in terms of RBC density separation. It was also observed that RNA expression was better preserved or less altered when the sample was kept in 4ºC compared to room temperature. In summary, blood samples were collected in EDTA tubes and stored on ice, and were treated with Dextran for RBC removal.

2.4.2 Post-processing after Single Labyrinth

High efficiency was observed in Labyrinth such that 95% of spiked cancer cells are recovered and about 2 log depletion of WBC contamination through a single Labyrinth process. However, the number of remaining WBCs in the collected product from Labyrinth was still much higher than the number of cancer cells, resulting in a rather low CTC purity. In general, several million WBCs were found in 1 mL of whole blood, while only tens of CTCs may appear in each milliliter of blood. The amount of WBCs could still be in the order of tens of thousands after single Labyrinth process, and the low concentration of CTCs could hinder further study on the targeted cells. Several approaches for post-processing after single Labyrinth were developed to further purify the isolated CTCs.

Affinity-based capture could not only be applied in CTC capture, but also in the depletion of WBC contamination. The CTC-chip is the first immuno-capture microfluidic technology for the

isolation of CTCs [18]. The PDMS-based device consists of thousands of microposts coated with antibodies against EpCAM, which allows the capturing of CTCs expressing the antigen using a one step process. By replacing EpCAM with WBC-specific antibodies, CTC-chip can be used as "WBC-chip" to capture WBCs (Figure 2.2) while CTCs can freely flow through the microposts in device. A cocktail of antibodies was chosen including CD45, CD11b, and CD15. CD45 is a receptor-linked protein tyrosine phosphatase expressed on the surface of most leukocytes. CD11b is an integrin family member that expressed on the surface of monocytes, neutrophils, natural killer cells, granulocytes and macrophages. CD15 is a cluster of differentiation antigen that can be found on neutrophils. The cocktail of antibodies is capable of binding most WBCs. The "WBC-chip" was tested through the experiments with blood samples to optimize the antibody concentration, cocktail combination, and sample flow rate. It was observed that, with the WBC-chip process after single Labyrinth, the WBC contamination could be further reduced by 2 log to an order of hundreds WBC per mL of blood.

Figure 2.2 DAPI labeled WBCs captured in WBC-chip.

Although being efficient in WBC capture, WBC-chip suffered from a few limitations. Throughput is a major concern with antibody-based technologies due to the limited shear conditions under which affinity binding occurs. WBC-chip operated at a flow rate of 1 mL hr^{-1}, adding an hour of processing time on top of single Labyrinth and diminishing the goal of high throughput CTC isolation. Another drawback is the non-specific capture of CTCs due to the size difference of cells. CTCs are in general larger in size compared to WBCs, and could be physically trapped in between the gap of two microposts.

An immune-magnetic technology termed magnetic sorter was applied to overcome the limitations of WBC-chip (Figure 2.3). Magnetic sorter applies antibody-coated magnetic beads to bind the targeted cells. The cells/magnetic beads duplet are then attracted by magnetic fields generated on one side of the microfluidic channel to separate targeted cells from unbounded cells.

In this study, the magnetic beads were coated with CD45 antibody to bind WBCs, and the bounded WBCs were then separated into side channel apart from the main stream consisting CTCs. A similar WBC removal efficiency compared to WBC chip was observed, while much fewer CTCs were lost during the process. However, the application of magnetic sorter was still limited by its low throughput. Another concern is the excess beads residue which could interfere with downstream analysis.

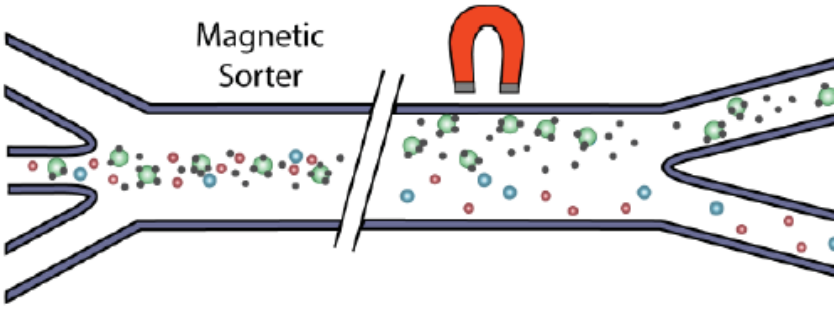

Figure 2.3 Illustration of the magnetic sorter for the depletion of WBCs.

A second Labyrinth was proposed as a simple yet efficient approach for further purification of CTCs. Processing of samples through a single Labyrinth even at a flow rate of 2.5 mL/min, which is considerably greater than the currently available label-free techniques, yielded comparable or better purity (13800 WBCs/mL average, n=9, compared to 32,000 WBCs/mL reported[63]). We adopted the strategy of using a double Labyrinth (LL), where two single Labyrinth devices were applied in series. This system furthers reduce the WBC contamination yet maintains equivalent CTC viability. As shown in Figure 2.4A-B, the recovery of MCF-7 cells using a double Labyrinth (91.1 ± 0.7%) was consistent with the results obtained using a single Labyrinth (91.5 ± 0.9%), but with lower WBC contamination (663 ± 647 WBCs/mL), representing a two-log improvement in tumor cell enrichment over the single Labyrinth. This mode of operation

yields higher purity than reported using other label-free methods[46, 63-72]. It is to be noted that the additional run through the Labyrinth adds less than 5 minutes to the total time versus a single run.

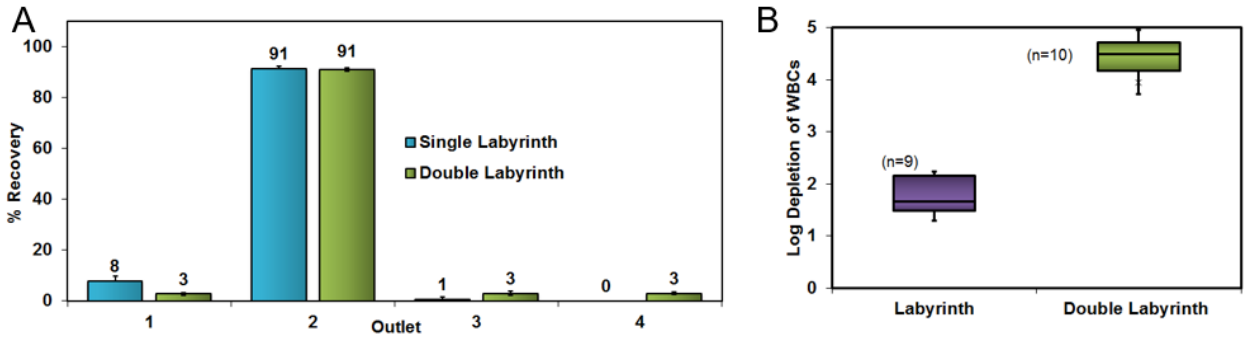

Figure 2.4 Comparison of performance using a single or double Labyrinth.
(A) Comparison of cancer cell recovery using a single or double Labyrinth for each outlet. Error bars represent the standard deviation of three replicates. (B) Log depletion of WBCs using the single (n=9) and double Labyrinth (n=10) to demonstrate high device purity.

2.4.3 Isolation of CTCs from Metastatic Breast Patient Samples

A total of 56 blood samples obtained from patients with metastatic breast cancer were processed through the Labyrinth to isolate CTCs. Of these, 9 samples were processed using a single labyrinth approach. As shown in Figure 2.5A, the average number of CTCs recovered from the breast cancer patients was 9.1 CTCs/mL (range 3-31). Since the objective was to obtain a high purity CTCs population for downstream analysis, we processed the rest of the samples using the strategy of double labyrinth (LL). In the 40 patient samples processed using the double Labyrinth strategy, the recovery of CTCs was 5.4 ± 4.6 CTCs/mL (range 0-21.7, Figure 2.5B). Figure 2.5C presents the number of WBCs in the enriched CTC population (663 ± 647 WBCs/mL, range 0-2900), which is by far the best purity reported among label-free methods. CTCs were identified as DAPI-positive nucleated cells that stained positive for pan-CK and negative for CD45. Figure 2.5D illustrates typical CTCs recovered from the double labyrinth (B41), including multi-nucleated CTC (B29), and clusters of CTCs (B45, B37, and B46). Since the clusters are of larger

size, they preferably migrate to the second outlet, which is the target collection outlet for CTCs.

Figure 2.6 shows more typical CTCs isolated from breast patient samples.

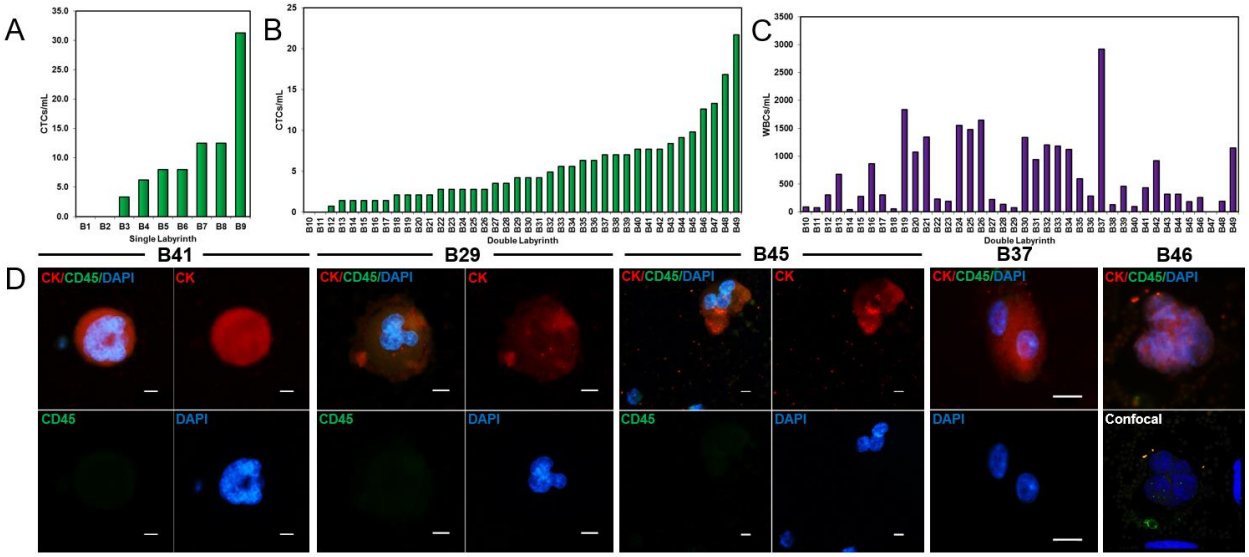

Figure 2.5 Results of breast cancer patient samples using Labyrinth.
(A) CTCs (CK+, CD45-, DAPI+) per mL for each patient sample processed with single Labyrinth. (B) CTCs per mL for each patient sample processed with double Labyrinth. (C) WBCs per mL for each patient sample processed with double Labyrinth. (D) Fluorescence microscopy images demonstrating typical, multi-nuclei, and clusters of CTCs separated by Labyrinth. Cells are stained with DAPI (blue), cytokeratin (red) and CD45 (green). Scale bar 10 μm.

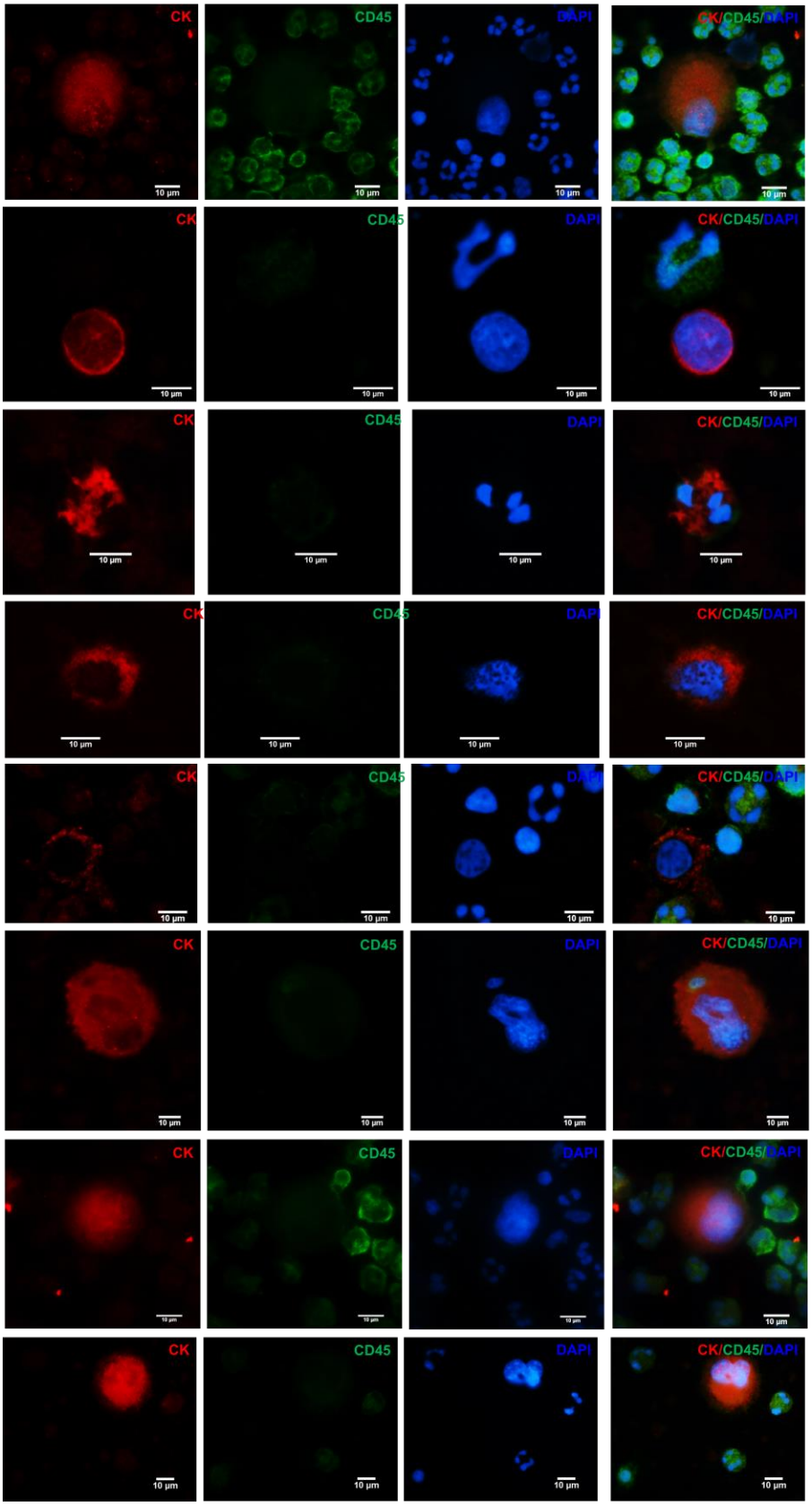

Figure 2.6 Gallery of CTCs recovered from breast cancer patients.

In three patients, we did side by side comparison of single and double labyrinth analysis and found that although the CTCs yields were comparable (Figure 2.7), the double Labyrinth processing reduced WBC contamination by two orders of magnitude more than the single Labyrinth.

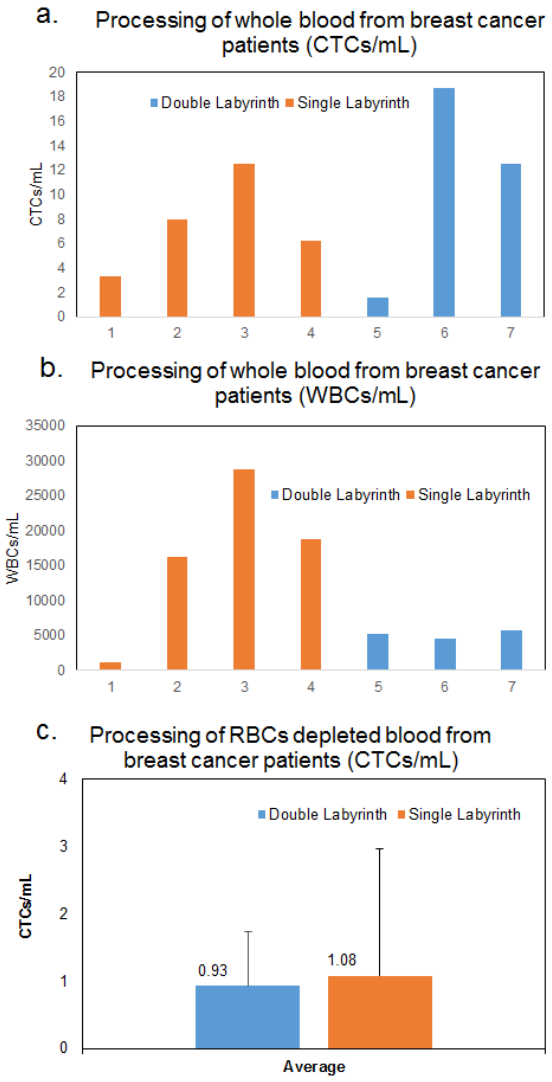

Figure 2.7 Comparison of single and double Labyrinth in metastatic breast patient samples. (A) CTCs/mL of blood recovered from seven breast cancer patients using whole blood with single and double Labyrinth. (B) WBC/mL of blood remained after processing whole blood (without any RBC removal/pre-processing) from seven breast cancer patients using both single and double Labyrinth. (C) Single vs Double Labyrinth CTC counts (per mL of whole blood) in breast cancer patients using pretreated blood for RBC removal.

Additionally, enriched CTCs from the Labyrinth were stained using antibodies against the epithelial marker EpCAM and the circulating stem cells (CSC) and EMT marker CD44. The results are presented in Figure 2.8A-B. In all 7 of the patients that were analyzed, we found CTCs that did not express EpCAM (Figure 2.8A). These cells would not have been identified as CTCs in EpCAM based affinity based capture techniques. Indeed, 52.3% ± 19.5% of the CK+ CTCs were EpCAM- and 47.7% ± 19.5% were EpCAM+. None of the isolated cells was observed to be EpCAM+/CK- . For the same 7 patients, we found CTCs that express CD44 in all of the patients (Figure 2.8B). Among these samples, 41.7% ± 14.1% of the CTCs were CD44+ and 58.3% ± 14.1% were CD44- . Cells expressing CD44+/CK- were only observed in two of the patients. Hence, the Labyrinth is capable of both isolating heterogeneous single CTCs and clusters of CTCs.

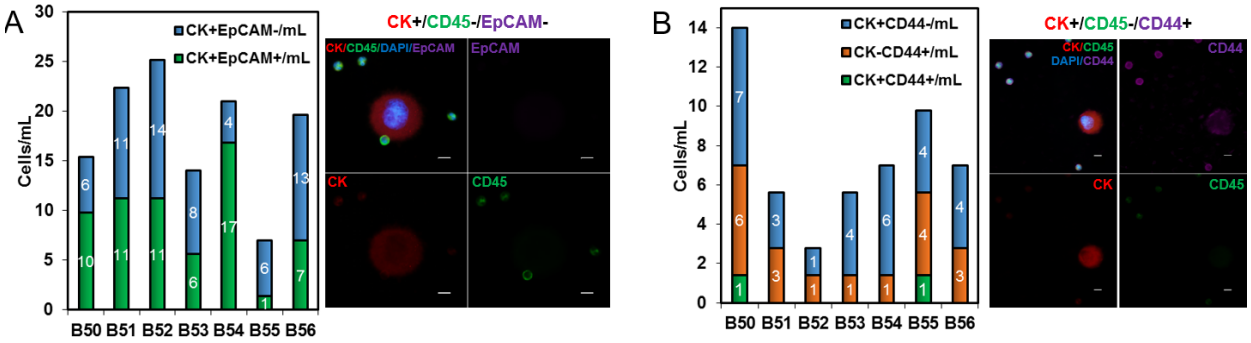

Figure 2.8 Immunostaining and quantification of enriched CTCs with epithelial marker EpCAM and the CSC and EMT marker CD44
(A) Representative images of CTCs with or without the expression of cytokeratin and EpCAM. (B) Number of CTCs with or without the expression of cytokeratin and CD44. Scale bar 10 µm.

2.5 Conclusion

The performances of most CTC isolation technologies were characterized through spiking experiments with cultured cancer cells. However, results from spiking experiments may not directly translate to the performance in clinical samples. Affinity-based isolation approaches were widely validated in clinical samples for the use in prognosis, therapeutic monitoring and molecular

diagnosis. However, these approaches have their shortcomings including their throughputs and the incapability of capturing heterogeneous population of CTCs. Since 2010, various label-free isolation technologies have been developed and tested in clinical trials. Nevertheless, each individual method has to compromise for either low throughput, low efficiency, or overall low performance.

The high throughput, label-free, and inertial-based Labyrinth device for the size-based separation of CTCs was optimized and applied in metastatic breast cancer patient samples. The blood samples were collected in EDTA tubes and stored on ice to be processed within 4 hours from blood drawn to ensure the preservation of cell integrity, cell viability, and RNA stabilization. The optimized protocol involves a sample pre-processing step using Dextran to remove the majority of RBCs, and the application of double Labyrinth in series that were operated at 2.5 mL min^{-1}. The total processing time was less than 90 minutes. The isolated CTCs from Labyrinth were then cytospun onto slides followed by the standard immunostaining process. A strict criteria to identify CTCs from contamination blood cells was adopted in the characterization and quantification of CTCs using fluorescent microscopy.

The isolation results of CTCs from 56 metastatic breast cancer patient samples demonstrate the sensitivity and specificity of the Labyrinth platform. CTCs were found in 93% of the patient samples (52/56), with a low contamination of WBCs (663 ± 647 WBCs/mL). CTCs with different morphologies were also observed in the isolated samples, including typical single cells, multinucleated cells, and cluster of cells. Moreover, the immunostaining and quantification of enriched CTCs with epithelial marker EpCAM and the CSC and EMT marker CD44 further confirmed Labyrinth's capability of isolating the heterogeneous populations of CTCs that could have been missed by affinity based approaches.

CHAPTER 3 Characterization of Circulating Cancer Stem Cells in Breast Cancer Patients at Single Cell Level

3.1 Abstract

The molecular and genetic profiling of CTCs presents a possible alternative to painful, costly, and invasive biopsies. To take advantage of the single cell profiling techniques in order to probe the heterogeneity of CTCs, we developed a completely label-free and surface expression independent platform combining the previously introduced Labyrinth device and the commercially available C1™ system which prepares CTCs in single cell level for further analysis. Multiplex gene expression analysis of seventy single cells recovered from patients identified different subpopulations of CTCs. Both inter- and intra-patient molecular heterogeneity at the single cell level were observed with cells expressing genes uniquely related to epithelial, MET, and EMT phenotypes. The Labyrinth platform allows a thorough molecular understanding of the heterogeneity among CTCs. This platform also shows CTCs potential as a biomarker to non-invasively evaluate tumor progression and response to treatment in cancer patients.

3.2 Motivation

CTC enumeration is a powerful tool in early screening, disease progression and treatment monitoring, and cancer relapse indication [73]. Sometime assessed as “liquid biopsy” in contrast to traditional biopsy, CTCs have more potential in providing clinical and therapeutic information when combining with downstream analysis [74]. In fact, studies have suggested that CTC enumeration alone is insufficient for the guidance of therapeutic decisions [75]. Analysis of CTCs at molecular level could be performed to determine the alteration of targeted therapy [76]. For instance, genetic mutations such as KRAS, EGFR, HER2, and estrogen receptor (ER) genes can be identified through the screening of CTCs [77]. The differences between individual CTCs and the primary tumor may bring new insights through the comparison of CTC genomes with the primary and metastatic tumors [73]. *Ex vivo* culture of patient-derived CTCs can be adopted in the test of drug efficacy [78] and enable multiplexed proteomic analysis of CTCs [79]. mRNA profiling or sequencing on CTCs offers the advantage of multiple transcripts of a single gene to assist in overcoming copy limitations associated with genomic DNA, and can provide extensive information to identify signaling pathways and splice variants relevant to metastatic potential and therapy resistance [80].

The molecular and genetic profiling of CTCs presents a possible alternative to painful, costly, and invasive biopsies. Single cell applications have been particularly important for analyzing the genomic, transcriptomic, proteomic, and metabolomic profiles of individual CTCs, the signatures of which may be masked by other blood cells present in far greater numbers that are often captured together with CTCs [81]. Multiple novel single-cell techniques have emerged in recent years, making the genome, transcriptome, and proteome of single cells accessible for detailed analyses. Such analyses would greatly contribute to an improvement of our fundamental understanding of both cancer biology and drug therapeutics, and most probably reveal multiple

novel insights into the metastatic process [82]. One of the strengths of single-cell technologies lies in their ability to analyze rare cell events. For example, for patients with cancer, single-cell technologies are playing an increasing role in the detection of minimal residual disease or in the analysis of circulating tumor cells in the peripheral blood [83]. Dawson et al. [84] compared CTCs and primary tumor DNA from breast cancer patients by Next-Gen sequencing and suggested that CTCs are more informative for detecting secondary mutations than primary tumors. Yu et al. [85] used single cell RNA sequencing of CTCs from pancreatic cancer mouse models and identified the role of WNT signaling pathways in pancreatic cancer. As more studies are expected to come in the near future, single cell CTCs profiling could provide distinct drivers for the detection of cancer metastasis.

Several studies have enabled the single cell mRNA profiling of CTCs in the past few years. Peeters introduced the combination of commercially available platforms CellSearch™ to isolate CTCs through EpCAM-labeled magnetic beads, and DEPArray system to molecularly characterize the CTCs through manipulating the cells with "electric cages" created by microelectrodes [86]. Ting et al. applied ^{neg}CTC-iChip to purify CTCs from pancreatic cancer patients using inertial- and magnetic-based microfluidic approaches, and manipulated individual cells identified with $CD45^{-}$ with micro transfer tips to prepare the sample for single cell RNA amplification and sequencing [87]. Schneck et al. reported an enrichment strategy combining different antibodies specific for surface proteins and extracellular matrix (ECM) components to capture $EpCAM^{neg}$ CTCs from blood samples of breast cancer patients, and micromanipulated cells through CellCelector (CC) to perform single cell genomic hybridization on micro array [88]. However, none of the published approaches are truly label-free for a completely unbiased single cell analysis. Up to date, all the single cell CTC studies either apply affinity based isolation technique to ensure a pure population

of CTCs, or manipulate the isolated CTCs using antibody-based labels to identify the cells among background contamination of blood components. Given the heterogeneous nature of CTCs, it is important to develop a label-free platform for the unbiased study (without either positive or negative selection) of CTCs at single cell level.

In an attempt to take advantage of the single cell profiling techniques in order to probe the heterogeneity of CTCs, we developed a completely label-free and surface expression independent platform combining the previously introduced Labyrinth device and the commercially available C1™ system (Fluidigm). CTC samples are purified through the Labyrinth devices, and isolated into individual chambers for the mRNA expression analysis. To our knowledge, this is the first high throughput inertial microfluidics based platform that enables the truly unbiased study of CTCs at single cell level. The Labyrinth platform can facilitate a thorough molecular understanding of CTCs and their subpopulations, having a direct impact upon patient care for early detection, monitoring treatment response, and developing personalized therapy.

3.3 Methods

3.3.1 Blood Samples from Human Subjects

All human subjects in this study were consented by the study team or research nurse prior to the scheduled blood draw using standard procedures for clinical research employed in the University of Michigan Comprehensive Cancer Center (UMCCC). Whole blood sample as control group was obtained from volunteer healthy people as part of an Institutional Review Board approved protocol (HUM00070190). Whole blood from patients with pancreatic cancer was obtained as part of an Institutional Review Board approved protocol (HUM00025339). Whole

blood from patients with metastatic breast cancer was obtained as part of an Institutional Review Board approved protocol (HUM00070190). All participants were over 18 years of age.

3.3.2 Patient Sample Processing using Labyrinth

Labyrinth was pre-flowed with 1% Pluronic acid solution to prevent cell clotting on channel walls. Blood samples from metastatic breast cancer patients were collected in EDTA tubes and stored on ice. Samples were processed through the Labyrinth within 4 hours of collection. RBCs in blood samples were removed using density separation with dextran solution (6 m/v% dextran and 0.87 m/v% sodium chloride in DNase/RNase-Free Distilled Water) prior to the Labyrinth process to prevent RBC interference with single cell analysis. The blood sample, typically from 5 mL of whole blood, with dextran solution was kept still in room temperature for 45 minutes to bring down the RBCs driven by density difference. The supernatant, which includes everything in whole blood except RBCs, was carefully taken out using pipettes, and was diluted to 25 mL with PBS. Blood samples were then processed through the device at a flow rate of 2.5mL/min using motorized syringe pump. The product from second outlet was collected and processed through second Labyrinth to achieve a higher purity. The final product after double Labyrinth devices was at an average volume of 1.4 mL, and was centrifuged to 10 µL for the single cell process using C1 (Fluidigm).

3.3.3 Single Cell Multiplex Gene Expression Analysis

Cells isolated using the double Labyrinth were mixed with suspension reagent and loaded onto a C1 chip (10-17 µm) to isolate up to 96 single cells using the C1 machine (Fluidigm, USA). The loading efficiency of C1 chip for a sample containing about 1500 cells/3uL is >90%. Captured cells within the 96 chambers of the C1 chip were examined under the microscope (IX-83 Olympus,

Japan) to differentiate chambers containing single cells from those with multiple cells or no cells. A typical patient sample loading onto C1 yields CTCs ranging 1-16, 10-40 WBCs and some RBCs. Then, lysis, RT and preAmplification reagents (Fluidigm and Ambion, USA) along with the pooled 96 selected TaqMan assays (Table 3.1, Life Technologies, USA) were added to the corresponding wells in the chip to generate preAmplified cDNAs for the 96 target genes for each single cell using the Fluidigm's STA protocol in C1 instrument. Single cell cDNA products were then subjected to qPCR using the 96 selected TaqMan assays (Life Technologies, USA), 96x96 chips, and BioMark HD instrument (Fluidigm, USA). Results were analyzed by SINGuLAR and R script software and presented as Log2Exp in HeatMap and PCA plots. The representative images of single breast cancer cells isolated within the C1 chip are presented in Figure 3.1, where fluorescent labeled cancer cells are captured in the chip. It is to be noted that cells of different sizes and morphology can be loaded on the same chip.

Table 3.1 List of 96 genes studied in single CTCs

GAPDH	**CD24**	**KRT5**	**CDH3**	**CTNNB1**	**IL6**
HPRT1	**CD44**	**KRT7**	**TGFb1**	**WNT2**	**IL6R**
RAB7A	**ALDH1a1**	**KRT8**	**TGFbR1**	**Twist1**	**gp130**
EpCAM	**ALDH1a3**	**AR**	**p53**	**SNAI1**	**IL8**
Vimentin	**CD133**	**KRT18**	**PTEN**	**SLUG**	**CXCR1**
HER2	**CCND1**	**KRT19**	**PI3K**	**ZEB1**	**CXCR4**
EGFR	**ANXA3**	**CDH1**	**AKT1**	**ZEB2**	**MTOR**
GSK3B	**GATA3**	**CDH2**	**AKT3**	**EZH2**	**NFKB1**
ESR1	**ABCG2**	**ID1**	**NOTCH1**	**MCL1**	**MKI67**
PGR	**ABCB1**	**ID2**	**NOTCH2**	**BAX**	**PCNA**
TAZ	**NESTIN**	**MET**	**NOTCH3**	**BCL2**	**CD3D**

YAP1	**LIN28A**	**BRCA1**	**NUMB**	**TSPAN6**	**CD11B**
SOX2	**ITGB3**	**MUC1**	**HES1**	**TM4SF1**	**CD14**
UXT	**ITGA6**	**STAP2**	**HEY2**	**TMEM57**	**CD20**
SOCS3	**FBXW7**	**AMOTL2**	**DLL1**	**NANOG**	**CD45**
p63	**MMP9**	**TNKS1BP1**	**JAG2**	**O ct4**	**CD146**

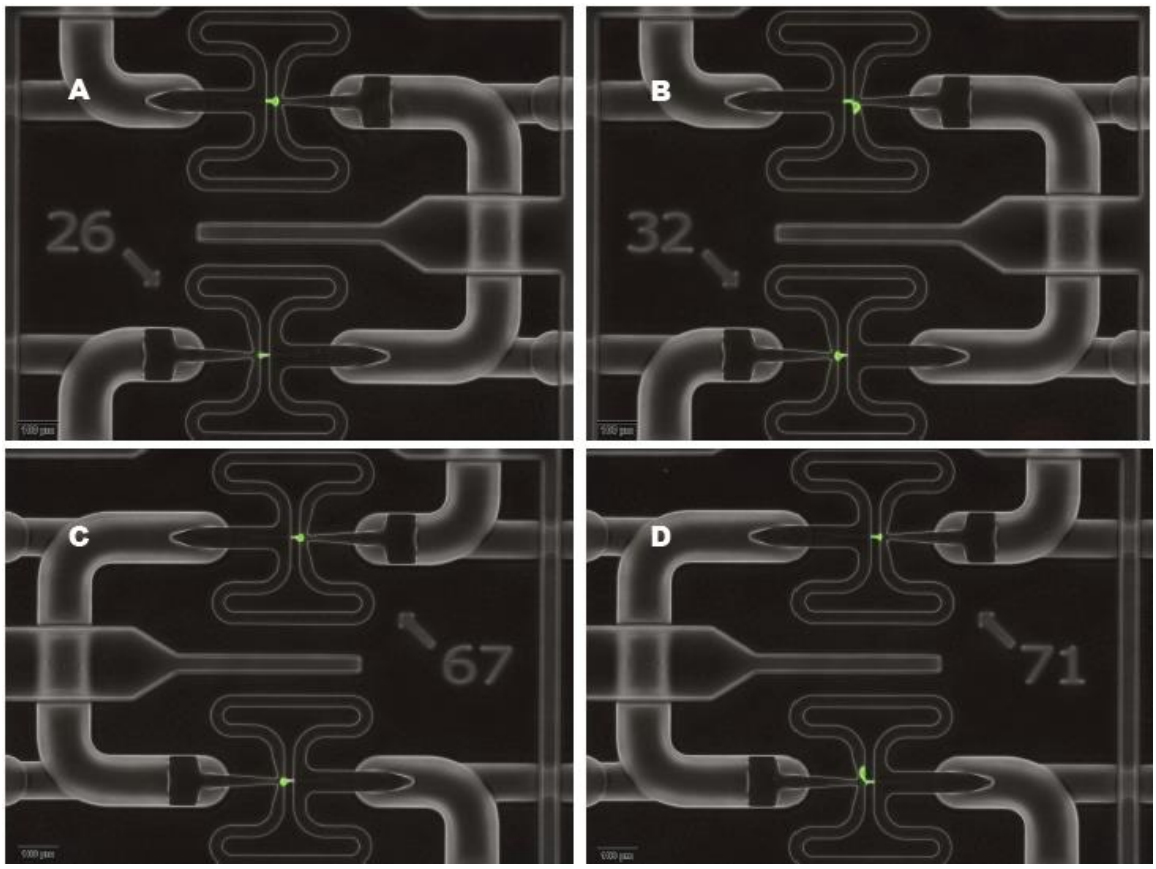

Figure 3.1 Representative images of single breast cancer cells isolated within the C1 chip.

3.4 Results

3.4.1 Validation of the established protocol

In control experiments with technical and biological replicates using T47D breast cancer cell line, the expression profiles variation was found to be minimal. Figure 3.2 demonstrates the

single cell gene expression from three replicates clustered together indicating that the variation of profiles among single cells using our protocol is reliable and reproducible.

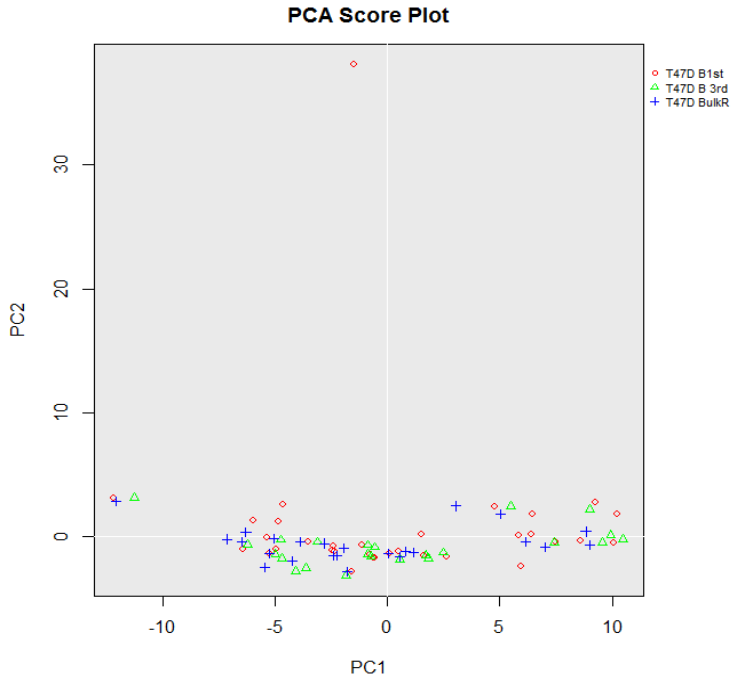

Figure 3.2 Principal component analysis (PCA) plot showing log2 gene expression data of single cells from T47D breast cancer cell line.
T47D B1st (Red) and T47D BulkR (Blue) are the same single cells isolated by C1 and analyzed by BioMark HD in 2 separate RT-qPCR experiments as technical replicates. T47D B3rd (Green) and T47D B1st (Red) are biological replicates of 2 independent C1/BioMark HD experiments.

In order to validate the RNA integrity in the analyzed CTCs, we included the apoptotic related genes in the 96 gene panel to confirm that the CTCs were not apoptotic in circulation and the RNA from these cells were not degraded. As shown in Figure 3.3, most of the cells showed no expression of pro-apoptotic marker BAX. The two cells that showed BAX expression also showed strong anti-apoptotic marker MCL1 expression with the ratio favoring MCL1, indicating the overall cell survival. In addition, as part of the protocol we routinely examined all single cells captured within the C1 chip under the microscope (representative images provided in Figure 3.1), where only intact and viable cells would be processed in the single cell analysis.

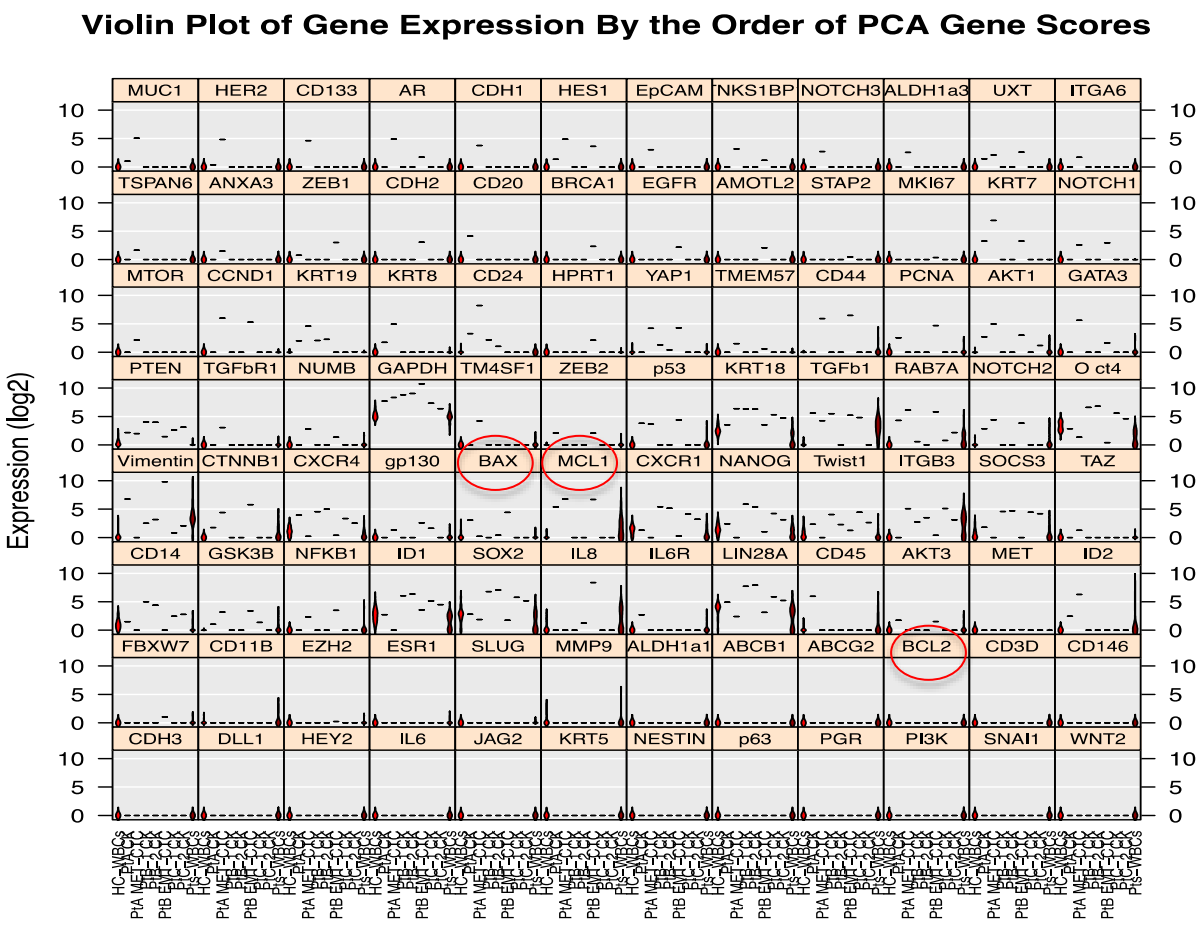

Figure 3.3 Violin plot of the gene expression of CTC samples.
Red circles highlight the pro-apoptotic gene BAX, and anti-apoptotic genes MCL1 and BCL2.

A comparison of single cell against bulk gene expression was performed using SUM149 breast cancer cell line to verify the accuracy of the established protocol. As depicted in Figure 3.4, the gene expression from single cell had similar profile to the one from bulk cells, indicating that the single cells did represent the bulk as expected in the case of cell line. The unbiased clustering of these two groups of cells further confirmed the observation (Figure 3.5).

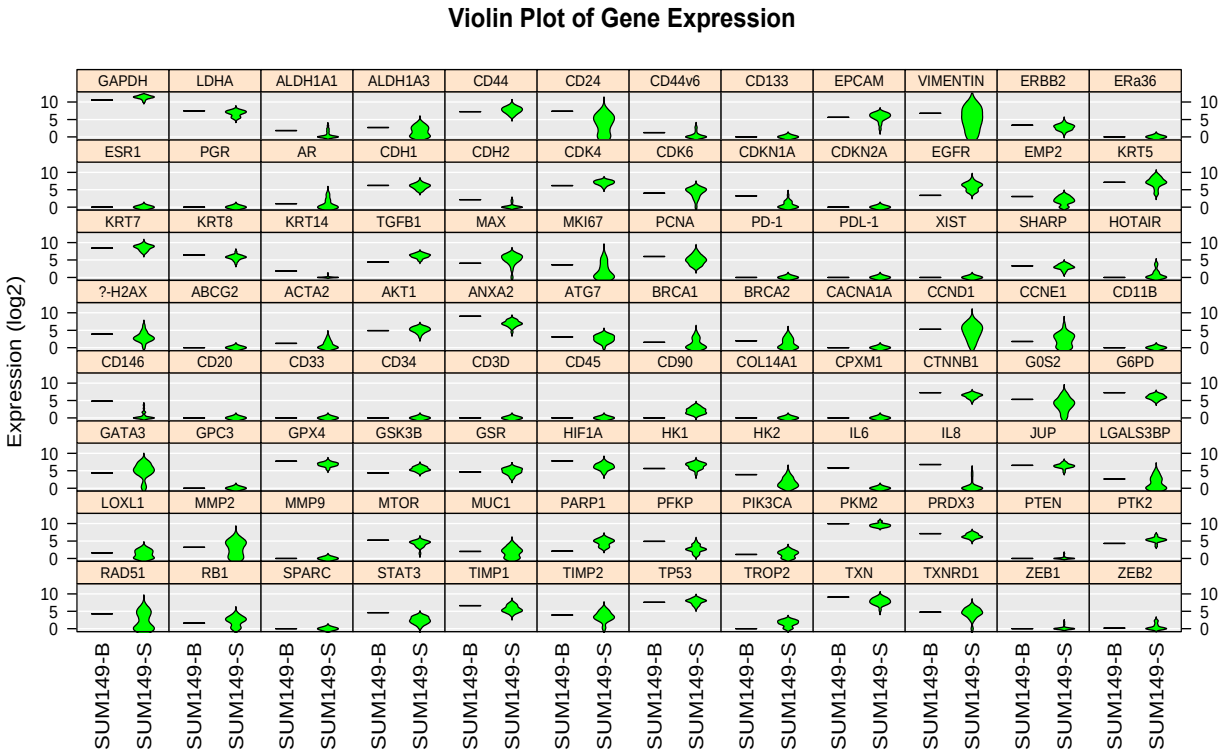

Figure 3.4 Comparison of gene expression profiles for bulk cells and individual single cells (n=23) from a breast cancer cell line (SUM149).

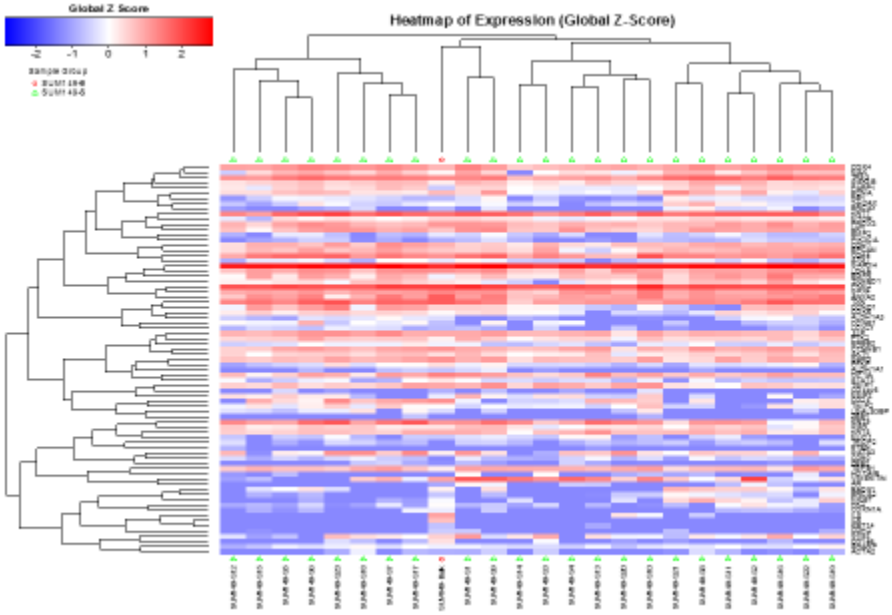

Figure 3.5 Unbiased heatmap cluster analysis of gene expression profiles of SUM149 cells analyzed as bulk cells and single cells.

3.4.2 Single cell multiplex gene expression analysis from metastatic breast cancer CTCs

Liu et al. introduced a molecular profiling to characterize the gene expression patterns of EMT and MET CSCs from a series of primary human breast cancers[89]. Applying this molecular profiling, we identified a 96 gene signature whose expression characterized and discriminated these differing CSC populations (Table 3.1). Among these genes are the epithelial CSC marker ALDH1a3 and the mesenchymal CSC marker CD44, as well as other genes involved in "stemness" and/or EMT/MET transitions. We utilized multiplex RT-qPCR to interrogate expression of each of these 96 genes in single CTCs isolated using double labyrinth purification followed by C1 and BioMark HD (Fluidigm® USA) analysis. We found that the MCF-7 cells (which are of luminal phenotype) exhibit high expression of E-Cadherin, CD133, EpCAM, HER-2 and ALDH1a3, whereas the Basal/ClaudinLow phenotype SUM159 cells expressed N-Cadherin, Zeb-1, Vimentin, TGFBeta-1, and CD44. Accordingly, and based on previous study [89], we classified the cells with the former signature as MET and the later signature as EMT. Based on these gene expression patterns, we classified CTCs into 4 different groups; CK CTCs, EMT CTCs, MET CTCs and Dual (EMT-MET) CTCs (Table 3.2).

Table 3.2 CTC categories for marker-based classification

CTC Category	Definition (based on marker expression)
EMT	**$CD44^{+}$ and $CD24^{low/-}$**
MET	**$ALDH1a3^{+}$**
Dual	**$ALDH1a3^{+}$, $CD24^{low/-}$ and $CD44^{+}$**
CK	**≥2 CK^{+} markers (CK 7, 8, 18, 19)**
WBC	**≥1 Blood marker (CD45, CD11B, CD20, and CD3D)**

Previous studies have identified $CD44^{+}CD24^{low/-}$ and ALDH as breast cancer stem cell (BCSC) markers, with cells displaying either marker being capable of initiating tumors in mice [90, 91]. Both EMT and MET CTCs are classified as BCSCs, with the difference being EMT CTCs are the cells expressing $CD44^{+}CD24^{low/-}$, and MET CTCs are the cells expressing $ALDH1a3^{+}$. Dual CTCs are the cells expressing both of the BCSC markers $CD44^{+}CD24^{low/-}$ and ALDH. CK CTCs are the cells expressing at least two cytokeratin markers but none of the BCSC markers. All the CTCs classified in these four groups expressed none of the blood markers applied in the study (CD45, CD11B, CD20, and CD3D).

Figure 3.6 depicts the heat map of the gene expression analysis of 47 single cells including 31 patient derived CTCs from 6 different patients, 8 patient derived contaminating WBCs (Pts-WBCs) and 8 WBCs from healthy controls (HC-WBCs). The color in each block represents the CT value of a specific gene from a single cell, with red showing highly expression, white showing moderate expression, and blue showing low or no expression. Each column represents the 96 gene expression from a single cell, and the columns are grouped based on their origin (Pt A-F and healthy control). The labels at the bottom of each column indicates the group that the specific cell was categorized into (group of cells are listed in Table 3.2). The genes in each row are grouped together based on the genotypic characterization including epithelial, mesenchymal, stem-like, oncogenic, tumor suppressor, proliferation, apoptotic, inflammatory, hormone receptors, and blood related genes.

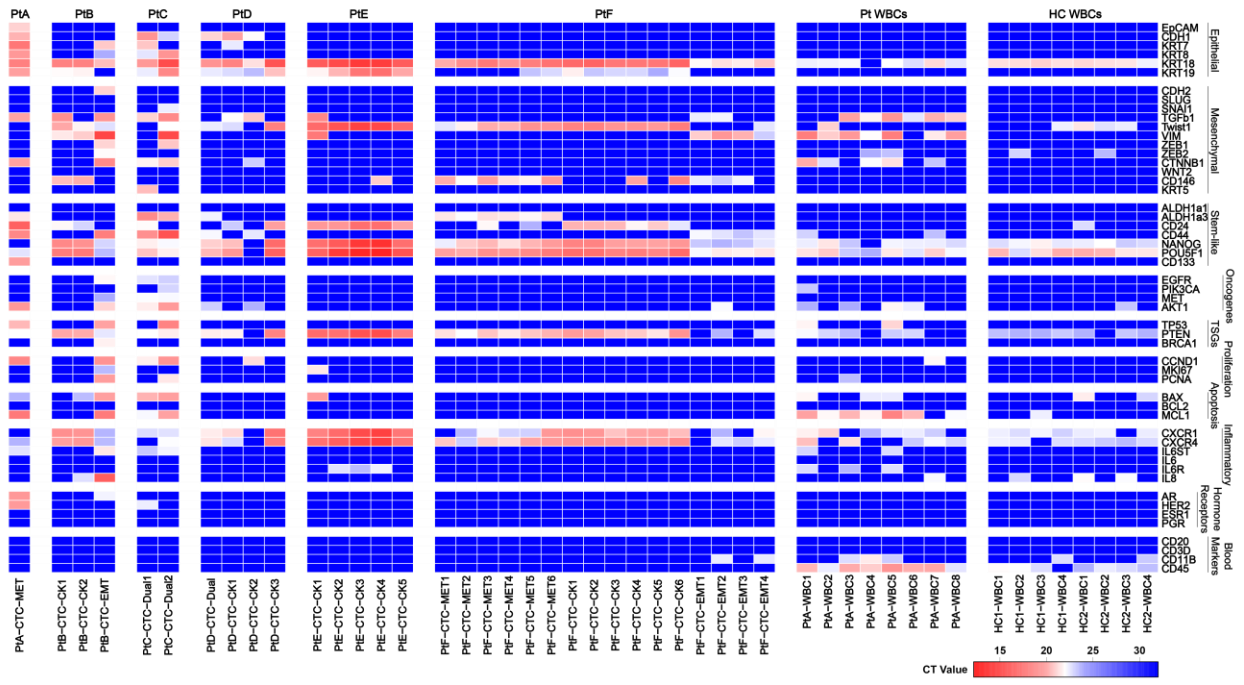

Figure 3.6 Single cell multiplex gene expression profile of isolated CTCs.
Blood samples from cancer patients and healthy controls were processed by Labyrinth as described in the methods. Heat map analysis of the gene expression levels of 47 single cells including 31 patient derived CTCs from 6 different patients, 8 patient derived contaminating WBCs (Pts-WBCs) and 8 WBCs from healthy controls (HC-WBCs). The genes are grouped based on the genotypic characterization as described in Table 3.2.

From the heatmap presented in Figure 3.6, we observed that CTCs presented a gene expression pattern that was distinct from WBCs, whereas Pts-WBCs were similar to HC-WBCs. For instance, both groups WBCs from patients and HC had lower expression on most cancer related genes and higher expression on at least one blood marker genes.

CTCs also showed varied profiles of gene expression. Patient A CTC exhibited MET profile whereas patient B had two CK CTCs and one EMT CTC. Patients C and D had several Dual CTCs along with CK CTCs. On the other hand, Patient E had several CTCs, all of which were CK CTCs. Patient F had a total of 16 CTCs that were analyzed on the Fluidigm BioMark HD chip, among which 6 of them were MET CTCs, 6 of them were CK CTCs, and 4 of them were EMT CTCs. Figure 3.7 presents the examples of inter and intra-patient heterogeneity of CTCs

along with relative expression levels of the relevant genes shown in Violin plot for HC-WBCs (n=8), Pt-WBCs (n=8), CK CTCs from two different patients B & C (n=2 each) along with EMT and MET CTCs. As shown in Figure 3.7A, the sample from patient A was found to have a MET CTC characterized by CDH1+/EpCAM+/ALDH1a3+/CD45-, whereas sample from patient B presents an EMT CTC characterized by CDH2+/EpCAM-/CD44+/CD24-/CD45-. Samples from patients B and C contained CTCs that did not express CSC markers, but were CK+/CD45-. Overall, MET CTCs expressed EpCAM, ALDH1a3, and CDH1 (E-Cadherin) and low level of Vimentin whereas. EMT CTCs expressed Vimentin, CD44, and CDH2 (N-Cadherin) and low levels of ALDH1a3 and CD24. A detailed characterization of all the different categories is presented in the Table 3.2. Furthermore, principal component analysis (PCA) showed separation of CTCs from the contaminating blood cells (Figure 3.7B). The single cell gene expression analysis of 16 CTCs isolated from a single breast cancer patient (Pt F) whose primary tumor was ER+/PR+/HER2- showed 3 distinct groups of CTCs in the unsupervised cluster analysis including: EMT CTCs (n=4) characterized by CD44+/CD24-/Vimentin+/ALDH1a3-/CD45-, MET CTCs (n=6) characterized by ALDH1a3+/SOCS3+/Twist1+/CD24+/CD44-/Vimentin-/CD45- and CK CTCs (n=6) characterized by KRT18+/KRT19+/CD45-. The Log2 expression values for genes in each of these subpopulations are presented as Violin plot in Figure 3.7C. In addition, the expression profiles of 3 groups of CTCs were distinctly different from each other as clearly demonstrated by the PCA analysis (Figure 3.7D).

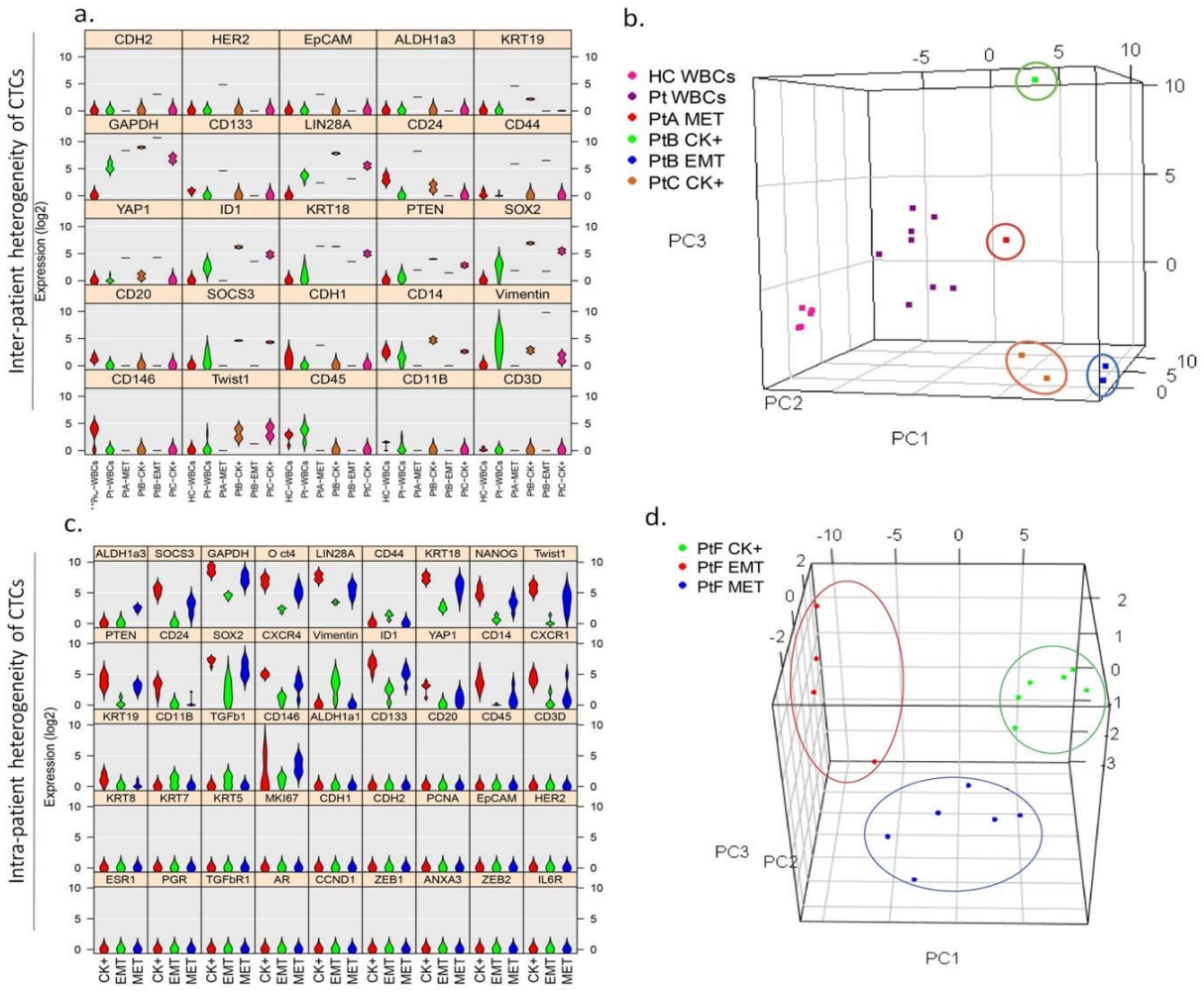

Figure 3.7 Inter-patient and intra-patient heterogeneity of patient derived CTCs.
Violin plot of Log2 expression of genes (A) and PCA (B) show the inter-patient heterogeneity between healthy controls (HC-WBCs), patient derived contaminating WBCs (Pt-WBCs), and patient derived CTCs from patients A, B and C. The Log2 gene expression data are also presented for 16 single CTCs isolated from a single breast cancer patient (Pt F) in Violin plot (C) and PCA (D). These 16 single CTCs show intra-patient heterogeneity as 3 distinct signatures are observed: MET (ALDH+) and EMT (CD44+/CD24-) CSCs, and CK+ non-CSCs.

3.4.3 Single cell multiplex gene expression analysis using alternative downstream approaches

In collaboration with Prof. Euisik Yoon, Dr. Yu-Chih Chen, and Yu-Heng Cheng, we were able to demonstrate the potential of Labyrinth in combination with an alternative downstream analysis technology – Hydro-Seq. Although we have incorporated Fluidigm C1™ technology for

the downstream analysis, Labyrinth output can be used with other downstream single cell tools including commercially available platforms DEPArray™ (Silicon Biosystems) and droplet digital PCR (Raindance) [92, 93], or technologies in development such as Hydrop-Seq. In fact, Fluidigm C1™ technology has a low cell loading efficiency and capacity that limits its application in rare cell samples. It was reported that the loading efficiency of C1 chip for a sample containing 1500 cells/3uL is 90% in 96 chambers, indicating an overall <6% loading efficiency (96/1500). The low recovery of cells suggested that only a small portion of CTCs from patients would be successfully analyzed, resulting in an incomplete study on these cells at single cell level.

Hydro-Seq is a microfluidic single-cell RNA sequencing (scRNA-seq) technology developed by Prof. Euisik Yoon, Dr. Yu-Chih Chen, and Yu-Heng Cheng (University of Michigan) for rare sample analysis (<1000 cells). With a high capture efficiency microfluidic design, Hydro-Seq can achieve >70% single cell capture efficiency with only 10-400 cells loaded. In addition to high capture efficiency, Hydro-Seq is also capable of on-chip washing to remove unwanted debris or particles in the cell suspension to prevent sample contamination. This ensures high-quality single cell analysis for clinical samples such as CTCs. Although there are many high performance CTC enrichment technologies, the output samples usually still contain some background platelets, red blood cells and white blood cells. With on-chip washing, Hydro-Seq effectively isolates tumor cells in each processing chamber without other cells that can contaminate mRNAs. For processing throughput, Hydro-Seq is currently designed with 800 chambers for CTC processing. The throughput can potentially be adjusted to meet different assay requirements. The performance of Hydro-Seq was validated by sequencing cell line samples with the identification of different cancer subtypes.

Hydro-Seq was applied as a next-gen platform for the single cell RNA sequencing of isolated CTCs from Labyrinth (Figure 3.8). Patient blood samples were processed through double Labyrinth as described in the Methods. The isolated CTCs were then processed through Hydro-Seq to separate cells into individual chambers, followed with cDNA preparation for RNA sequencing.

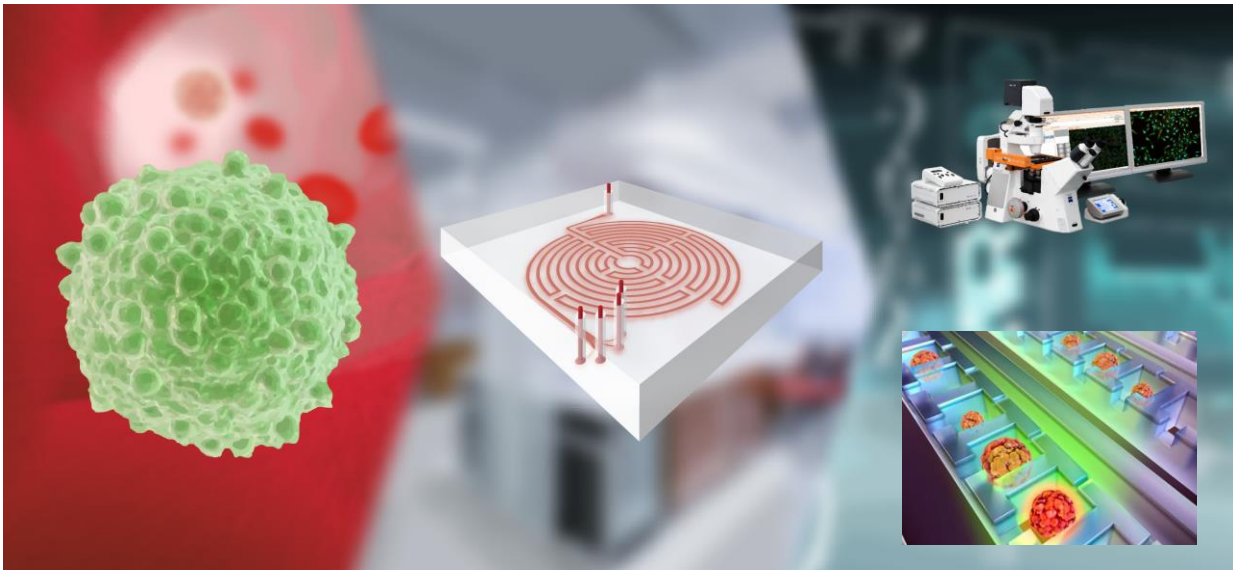

Figure 3.8 Illustration of next generation single cell sequencing of CTCs.
CTCs are first enumerated through Labyrinth devices, and then processed through Hydro-Seq device to separate cells into individual chambers, followed with cDNA preparation for RNA sequencing.

In Figure 3.9, we demonstrated that Hydro-Seq was able to isolate single CTCs from metastatic breast cancer patient into individual chambers. We achieved an extremely high sample purity containing no RBC contamination and 90% overall CTC purity, and a total processing time of four hours including Labyrinth to Hydro-Seq. The optimized Labyrinth/Hydro-Seq protocol was applied in over ten patient samples with an average of 12-18 mL of blood processed, and successfully retrieved over 10 single CTCs from every sample processed.

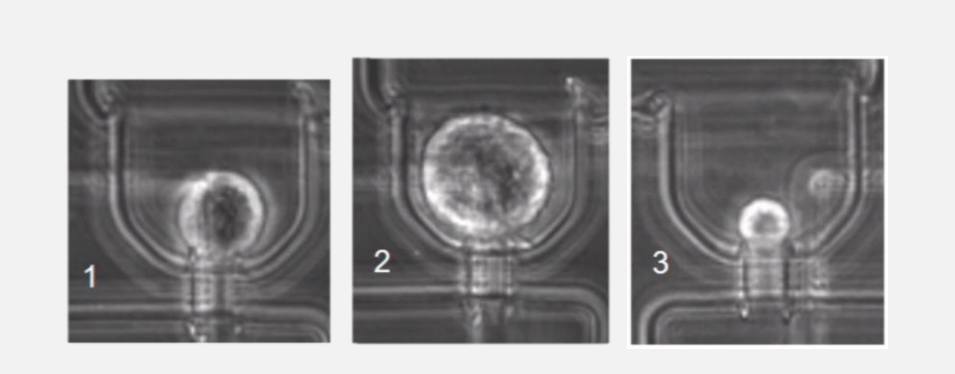

Figure 3.9 Single CTCs from metastatic breast cancer patient isolated in Hydro-Seq.

A total of 4 cancer patient samples (2 breast and 2 pancreatic cancers) processed with Labyrinth and Hydro-Seq were sequenced through Sequencing Core (University of Michigan) to identify the mRNA expression on isolated single cells. 68 CTCs were characterized from these 4 samples based on $CD45^-$ expression, where 29 WBCs were identified with $CD45^+$ expression. This suggested a high recovery of CTCs (average of 17 CTCs from each sample), and a high overall sample purity of 70.1%. Among the 68 CTCs identified, we observed the clustering of CTCs from the same patient in terms of gene expression on tSNE and PCA plots (Figure 3.10). Figure 3.11 presented a normalized heatmap of over 1000 genes analyzed in these cells, further demonstrated the potential of this approach in acquiring orders more data compared to gene panel applied in C1™.

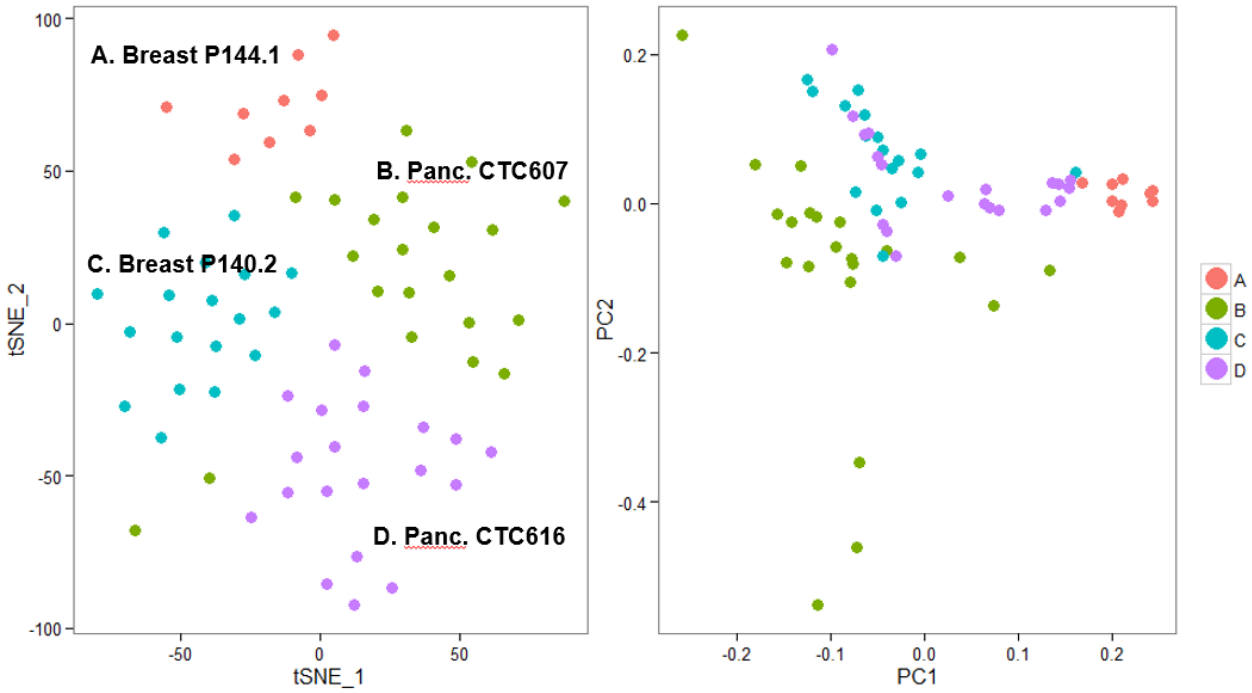

Figure 3.10 tSNE and PCA plots of isolated single CTCs from 4 patients.
Sample A & C are metastatic breast cancer patient samples, and sample B & D are metastatic pancreatic cancer patient samples. CTCs from each patient are plotted in distinct colors.

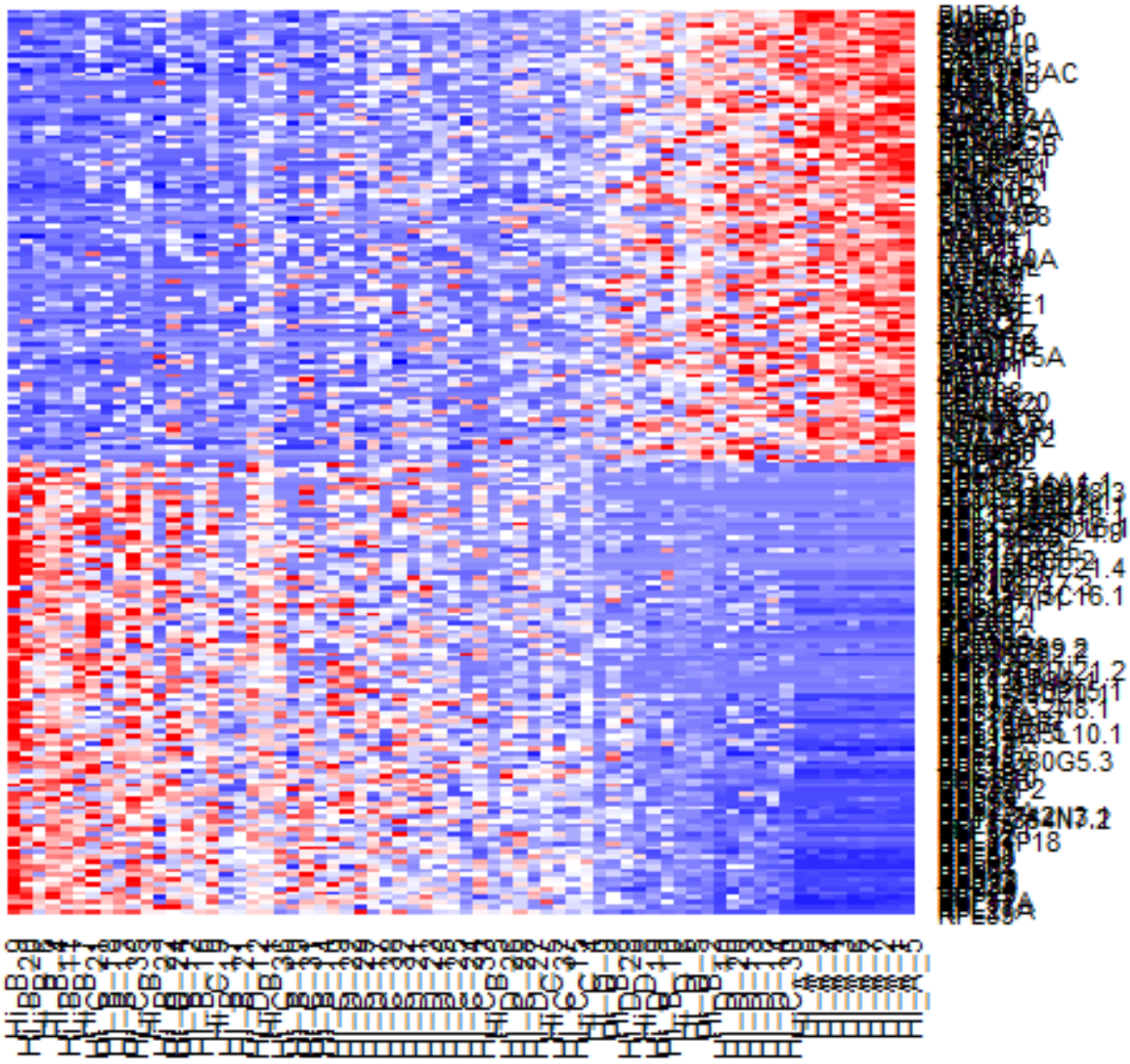

Figure 3.11 Normalized gene expression heatmap of isolated single CTCs from 4 patients.

3.5 Conclusion

With the presented Labyrinth, we were able to demonstrate a high throughput, continuous, and a true biomarker independent (without positive or negative selection) microfluidic separation technology to isolate CTCs from whole blood. Classical genomic analysis techniques use population average readouts. However, these approaches mask cellular heterogeneity and dynamics and are limiting for studying rare and heterogeneous cell populations, including cancer

stem cells. Techniques for single-cell analysis allow quantification of molecular dynamics and genotypic characteristics and can identify the signature from fewer rare CSCs that are present among other CTCs, which would have been missed if we did bulk CTC analysis. We demonstrated that the cells isolated using Labyrinth contain subpopulations of CTCs expressing markers of epithelial and mesenchymal stem-like cells at single cell resolution. Although we have incorporated Fluidigm technology for the downstream analysis, Labyrinth output can be used with other downstream single cell tools including but not limited to DEPArrayTM (by Silicon Biosystems) and droplet digital PCR (Raindance) [92, 93].

Over the past several years, a tremendous amount of effort has been invested in the development of new therapeutic agents that can take advantage of the "Achilles' heel" of CSCs by targeting cell-surface molecular markers or various signaling pathways [94-97]. A number of agents capable of targeting breast and pancreatic cancer stem cells in preclinical models are currently entering clinical trials [98]. However, one of the serious limitations has been the lack of proper metrics to evaluate the dose response and efficacy of these therapies. Most targeted therapies do not result in tumor shrinkage but act on subpopulation of tumor with the goal of killing the specific lethal types. The lack of proper biomarker endpoints has resulted in difficulty in assessing the effects on CSCs in these studies. The high throughput Labyrinth enables single cell isolation and gene expression characterization and opens opportunities to monitor heterogeneous subpopulations at a single cell resolution through treatment. Hence Labyrinth enables dynamic and rapid evaluation of the efficacy of the targeted therapies by measuring the specific pathway inhibition through gene expression analysis. Future research will involve more extensive application of innovative microfluidic systems that target the use of CTCs as a reliable biomarker for early detection, treatment selection, and monitoring of cancer patients.

CHAPTER 4 Efficient Label-Free and High-Throughput Purification of Isolated Muscle Satellite Cells Using Microfluidic Inertial Separation

4.1 Abstract

Beyond CTC isolation, Labyrinth was applied in the study of skeletal muscle satellite cells in collaboration with Dr. Brian C. Syverud and Prof. Lisa M. Larkin. Skeletal muscle satellite cells play an essential role in repairing muscle damage and have tremendous therapeutic potential in cell therapy or skeletal muscle tissue engineering. Obtaining a sufficiently pure satellite cell population, however, presents a significant challenge. We hypothesized that the size difference between satellite cells (8-13 μm) and fibroblasts (10-22 μm), two primary cell types obtained from our skeletal muscle dissociation process, would allow for label-free, inertial separation in a Labyrinth microfluidic device and that these purified satellite cells could be used to engineer skeletal muscle. Throughout our engineered tissue fabrication process, Labyrinth purified cells were compared to unsorted controls to assess the efficiency of this novel sorting process and to examine potential improvements in myogenic proliferation, differentiation, and overall engineered tissue function. Immediately after dissociation and Labyrinth sorting, aliquots of cells were fixed

via Cytospin and immunostained to identify myogenic cells and identify fibroblast progenitors. Remaining cells were cultured for 14 days to form a confluent monolayer that was induced to delaminate and was captured as a 3D skeletal muscle construct. During monolayer development, myogenic proliferation (BrdU assay on Day 4), differentiation and myotube fusion index (α-actinin on Day 11), and myotube structural development (light microscopy on Day 14) were assessed. Isometric tetanic force production was measured in 3D constructs on Day 16. From the Cytospin analysis, unsorted cells exhibited a myogenic purity of 39.9 ± 3.99%, and this purity was enriched approximately twofold to 75.5 ± 1.59% by microfluidic separation. The BrdU assay on Day 4 similarly showed significantly enhanced myogenic proliferation: in unsorted controls 47.0 ± 2.77% of proliferating cells were myogenic, in comparison to 61.7 ± 2.55% following purification. Myogenic differentiation and fusion, assessed on Day 11 by quantification of fusion index, showed improvement from 82.7 ± 3.74% in control to 92.3 ± 2.04% in the purified cell population. Myotube density in unsorted controls (18.6 ± 3.26 myotubes/mm^2) was significantly enriched in the purified cell population to 33.9 ± 3.74 myotubes/mm^2. Constructs fabricated from Labyrinth-purified cells also produced significantly greater tetanic forces (143.6 ± 16.9 μN) than unsorted controls (70.7 ± 8.03 μN). These results demonstrate the promise of microfluidic sorting in purifying isolated satellite cells and for tissue engineering. This unique technology could assist researchers in translating the regenerative potential of satellite cells to cell therapy and tissue engineering therapies.

4.2 Introduction

Skeletal muscle has the ability to regenerate itself in response to damage [99], largely due to the presence of potent muscle progenitor cells [100]. As the most abundant tissue in the body [101], skeletal muscle requires this regenerative capacity for maintaining homeostasis and

restoring function after injury. The resident skeletal muscle stem cell, the satellite cell, plays an essential role in repairing muscle damage [102, 103]. In cases of severe injury, however, the native skeletal muscle repair mechanism is overwhelmed, and external intervention is indicated. With volumetric muscle loss, surgical or traumatic loss of muscle tissue resulting in a functional deficit [104], natural repair is insufficient, and fibrotic scar tissue instead accumulates in the defect site [105]. Current treatment options, free functional muscle transfer and composite tissue allotransplantation, involve grafting healthy muscle, innervation, and vasculature into the defect, but limitations such as donor site morbidity and limited tissue availability often prevent complete recovery [106-108]. In addition, muscular dystrophies are a family of inherited degenerative disorders characterized by systemic muscle weakness [109-111]. Duchenne muscular dystrophy is particular distressing, due to its early onset and the lack of an effective treatment [112-114]. To address these clinical challenges, researchers have proposed using satellite cells in cell therapy [115-118] or tissue engineering approaches [119-123]. Although other cell types have been implicated as contributors to skeletal myogenesis [124-126], recent research shows that satellite cells act as the primary source of regeneration of adult skeletal muscle [102, 127]. Due to this tissue-specific regenerative ability, satellite cells have tremendous therapeutic potential.

Obtaining a suitable population of satellite cells, however, presents a continuing challenge. Satellite cells are relatively few in number, only accounting for 2-7% of the nuclei associated with a muscle fiber [126, 128], and current isolation methods have difficulty yielding both the population size and purity required [129-131]. Enzymatic dissociation yields a large quantity of cells with mixed myogenic and non-myogenic populations, requiring a need for additional purification [118, 130, 132], whereas single fiber explant culture isolates small satellite cell populations with purity of 95% or higher [133-135].

The prevailing technique is to combine enzymatic isolation techniques with subsequent purification methods, but each has its associated drawbacks. Pre-plating, allowing rapidly adhering non-myogenic cells attachment to a substrate to obtain a purified population of non-adherent myogenic cells [118, 136, 137], provides a technically simple and scalable approach for purification. It is limited, however, by sensitivity of the pre-plate timing and potential for loss of myogenic cells. Alternatively, fluorescence activated cell sorting (FACS) has successfully purified CD34+/CD45-/Sca1- myogenic cells from the heterogeneous isolated cell population [124, 138-140]. Because of the heterogeneity of surface markers within the satellite cell pool [141, 142], however, retention of the full satellite cell population is difficult. Furthermore, FACS requires modification of the cells being analyzed through the addition of exogenous dyes or the electrical perturbations of the sorting process itself [143]. Magnetic activated cell sorting (MACS) is another purification method, using magnetic microbeads conjugated to antibodies for specific markers of interest, that has been demonstrated [144]. Direct comparison to other methods indicated less efficient purification with MACS in comparison to pre-plating [145], and concerns about labelling with microbeads have been raised as well. Microfluidic characterization and sorting of fluorescently-labelled skeletal muscle cells has been demonstrated as an alternative [141, 146] but is currently limited to small throughputs of hundreds of cells or less. By examining the existing techniques, it is clear that an efficient, label-free, high-throughput method for purifying satellite cells following isolation is required.

Inertial microfluidics has the potential to fill this pressing need. The inertial migration of particles in a microfluidic device was first observed by Segré and Silberberg in the 1960s [50] and recently described by Di Carlo [44]. In short, particles in straight microfluidic channels experience stresses that act over the entire channel surface: 1) shear stress that yields drag forces, 2) normal

stress that yields lift forces perpendicular to the direction of flow, and 3) a wall lift effect [39, 44, 147]. The combination of these forces focuses the particles to certain equilibrium positions according to the density of particles and the geometry of microfluidic channel. In a curved channel, centrifugal effects induce secondary flow (Dean flow) on the cross section of the channel. The generated double recirculation (Dean Vortices), along with the aforementioned forces, migrate particles transversely. Particle migration is correlated to the particle size and the curvature of the channel, resulting in new profile of equilibrium positions which separates distinct size classes of particles50. In our case, a typical skeletal muscle cell isolate contains a mixture of satellite cells ranging from 8-13 μm [135, 141] and myofibroblasts ranging from 10-22 μm [148, 149], in addition to smaller populations of hematopoietic, neural, and immune cells.

A microfluidic device, termed "Labyrinth", was previously designed for and applied in the separation of circulating tumor cells (15-25 μm) from white blood cells (7-12 μm) using inertial microfluidics-based separation. It is a high throughput (1800-2500 μL/min), continuous, and biomarker independent microfluidic separation technology. The design of the Labyrinth (Figure 4.1A), inspired by the Labyrinth in Greek mythology, incorporates 11 loops and 56 corners in a total channel length of 637 mm. The loops have small curvature ratios, providing enough channel length for complete focusing of cells, whereas sharp right-angle corners have high curvature ratios to further enhance focusing of smaller cells. Four separate outlets are designed to collect the focused individual streams of cells with differing sizes. Combining these features, the Labyrinth enables the enumeration of cells in different size classes with high efficiency.

In this study, we demonstrate the power of inertial microfluidic separation for purification of isolated satellite cells. We hypothesized that the size difference between satellite cells and fibroblasts, two primary cell types obtained from chemical dissociation of muscle, would allow

for label-free, inertial separation in a microfluidic device and that purified satellite cells could be used to engineer our skeletal muscle units (SMUs). Throughout the engineered tissue fabrication process described extensively in previous work [123, 150-152], purified cells were compared to unseparated controls to assess the efficiency of the microfluidic separation process and to examine potential improvements in myogenic proliferation, differentiation, and overall engineered tissue function as a result.

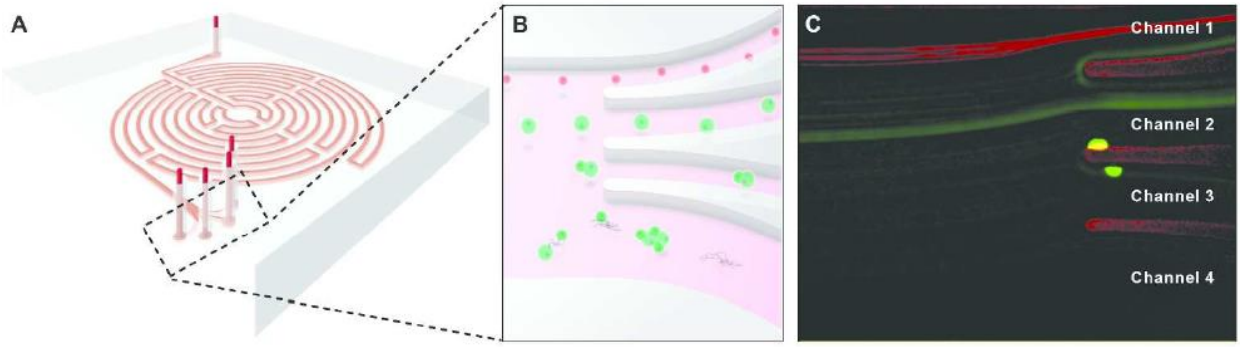

Figure 4.1 Microfluidic Inertial Separation in the Labyrinth Device
A schematic representation of the Labyrinth is shown in (A). Cells in suspension enter the device at the top of the image and rapidly flow (1800 μL/min) along the circuitous path created by a series of curved channels. Dean forces proportional to cell size and channel curvature act on the cells transversely to the flow direction, separating distinct size classes of particles at the outlets as pictured in (B). Specifically, we intended to separate satellite cells, with a size range of 8-13 μm, from myofibroblasts, with a typical diameter of 10-22 μm. The Labyrinth was designed to focus the smaller satellite cells into Channel 1 (top), larger myofibroblasts into Channel 2 (second from top), and cell aggregates and debris into Channels 3 and 4 (bottom). (C) Visualization of a mixed population of Pax7+ satellite cells expressing red tdTomato fluorescence and Achilles tendon fibroblasts labeled with CellTracker Green fluorescent dye during sorting confirmed efficient separation of these two cell types based on their difference in size.

4.3 Methods

4.3.1 Animal Care

All animal care procedures followed *The Guide for Care and Use of Laboratory Animals* [153], according to a protocol approved by the University Committee for the Use and Care of

Animals. Validation of the Labyrinth was performed using fluorescently labelled primary mouse cells. Pax7-positive satellite cells expressing red fluorescence were isolated from a transgenic Pax7CreERT2-r26-tdT mouse, provided by collaborators in the lab of Dr. Chris Mendias, Department of Orthopedic Surgery at the University of Michigan. To induce tdTomato fluorescence expression, mice were injected intraperitoneally with tamoxifen (Sigma-Aldrich, St. Louis, MO, cat. no. T5648) in corn oil (Sigma, cat. no. C8267) at a dose of 0.5 mg diluted to 10 mg/mL. Injections were repeated for five consecutive days, and cells were isolated at least ten days after the final injection. Mouse Achilles tendon fibroblasts were isolated from C57BL6 mice supplied by Charles River Laboratories Inc. (Wilmington, MA, USA) and were fluorescently labelled using CellTracker Green CMFDA Dye (Life Technologies, Carlsbad, CA, cat. no. C7025) according to the manufacturer protocol.

SMUs were engineered using soleus muscles and bone marrow from 145-155g female Fischer 344 rats, supplied by Charles River Laboratories. Animals acclimated to colony conditions for one week prior to any procedure and were fed Purina Rodent Chow 5001 and water ad libitum. Intraperitoneal injections of sodium pentobarbital (50 mg/kg for mice, 65 mg/kg for rats; Merck Animal Health, Madison, NJ, NADA # 119-807) was used to induce a deep plane of anesthesia. Supplemental pentobarbital doses were administered as required to maintain adequate anesthesia depth.

4.3.2 Muscle Dissection and Cell Isolation

From rats, both soleus muscles were removed under aseptic conditions and sterilized in 70% ethanol. All hindlimb muscles were dissected when isolating mouse muscle cells. The muscles were then minced using a razor blade, placed under ultraviolet light for 15 min in 15mL of Ham's F12 (Gibco BRL, Carlsbad, CA, cat. no. 11765-047), and added to a dissociation solution

consisting of 32U dispase (1.8 U/mg; Gibco, cat. No. 17105-04) and 2390U type IV collagenase (239 U/mg; Gibco, cat. no. 17104-019) in 20mL of Ham's F12. The mixture was maintained at 37°C with agitation for 90 min. The resulting suspension was then filtered with a 100 µm mesh filter (Fisher Scientific, Waltham, MA, cat. no. 22363549) prior to centrifugation. The dissociation solution was aspirated off and the cells were resuspended in growth medium.

4.3.3 Microfluidic Device Fabrication

The mold for the Polydimethylsiloxane (PDMS) device was fabricated following a standard protocol of soft lithography. Using a spin-coater, a negative photoresist layer of SU-8 100 (MicroChem, Westborough, MA, cat. no. SU-8 100) was deposited onto silicon wafer with 2450 rpm rotation for 1 minute. The wafer was then soft-baked for 10 minutes at 65°C and 70 minutes at 95°C. A mask with the device geometry was aligned to the wafer and exposed to UV light for 20 seconds to cure the photoresist. Post-exposure-baking was applied for 3 minutes at 65°C and 10 minutes at 95°C. Next, the wafer was soaked in developer solution (MicroChem, cat. no SU-8 Developer) for 6 minutes and in isopropyl alcohol (Sigma, cat. no. W292907) for 1 minute to remove the inactivated photoresist. It was finally hard baked for 4 minutes at 150-180°C. The resulting height of the mold on silicon wafer was 100 µm, and the width of the channel was 500 µm.

The flow chamber for Labyrinth was made from PDMS (Sylgard 184; Dow Chemical Corp., Midland, MI, cat. no. 4019862). 30 mL Sylgard polymer base and 3 mL curing agent were thoroughly mixed and poured onto a silicon mold. The mixture was placed into a desiccator for 2 hours to remove air bubbles from the mixture and then heated at 65°C overnight to harden the polymer. The polymer was next cut into the desired shape, and punched with a needle for tubing insertion. The PDMS device was then bonded to standard sized glass slides via plasma surface

activation of oxygen. The bonded device was plumbed with 0.76 mm diameter tubes (Cole-Parmer, Vernon Hills, IL, cat. no. 06419-00).

4.3.4 Microfluidic Inertial Separation

The Labyrinth device was pre-flowed with 1% Pluronic acid solution (Sigma, cat. no. P2443) in Dulbecco's Phosphate-Buffered Saline (DPBS; Fisher, cat. no. 14190144) at 100 μL/min for 10 minutes and then incubated for 10 minutes to prevent cell clotting on channel walls. Cell samples in suspension were then pushed through the Labyrinth at a flow rate of 1800 μL/min. The products from each of the four outlets was collected separately after 60 seconds of flow stabilization.

4.3.5 SMU Formation

SMUs were engineered in 60 mm polystyrene plates (Fisher, cat no. 353002), and ICC was performed on 35 mm plates (Fisher, cat. no. 353001) as described previously [152, 154]. Briefly, a substrate of PDMS was cured onto each plate, followed by coating with laminin (Natural Mouse Laminin, Gibco, cat. no. 23017-015) at 1mg/cm^2. Isolated cells were seeded in muscle growth medium (MGM) at 600,000 cells per 60 mm plate or 150,000 cells per 35 mm plate. MGM contained 30mL F-12 Kaighn's Modification Nutrient Mixture (Gibco, cat. no. 21127-022), 12.5mL Dulbecco's modified Eagle's medium (DMEM; Gibco, cat. no. 11995- 065), 7.5mL fetal bovine serum (FBS; Gibco, cat. no. 10437-028), 2.4 ng/mL basic fibroblast growth factor (bFGF; Peprotech, Rocky Hill, NJ, cat. no. 100-18B), and 0.5mL antibiotic-anti-mycotic (ABAM; Gibco, cat. no. 15240- 062). After initial plating for four days to allow attachment, cells were subsequently fed MGM every two days until becoming fully confluent on Day 7 with a network of elongating myotubes. At this point, 5 mm tissue engineered bone-tendon anchors were pinned onto the cell

monolayers at a spacing of 2.5 cm, and the media was switched to muscle differentiation medium (MDM). MDM was composed of 35mL M199 (Gibco, cat. no. 11150-059), 11.5mL DMEM, 3mL FBS, 50µL insulin-transferrin selenium-X (Sigma, cat. no. I1884), 0.5mL ABAM, and 36.2µL 50mM ascorbic acid 2-phosphate (Sigma, cat. no. A8960). After a week on MDM, re-supplied every other day, the monolayers delaminated from the plates on Day 14, rolling into cylindrical muscle constructs, held at length by the engineered bone anchors.

4.3.6 Immunocytochemical Analysis

At specific time points during SMU fabrication, samples were fixed in 20°C methanol for 10 min and set aside for immunocytochemistry (ICC). Samples were washed for 10 min in 0.1% Triton X-100 (Sigma, cat. no. T8787) in DPBS (PBST) and blocked with PBST containing 3% Bovine Serum Albumin (PBST-S; Sigma, cat. no. A2153) at room temperature. Samples were then incubated overnight at 40°C with primary antibodies diluted in PBST-S. Immunofluorescent staining was performed using the following primary antibodies: mouse monoclonal anti-desmin (1:20 dilution; Developmental Studies Hybridoma Bank, Iowa City, IA, cat. no. D3), mouse monoclonal anti-Pax7 (1:100 dilution; Abcam, Cambridge, MA, cat. no. ab199010), rabbit polyclonal anti-PDGFRα (1:100 dilution; Santa Cruz Biotech, Dallas, TX, cat. no. sc-431), biotin conjugated sheep polyclonal anti-BrdU (1:50 dilution; Abcam, cat. no. ab2284), mouse monoclonal anti-MyoD (1:100 dilution; BD Biosciences, San Jose, CA, cat. no. 554130), rabbit polyclonal anti-fibroblast-specific protein 1 (FSP1; 1:100 dilution; Abcam cat. no. ab27957), and mouse monoclonal anti-α-actinin (1:200 dilution; Sigma, cat. no. A7752). Plates stained with anti-BrdU had previously been incubated for 24 hours with a BrdU labelling reagent (Life Technologies, cat. no. 00-0103) in the culture media. Following 3 PBST washes for 5 min each, samples were incubated in 1:500 dilutions of with Alexa Fluor anti-mouse, anti-rabbit, or

streptavidin secondary antibodies (Life Technologies) for 3 hours at room temperature. Following 3 washes in PBST for 15 min each, samples were preserved in Prolong Gold with DAPI (Life Technologies, cat. no. P36935) and cover slipped. Samples were examined and photographed with a Leica Inverted microscope, and images were analyzed using the Image J software package. For ICC analysis, samples from each experimental group were fixed and stained (on Day 0 for Cytospin; Day 4 for BrdU; and Day 11 for α-actinin). Cells fixed on Day 0 were attached to microscope slides via Cytospin at 800 RPM for 8 min. From each sample, ten random areas were imaged, and the number of positively stained nuclei in each image was counted.

4.3.7 Myotube Fusion Index Calculation

From the α-actinin images, the percentage of myogenic nuclei was first calculated by dividing the total number of nuclei by the number of α-actinin-positive nuclei. The structural protein α-actinin is often used to identify Z-lines in skeletal muscle sarcomeres, but α-actinin is also expressed in the stress fibers of myoblasts prior to fusion [155-157]. To calculate myotube fusion index, α-actinin-positive cells were quantified depending on the number of nuclei contained. Specifically, cells were divided into groups with one, two, three, and four or more nuclei, and these values were reported as a percentage of the total number of α-actinin-positive nuclei.

4.3.8 Animal Care

SMUs were engineered using soleus muscles and bone marrow from 145-155g female Fischer 344 rats, supplied by Charles River Laboratories. Animals acclimated to colony conditions for one week prior to any procedure and were fed Purina Rodent Chow 5001 and water ad libitum. Intraperitoneal injections of sodium pentobarbital (50 mg/kg for mice, 65 mg/kg for rats; Merck Animal Health, Madison, NJ, NADA # 119-807) was used to induce a deep plane of anesthesia.

Supplemental pentobarbital doses were administered as required to maintain adequate anesthesia depth.

4.3.9 Myotube Size and Density Analysis

On Day 14 after initial seeding, light micrographs of developing monolayers were captured. Specifically, ten random areas from each 60 mm plate were imaged. Every myotube from these images was then measured in ImageJ to determine its size and the overall density of the myotube network.

4.3.10 SMU Contractile Measurements

SMU force production was measured on Day 16 following roll-up into 3D cylindrical form. The protocol for measuring contractility of engineered muscle constructs has been described previously [122, 157, 158]. Briefly, the pin on one end of the SMU was attached to a force transducer. Platinum wire electrodes were placed along either side of the SMU for field stimulation. The temperature of the construct was maintained at 37° C, using a heated aluminum platform. Twitch contractions were elicited using a single 2.5 ms pulse at 10, 30, 60 and 90 mA, whereas tetanic force was determined using a 1 s train of 2.5 ms pulses at 90 mA and 10, 20, 40, 60 and 80 Hz. Data files for each peak twitch force and peak tetanic force trace were recorded and subsequently analyzed using LabVIEW 2013.

4.3.11 Statistical Analysis

Values are presented as mean ± standard error. Measurements of significant differences between means were performed using R software. Means were compared using either a Student's

t-test or one-way ANOVA with Tukey post-hoc comparisons. Differences were considered significant at $p<0.05$.

4.4 Results

4.4.1 Initial Validation of Microfluidic Satellite Cell Purification

The sorting efficiency of the Labyrinth microfluidic device was validated using fluorescently labelled primary mouse cells. A combination of Pax7-positive satellite cells ubiquitously expressing red tdTomato fluorescence and Achilles tendon fibroblasts labelled with CellTracker Green fluorescent dye were separated at several different fluid flow rates. Visualization of the fluorescent cells during sorting (Figure 4.1C) indicated improved separation distances between satellite cells and fibroblasts at lower flow rates (1800 µL/min: 148 µm, 2000 µL/min: 135 µm, 2200 µL/min: 128 µm, 2500 µL/min: 112 µm). Based on these results, a flow rate of 1800 µL/min was used for all subsequent sorting runs. Sorting of the fluorescently labelled cell populations was repeated, and the separated cells were quantified with a hemocytomer (Table 4.1A). From these results, it is clear the Labyrinth separated the cell populations as intended, significantly enriching the satellite cell population in Channel 1 ($p = 0.015$) and the fibroblast population in Channel 2 ($p > 0.001$) as compared to unsorted controls.

Table 4.1 Purity of Separated Cell Populations Following Sorting.
Purity in mouse cells (A) refers to the percentage of fluorescent cells (red for Pax7+ satellite cells, green for fibroblasts) among the total cells counted in each Labyrinth channel. It is worth noting that very few cells were present in Channel 4, and none of these cells were Pax7+. In rat isolates (B), cells were characterized as myogenic if expressing either Pax7 or desmin, and fibrogenic based on expression of PDGFRα. The difference in sorted mouse and rat populations, evident in Channels 3 and 4, can be explained by the methods used to label these cells. The mouse cells contained a population of unlabeled fibroblasts from enzymatic digestion of the muscle biopsy. It is expected that these unlabeled fibroblasts represented a sizeable portion of the mouse cells sorted into Channels 3 and 4. In all tables and figures, values are presented as mean ± standard error. * indicates significant increases relative to unsorted controls.

A) Primary Mouse Cells	**Unsorted Control**	**Sorted Channel 1**	**Sorted Channel 2**	**Sorted Channel 3**	**Sorted Channel 4**
Pax7+ Purity (n = 3)	33.3 ± 3.36 %	**66.5 ± 6.03 % ***	27.2 ± 5.76 %	21.2 ± 11.6 %	0.00 ± 0.00 %
Fibroblast Purity (n = 3)	43.2 ± 2.57 %	11.9 ± 4.81 %	**70.6 ± 1.28 % ***	17.4 ± 2.96 %	0.18 ± 0.13 %
B) Primary Rat Cells					
Myogenic Purity (n = 6)	39.9 ± 3.99 %	**75.5 ± 1.59 % ***	27.5 ± 4.17 %	12.0 ± 1.56 %	7.36 ± 1.30 %
Fibrogenic Purity (n = 6)	45.6 ± 3.14 %	21.9 ± 1.94 %	57.4 ± 2.65 %	**60.8 ± 4.86 % ***	**78.3 ± 4.47 % ***

4.4.2 Isolated Cell Populations Immediately Following Microfluidic Sorting

The Labyrinth device demonstrated similar sorting efficiency in separating isolated primary rat cells (Table 4.1B). Following isolation and sorting, cells attached to microscope slides via Cytospin were immunostained with Pax7 and desmin to characterize myogenic cells and PDGFRα to identify fibroblast progenitors. Analysis of images from the separated cell populations indicated that a purified population of myogenic cells was evident in Channel 1 of the Labyrinth device. Specifically, compared to the unsorted muscle dissociation, with a myogenic cell purity of 39.9 ± 3.99%, Labyrinth-sorted cells were significantly enriched with myogenic cells, approximately two-fold, to 75.5 ± 1.59% ($p < 0.001$). Because of their larger cell size, the fibroblast progenitors were separated into Channels 2, 3, and 4 by the Labyrinth device. In comparison to the unsorted dissociation with a fibrogenic cell purity of 45.6 ± 3.14%, channels 2, 3 and 4 demonstrated increased fibroblast purities of 57.4 ± 2.65% ($p = 0.1091$), 60.8 ± 4.86% ($p = 0.023$), and 78.3 ± 4.47% ($p < 0.001$), respectively.

4.4.3 Effects of Microfluidic Sorting on Cell Proliferation

To assess the influence of the microfluidic separation process on cell proliferation, Labyrinth sorted cells were seeded and cultured normally. ICC analysis was performed on Day 4 following seeding to identify proliferating cells expressing BrdU, a synthetic nucleoside analog of thymidine. Expression of MyoD and FSP1 was examined simultaneously to identify myogenic cells and matrix-secreting fibroblasts, respectively. From BrdU analysis of plates ($n = 10$), it was clear that microfluidic sorting did not have a significant effect on overall cell proliferation (Figure 4.2). In unsorted controls $91.2 \pm 1.23\%$ of cells were proliferating, whereas cells sorted into Channel 1 of the labyrinth exhibited $91.6 \pm 1.01\%$ ($p = 0.556$). Co-staining for MyoD, however, demonstrated a significant increase ($p = 0.004$) in proliferating myogenic cells sorted into Channel 1 ($57.1 \pm 2.97\%$) as compared to unsorted controls ($44.3 \pm 2.81\%$). In contrast, FSP1 co-staining indicated that the percentage of proliferating fibrogenic cells in unsorted controls, $46.9 \pm 1.86\%$, was significantly decreased to $34.5 \pm 1.90\%$ by microfluidic sorting ($p < 0.001$). It is worth noting that insufficient myogenic cells were present in Channels 2, 3, and 4 for SMU fabrication, so only unsorted controls and Channel 1 cells were compared for this and subsequent analysis.

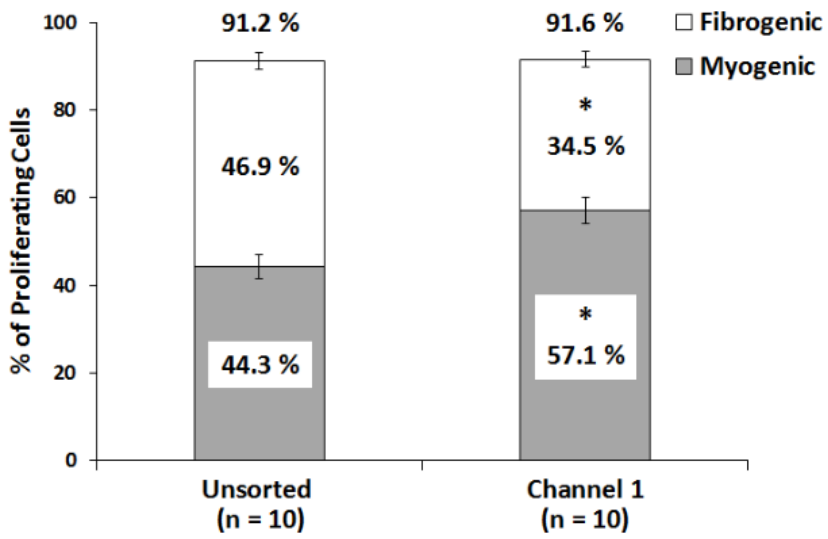

Figure 4.2 Myogenic and Fibrogenic Proliferation of Sorted Cells.
Incorporation of BrdU on Day 4 of SMU fabrication was used to identify proliferating cells. No difference in overall proliferation was observed between unsorted controls (91.2 ± 1.23%) and cells sorted into Channel 1 (91.6 ± 1.01%, $p = 0.556$), suggesting the sorting process did not adversely affect cell growth. Immunostaining for MyoD and FSP1 indicated myogenic and fibrogenic cells, respectively. Proliferating myogenic cells were significantly enriched ($p = 0.004$) after sorting into Channel 1 (57.1 ± 2.97%) as compared to unsorted controls (44.3 ± 2.81%). In contrast, FSP1 staining indicated proliferating fibrogenic cells in unsorted controls, 46.9 ± 1.86%, were significantly decreased to 34.5 ± 1.90% by microfluidic sorting ($p < 0.001$). * Indicates statistical difference from control.

4.4.4 Myogenic Differentiation and Myotube Fusion Following Microfluidic Sorting

Myotube fusion index was measured to assess the ability of sorted cells to form a network of myotubes following microfluidic separation. Expression of α-actinin on Day 11 of SMU fabrication was used to identify fused myotubes and sarcomeric structure. Myotubes in both control and Channel 1 plates exhibited dense networks of longitudinally-aligned myofibrils with advanced sarcomeric structure (Figure 4.3A-B). Quantification of the number of nuclei associated with α-actinin-positive cells yielded a myotube fusion index value. From a t-test, the overall percentage of nuclei associated with cells expressing α-actinin in unsorted control plates ($n = 8$) of 52.0 ± 2.76% was not significantly different ($p = 0.142$) from plates seeded with cells sorted

into Channel 1 57.0 ± 2.06% (Figure 4.3C). However, the number of fused myotubes with four or more nuclei in unsorted control plates, 82.7 ± 3.74%, was significantly increased to 92.3 ± 2.04% in Channel 1 plates ($p < 0.001$, Figure 3D).

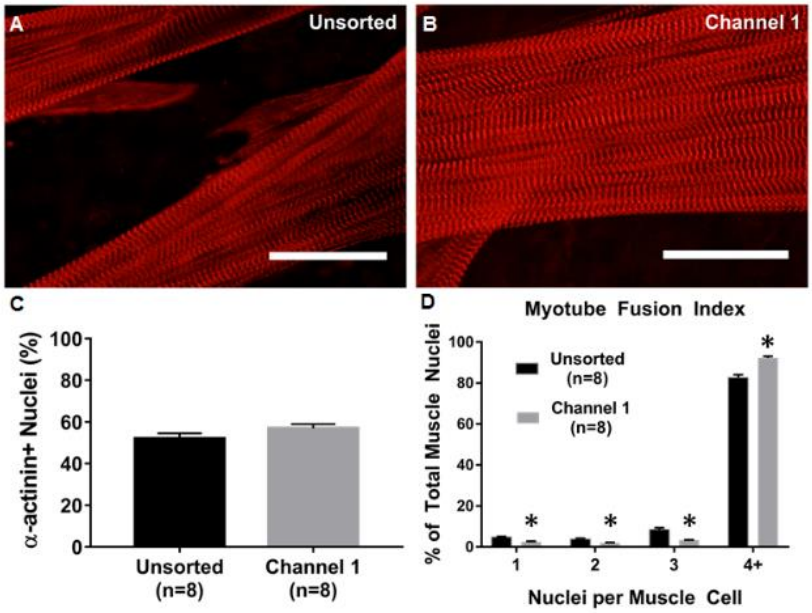

Figure 4.3 Structural Maturation following Microfluidic Sorting.
(A&B) Advanced sarcomeric structure within highly-aligned myofibrils, evident from immunostaining for α-actinin, was observed on Day 11 in both unsorted controls and Channel 1 plates. Scale Bar = 50 μm. (C) No significant difference was recorded in the total nuclei associated with α-actinin-positive muscle cells ($p = 0.142$). (D) Quantification of myotube fusion index, the percentage of muscle cells with either 1, 2, 3, or 4+ nuclei, indicated greater fusion following microfluidic sorting. In particular, the percentage of fully fused myotubes with 4+ nuclei significantly increased from 82.7 ± 3.74% in unsorted controls to 92.3 ± 2.04% in Channel 1 ($p < 0.001$). * Indicates statistical difference from control.

Further analysis of the myotube network was performed on Day 14 of the fabrication protocol using light microscopy. The average myotube diameter in unsorted controls (n = 10) was 16.0 ± 1.31 μm. This value was nearly identical ($p = 0.938$) to the myotube diameter of 16.18 ± 1.38 μm in cells sorted into Channel 1 (Figure 4.4). In contrast, the density of the myotube networks in unsorted and sorted samples exhibit a stark difference. Specifically, unsorted control

plates averaged 18.6 ± 3.26 myotubes/mm^2, whereas cells sorted into Channel 1 formed a significantly denser network (p = 0.004) averaging 33.9 ± 3.74 tubes/mm^2.

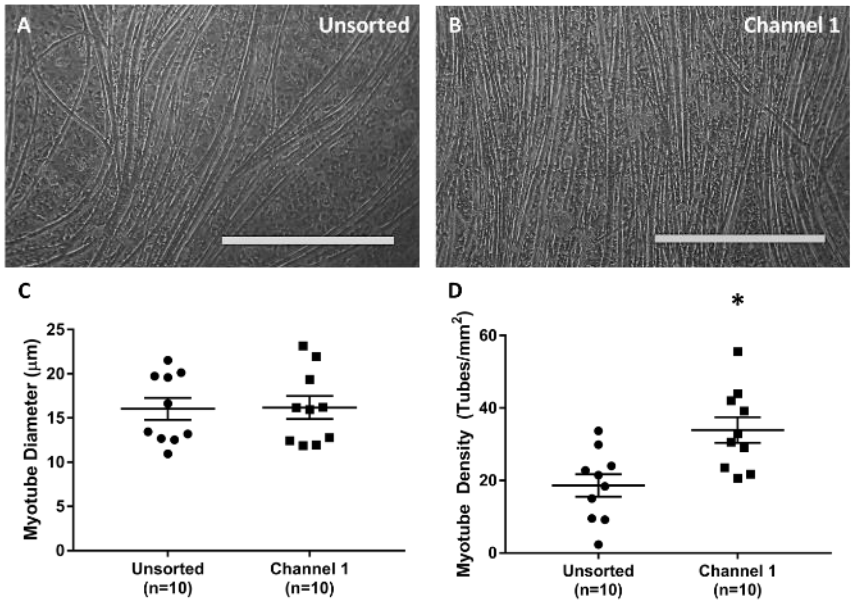

Figure 4.4 Effects of Microfluidic Sorting on Myotube Growth.
Shortly before delamination, light microscopy images were captured on Day 14 to assess the size and density of myotubes within the developing muscle monolayer. (A&B) Representative images of monolayers from unsorted cells and cell sorted into Channel 1. Scale Bar = 500 μm. (C) The average myotube diameter was indistinguishable between the two groups: 16.0 ± 1.31 μm in controls and 16.18 ± 1.38 μm in Channel 1 (p = 0.938). (D) Channel 1 cells, however, exhibited a significantly denser myotube network (p = 0.004), with 33.9 ± 3.74 tubes/mm2 in comparison to 18.6 ± 3.26 myotubes/mm2 in unsorted controls. * Indicates statistical difference from control.

4.4.5 Force Production in 3D SMUs after Microfluidic Sorting

Finally, overall function of engineered SMUs was assessed by contractile force production on Day 16, following monolayer delamination and capture in 3D form. As shown in Figure 4.5, the peak isometric tetanic force production in unsorted control SMUs (n = 8) of 70.7 ± 8.03 μN was significantly increased (p = 0.002) approximately two-fold to 143.6 ± 16.9 μN in SMUs fabricated from cells sorted into Channel 1 of the Labyrinth microfluidic device.

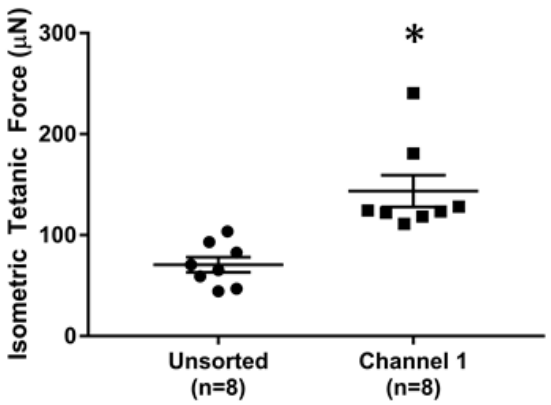

Figure 4.5 SMU Functional Development with Microfluidic Sorting.
Functional measurement of isometric tetanic force in 3D SMUs on Day 16 indicated a significant effect of sorting: unsorted control SMU force production of 70.7 ± 8.03 μN was significantly increased ($p = 0.002$) approximately two-fold to 143.6 ± 16.9 μN in Channel 1 SMUs. * Indicates statistical difference from control.

4.5 Discussion

[137]Cells separated with microfluidic sorting were analyzed to assess effects on the myogenic purity of the isolated population, along with capability for subsequent proliferation, differentiation, and function. Immediately following microfluidic sorting, two-fold enrichment of the myogenic population was observed in Channel 1 of the Labyrinth device. This enrichment was expected based on the design of the Labyrinth device for focusing smaller particle and cells, including satellite cells and myogenic progenitors, into Channel 1. In contrast, the fibroblast population was enriched in Channels 2, 3 and 4. Again, this result was intended, since the Labyrinth was designed to focus the larger fibroblasts into these channels. A minority population of fibroblasts was present in Channel 1, however, and a similar population of myogenic cells was captured in Channel 2, indicating that microfluidic sorting did not occur with maximal efficiency. It is expected that the overlap in the size distributions of satellite cells (8-13 μm [135, 141]) and of fibroblasts (10-22 μm [148, 149]) led to this reduced sorting efficiency. Alternatively, large

aggregates of undigested, fibrillar extracellular matrix debris was observed in the microfluidic device during sorting and in outlet Channels 3 and 4 (data not shown). This debris may have impeded fluidic focusing of the different cell populations and reduced the overall sorting efficiency. Nevertheless, the majority of satellite cells and fibroblasts were consistently separated as desired by the Labyrinth device.

After microfluidic sorting, cells separated into Channel 1 were not adversely affected by the high shear forces imposed during flow through the Labyrinth device. These sorted cells exhibited similar overall proliferation to unsorted cells, in addition to improved myogenic proliferation and suppression of non-myogenic proliferation. We know that these sorted cells were more myogenically pure at seeding from our ICC analysis immediately after microfluidic separation, and observation of improved myogenic proliferation confirms this result. Improved myogenesis continued as sorted cells differentiated and fused to form skeletal muscle myotubes. Increased myoblast fusion index was observed in cells sorted into Channel 1, resulting in a denser network of myotubes in the differentiation phase of SMU formation. Additionally, structural maturation of the muscle monolayers, indicated by advanced sarcomeric structure within highly aligned myofibrils, was observed in both unsorted control and Channel 1 plates. Ultimately, these improvements in myogenic proliferation and differentiation translated to greater force production in SMUs fabricated from Channel 1 cells. In conclusion, microfluidic sorting efficiently separated satellite cells and fibroblasts while improving the capability for myogenic proliferation, differentiation, and function.

Microfluidic sorting, as demonstrated in this study, offers an alternative approach to purification of satellite cells enzymatically digested from a muscle biopsy. The most comparable approach, pre-plating to remove rapidly adhering non-myogenic cells, can achieve greater than

80% myogenic purity [137]. The primary drawbacks to pre-plating, however, are the length of time required (5 days) and the potential for decreased cell yields. Recently, purification of isolated satellite cells through FACS has gained popularity due to its ability to rapidly sort Pax7+ satellite cells with greater than 90% purity [138, 139]. With FACS, labelling with exogenous dyes is required, and incubation with these antibodies decreases throughput. Microfluidic sorting has the potential to fill a niche distinct from these established methods. Although the myogenic purity of cells separated with the Labyrinth devices was slightly lower at 75%, the sorting process was label-free and required approximately 5 minutes. For tissue engineers, this high-throughput and label-free purification process presents an exciting alternative.

CHAPTER 5 Other Applications of Labyrinth in Transformative and Collaborative Projects for High Throughput Size-Based Cell Separation

5.1 Abstract

Improvement in pancreatic cancer treatment represents an urgent medical goal that has been hampered by the lack of predictive and biomarkers. Circulating Tumor Cells (CTCs) may be able to overcome this issue by allowing the monitoring of therapeutic response and tumor aggressiveness through *ex vivo* expansion. The successful expansion of CTCs is challenging due to low number in blood and the high contamination of blood cells. Here, we explored the utility of pancreatic CTC cultures as a preclinical model for treatment response. CTCs were isolated from newly diagnostic and locally advanced pancreatic cancer patients disease using the Labyrinth device and expanded three CTC samples in adherent and spheroid cultures. Proliferation and CTC phenotype were evaluated in culture and compared to the original patient specimen. Additionally, we evaluated take rate and metastatic potential in vivo and examined the utility of CTC lines for cytotoxicity assays. Our results demonstrate that CTC cultures are possible and provide a valuable

resource for translational pancreatic cancer research while also providing meaningful insight into the development of treatment resistances and distant metastasis.

5.2 Motivation

Labyrinth was developed as a high throughput, high performance, and truly label-free platform for the isolation of breast cancer CTCs to enable the genomic analysis at single cell level. However, the application of Labyrinth is not limited to the research in breast cancer, and is even further beyond the study of CTCs. Labyrinth is capable of isolating small cells or particles (7-12 μm) from larger ones, making it an efficient microfluidic approach for cell purification from different size classes. Labyrinth is widely adopted in Nagrath lab for the isolation of CTCs from various types of cancers, including but not limited to adenoid cystic carcinoma (ACC), hepatocellular carcinoma (HCC), lung, and pancreatic cancers. Besides enumeration, the isolated CTCs were also used in a wide range of studies, such as *ex vivo* culture of live CTCs from pancreatic patients and generating xenograft tumor model in mice from expanded CTCs.

In this part of thesis described below, I participated in the pancreatic cancer projects in which Labyrinth technology developed by me was incorporated. In these projects, I played a critical role in determining the optimal operating parameters, resolving technical issues, and optimizing experiment protocols.

Pancreatic cancer is the third leading cause of cancer-related death in the United States [159]. In fact, its survival probability has not improved substantially over nearly 40 years [159, 160]. While surgical removal of the tumor represents the best treatment option for pancreatic cancer patients, only 20% of patients qualify for surgery [160, 161]. Chemotherapy or chemotherapy combined with radiation is typically offered to patients with locally advanced disease [161, 162].

A major challenge in the management of these patients is the early assessment of response to therapy that would allow the selection of the appropriate therapy and limit toxicity in treatment-resistant patients. Computed tomography (CT) is routinely used to stage and reassess patients following treatment. However, a number of studies have demonstrated that CT-detected treatment responses are infrequent [163]. Obtaining tissue from pancreatic cancer patients with locally advanced disease for histological diagnosis and acquiring pre- and post-monitoring presents a substantial challenge.

Over the past few years, several studies have studied circulating tumor cells (CTCs) in many epithelial cancers and suggested that CTCs can be used as clinical biomarkers of treatment response and prognosis [164-170]. CTCs are cancer cells that have shed into the vasculature or lymphatics from a primary tumor and are carried around the body in the circulation. CTCs are believed to have the potential to develop into distant metastases, which are the major cause of cancer related mortality. However, the isolation of viable CTCs is an actively research area with limited success. Hence, the dire need of such technologies hamper culture approaches.

The current gold standard for CTC isolation is the CellSearch™ system, which uses magnetic beads functionalized with antibodies against the epithelial cellular adhesion molecule (EpCAM) [170-172]. Due to the use of antibodies for CTC capture, this system fails to detect cancer cells with reduced EpCAM expression and may thus only enrich a small subpopulation of CTC [173-176]. Hence, to address the shortcomings of the FDA-approved CellSearch™ system, the development of new technologies with higher sensitivity is desired. This can be overcome by the use of microfluidic technologies that allow for unprecedented spatio-temporal control of cells [168]. Their application in cancer research is now well established [177] with a number of studies demonstrating successful isolation and characterization of CTCs from clinical samples [178].

Microfluidic CTC isolation technologies are mainly categorized by their exploitation of either CTCs' distinctive (i) biological properties or (ii) physical properties [177]. The former is based on the expression of cell surface markers, while the latter includes size, deformability, density, and electric charge [179]. The use of CTCs' physical properties to develop microfluidic devices allows label-free isolation, which overcomes biased cell selection using the CTCs' biological properties, such as protein expression and molecular markers. Furthermore, isolated cells using label-free technology are not modified, which permits greater flexibility for downstream characterization of CTCs. In summary, advances in label free microfluidic technologies allow the reliable detection and isolation of CTCs from clinically available blood draws. This will in turn allows functional characterization of CTCs to understand the utility of CTCs as predictive and prognostic markers and may serve as a surrogate tumor biopsy. However, previously reported clinical studies have mostly focused on CTC enumeration in guiding prognosis in metastatic cancer patients, and current research is exploring the pharmacodynamic and predictive biomarker utility of CTCs.

A number of studies have isolated and evaluated CTCs in patients with pancreatic adenocarcinoma [180]. Early studies identified CTCs in pancreatic cancer patients with metastatic disease using several tumor cell markers including CK20, CEA, and c-MET and demonstrated that compared to other types of malignancies, these patients have relatively low numbers of CTCs [181-185]. Recent reports have concentrated on CTCs in patients with locally advanced pancreatic cancer. Ren et al. examined CTCs in 31 patients with stage III and nine patients with stage IV pancreatic cancer. Eighty percent of these patients were found to have CTCs prior to chemotherapy, and this number decreased to 29% after treatment [186]. Bidard et al. analyzed blood samples of 79 patients with locally advanced pancreatic cancer treated on a clinical trial for

CTC detection. This study identified CTCs in only 11% of patients; however, the presence of CTCs was associated with poor outcome [170].

Beyond CTC enumeration, an *ex vivo* expansion and functional characterization of patient-derived CTCs will help to elucidate the clinical application of CTCs in pancreatic cancer. Due to their low frequency in pancreatic cancer patients [180] expanding such cells becomes a dire need of any CTC study. To our knowledge, no CTC cultures in pancreatic cancer have been reported. However, some success has been reported across other types of cancers using affinity based approaches. In breast cancer, CTC cultures were reported by Yu et al. using the CTC-iChip [187]. Cultures were done under hypoxic and non-adherent culture conditions, achieving success for 6/36 breast samples. In colon cancer, Cayrefourcq et al. was also able to expand CTCs from 2/71 colon cancer patients [188]. Our own research group reported CTC culture in lung cancer using a microfluidic co-culture device, where 14 out of 19 samples were expanded [189]. While these technologies have shown the ability to expand CTCs, the inherent biased CTC selection of immunoaffinity based technologies limits the *ex vivo* functionality study of all distinct subpopulations of CTCs.

In order to further validate the utility of expanded CTCs, researchers have started developing CTC-derived xenografts (CDX) models. Such models serve as a method to examine expanded CTCs' in vivo properties including tumorigenicity and drug susceptibility. For example, Cayrefourcq et al. showed the generation of colon tumors from a CTC-derived cell line in immunodefficient mice [188]. In breast cancer, Yu et al. successfully established five CTC cell lines, where three were tumorigenic in mice [187]. In small-cell lung cancer, Hodgkinson et al. demonstrated that CTCs from patients with either chemosensitive or chemorefractory tumors are tumorigenic in immune-compromised mice. Furthermore, their findings mirrored the donor

patient's response to platinum and etoposide chemotherapy [190]. In order to successfully perform these in vivo CTCs studies, a high initial concentration of CTCs was required (>106 cells) for all studies, making CTC expansion essential.

Recently, we developed and optimized a microfluidic device, the “Labyrinth”, for the high throughput label free isolation of CTCs, which takes a hydrodynamic approach for the size based isolation of CTCs (Chapter 1). The Labyrinth is an inertial microfluidics based separation technology that demonstrated greater than 90% recovery when tested with various cell lines including pancreatic cancer cell lines, while achieving an 89% WBC removal. In our approach, since no positive or negative selection of cells is needed, the Labyrinth enables the study of CTC heterogeneity and allows the identification of multiple CTC subpopulations through further downstream biological and functional studies. Our study showed the presence of CTCs that have undergone the epithelial-to-mesenchymal transition (EMT) across all pancreatic cancer patients. The use of our label free Labyrinth device enables the study on viable EMT-like CTCs, which are believed to be the most aggressive subtype of CTCs [191-193]. Building upon our previous expansion work on lung cancer, this study uses the Labyrinth to expand CTCs using a monoculture approach to maintain the simplicity of the Labyrinth by eliminating the need of CTC purification from other cell lines.

In the present study we explore the utility of pancreatic CTC cultures as a preclinical model for treatment response. CTCs were isolated from the blood of pancreatic cancer patients with locally advanced disease using the Labyrinth and expanded *in vitro*. CTC cultures were then characterized in both 2D (adherent) and 3D (spheroid) conditions. Such characterization was performed through the examination for epithelial and EMT features and compared to the original patient specimen. Furthermore, we evaluated tumorigenicity *in vivo* by injecting cultured CTCs

into a NOD/SCID mice, thus creating a pancreatic CDX model. To our knowledge, these are the first ever pancreatic CTC cultures developed from pancreatic patient samples. The isolation and expansion of CTCs can provide meaningful information to elucidate the process of pancreatic tumorigenesis and dissemination to preempt its fatal result.

5.3 Methods

5.3.1 Patients

10 ml of whole blood for CTC extraction was obtained from ten patients with locally advanced pancreatic cancer as part of an Institutional Review Board approved protocol (HUM00085016). Informed consent was obtained from all participating patients.

5.3.2 CTC isolation using Double Labyrinth

Red blood cells were removed from the samples using density separation (6% dextran solution, M.W. 250,000) prior to the labyrinth. The sample-dextran solution was kept still in room temperature (RT) for 1h to sediment the red blood cells. The supernatant was removed and diluted with PBS buffer at a 1:3 ratio. Samples were then processed through the pre-flowed labyrinth, at a flow rate of 2.5mL/min. To achieve higher purity all the second outlet product for all samples were diluted 1:2 samples and run through another labyrinth. The purified CTCs were used for characterization by immunofluorescence and culture.

5.3.3 CTC culture

The output from second outlet was processed using a RBC lysis buffer at a 2:1 (buffer:sample) and incubated on ice for 3min. Samples were then spun down and the pellet

resuspended in culture medium (RPMI1640) supplemented with 10% FBS and 1% antibiotics. For adhered cultures, the cell suspension was plated into fibronectin coated 24 well plates. For spheroid cultures, CTCs were seeded on hanging drop array plates with 10cells/drop using serum supplemented RPMI. Confocal microscopy for live/dead staining using calcein and ethidium homodimer at Day 14, indicate high viability within CTC spheroids.

For growth curve analysis, CTC cultures were seeded in 96 well dishes at 1000 cells per well. Cell proliferation was evaluated using Alamar blue per the manufacture's guidelines for 6 days. Absorption was measured using the Biotek-Synergy Neo-Plate reader.

5.3.4 Immunofluorescence staining

CTCs were processed using Thermo Scientific™ Cytospin 4 Cytocentrifuge according to the manufactures guidelines. Cytoslides were fixed using 4% PFA and stored at 4°C until staining.

For immunostainings, samples were permeabilized with 0.05% PBST solution for 15min and blocked using 20% donkey serum for 30min at RT. A cocktail of primary antibodies was added and incubated at 4°C in a humidified chamber overnight. Samples were incubated in dark with secondary antibodies for 45min at RT and mounted with Prolong Gold () with DAPI. CTCs were classified PanCK and DAPI positive and CD45 negative. White blood cells (WBC) were considered to be CD45 and DAPI positive.

Slides with spheroid sections were deparaffinized and rehydrated by dipping three times in xylene, two times in 100% ethanol and once each in 95% and 70% ethanol. Antigen retrieval was performed by boiling slides in citrate buffer (pH=6.0) for 10min. Chamber slides with cultured cells were fixed with 4% Paraformaldehyde (Electron Microscopy Sciences) for 10min and then washed with PBS. Samples were then permeabilized with ice-cold 1:1 Methanol:Acetone for 1min and washed with PBS. Blocking buffer consisting of 5% goat serum (Sigma Aldrich) diluted in

PBS was applied at room temperature for 30min to prevent non-specific adhesion. Monoclonal anti-vimentin (5µg/ml, Thermo Fisher: MA1-10459) was diluted in blocking buffer and applied to samples overnight at 4oC. Samples were washed 3 times for 5minwith PBS. Goat anti-mouse IgM CF770 (4µg/ml, Biotium: 20385), anti-Pan-Keratin Alexa Fluor 555 (0.64µg/ml Cell Signaling Technology: 3478S), anti-EpCAM APC (0.24µg/ml BD Biosciences: 347200), anti-CD44 BV510 (1µg/ml, BioLegend: 103043), and anti-CD45 FITC (1µg/ml, BioLegend: 304005) were diluted in blocking buffer and applied to samples overnight in a refrigerator at 4oC. Samples were again washed 3 times for 5min with PBS. DAPI (1µg/ml, Thermo Fisher) diluted in PBS was applied for 10min at room temperature to label nuclei. A drop of Prolong® Diamond Antifade Mountant (Thermo Fisher) was then added and coverslips were mounted onto the slides for imaging.

5.3.5 Flow cytometry

Cells were trypsinized, washed with ice-cold PBS, and fixed at a concentration of 2 × 106 cells/ml in ice-cold 70% ethanol. For γH2AX analysis, samples were incubated with a mouse anti–γH2AX-specific antibody (clone JBW301; Millipore) overnight at 4°C followed by incubation with a fluorescein isothiocyanate–conjugated secondary antibody (Sigma). For quantification of γH2AX positivity, a gate was arbitrarily set on the control, untreated sample to define a region of positive staining for γH2AX of approximately 5%. This gate was then overlaid on the treated samples. Samples were stained with propidium iodide to measure total DNA content and analyzed on a FACScan flow cytometer (Becton Dickinson) with FlowJo software (Tree Star).

5.3.6 Immunohistochemistry

Xenograft tumors were excised, fixed and paraffin embedded. Paraffin tissue sections were cut, dried and dewaxed. Endogenous peroxidase was blocked in 3% hydrogen peroxide for 10 min.

Microwave antigen retrieval was carried out under pressure at 120C for 10 min in 10 mM Citrate buffer, pH 6.0 using a T/T Mega microwave oven. Endogenous biotin was blocked in Vector's biotin blocking kit, and then slides were labeled with primary antibodies to cytokeratin (DAKO, Glostrup, Denmark, AE1/AE3, 1:200) and Smad4 overnight. Biotinylated anti-mouse IgG incubations were carried out followed by streptavidin biotin detection system (Signet Pathology System, Deham, MA, USA) for 30min each Immunoreactivities were revealed by incubation in Nova Red substrate (Vector Lab, Burlingame, CA, USA) for 5min and counterstained in Mayer's haematoxylin.

5.3.7 Cell Proliferation Assay

Cultured cells were seeded at a concentration of 500 cells/well in 100µL of RPMI media into 96 well plates. Cells were incubated from 1-6 days at 37ºC and 5% CO_2. 10µL/well Cell Proliferation Reagent WST-1 (Roche) was added and incubated for 1h and. Plate shaken for 1min on a shaker. The absorbance was measured at an emission wavelength of 450nm, using a BioTek-Synergy Neo multi-purpose plate reader.

5.3.8 Treatments

Cultured cells were seeded at a concentration of 1000 cells/well in 100 µL of RPMI media into 96 well plates. Cells were incubated for 24h at 37ºC and 5% CO2. Media was exchanged for Gemcitabine (0, 0.05 0.1, 0.5, 1, 5 uM) or 5-FU (0, 1, 5, 10, 50, 100 uM) diluted on RPMI media. Cells were incubated for 24h, the media was replaced and cells cultured for 48h. 10µL/well Cell Proliferation Reagent WST-1 (Roche) was added and incubated for 1h. Plate was then shake for 1min on a shaker. The absorbance was measured at an emission wavelength of 450nm, using a BioTek-Synergy Neo multi-purpose plate reader.

For radiation treatments, cells were treated with a single dose of 4Gy at 60% confluency and fixed for flow cytometry 16h after treatment. For gemcitabine treatments, cells were treated with 100nM gemcitabine for 2h and fixed for flow cytometry 22h after treatment.

5.3.9 Xenografts

Animal experiments were carried out using protocols approved by the University Animal Care Committee (PRO00006457) under the guidelines of the Association for Assessment and Accreditation of Laboratory Animal Care.

For CTC xenografts, 106 cells were injected subcutaneously into the flank of 4-5 week old NOD/SCID mice. Tumors were grown until the humane endpoint of ~1cm in diameter or distress due to ascites or metastasis. Tumor size was evaluated twice a week using calipers.

5.3.10 STR Fingerprinting

The UM DNA Sequencing Core performed cell identity verification using the Applied Biosystems IdentifilerPlus kit to assess CODIS markers. DNA testing was performed according to manufacturer's recommended protocols. Resulting fragments were assessed on an ABI 3730XL Genetic Analyzer. Analysis of resulting electropherograms were performed using ABI GeneMapper V5.0 software, as per manufacturer's recommended protocols.

5.4 Results

5.4.1 Isolation of CTCs from pancreatic cancer patients using single Labyrinth

CTC analysis was performed using blood samples collected from 20 patients with a new diagnosis of pancreatic cancer, as shown in Figure 5.1A. These whole blood samples were all

processed without any pre-processing as described in methods. All of the samples had measurable CTCs, identified as DAPI positive nucleated cells staining positive for CK-19 and negative for CD45. CTC Enumeration in these twenty patients showed a yield of 51.6 ± 25.5 pancreatic CTCs per mL blood, whereas less than 2 CTC-like cells/mL were found in healthy controls.

Pancreatic CTCs were further evaluated to determine what percentage of the cells displayed epithelial versus mesenchymal-like features. To quantitate epithelial-like cells, expression of EpCAM and CK-19 was assessed, while for quantification of mesenchymal-like cells, the EMT markers ZEB1 and ATDC were used. All patient samples contained not only CK+ CTCs but also EMT marker positive CTCs. An average of 53 ± 17% of the captured CTCs stained positive for EMT-related markers along with CK-19. Figure 5.1B presents three CTC subpopulations obtained from the same patient differentially expressing epithelial and mesenchymal markers, demonstrating intra-patient CTC heterogeneity. The molecular characteristics of CTCs were further explored by mutational analysis of select genes using the DNA isolated from captured CTCs. DNA was extracted from CTCs isolated from five pancreatic patient samples. The qBiomarker Somatic Mutation PCR Array: Human Pancreatic Cancer (Qiagen) was chosen to represent a comprehensive spectrum of frequently mutated genes in pancreatic cancer. The array includes multiple assays for genes including APC, BRAF, CDKN2A, CTNNB1, KRAS, NRAS, PIK3CA, SMAD4, and TP53. Using this array, mutations in at least one gene were detected in all samples tested. All of the samples tested were positive for mutations in KRAS, which is mutated in not only PDAC patients (>95%), but also in pancreatic intraepithelial neoplasias (PanINs), the earliest pre-neoplastic stages of pancreatic cancer progression. As expected, no mutations were detected in the healthy control.

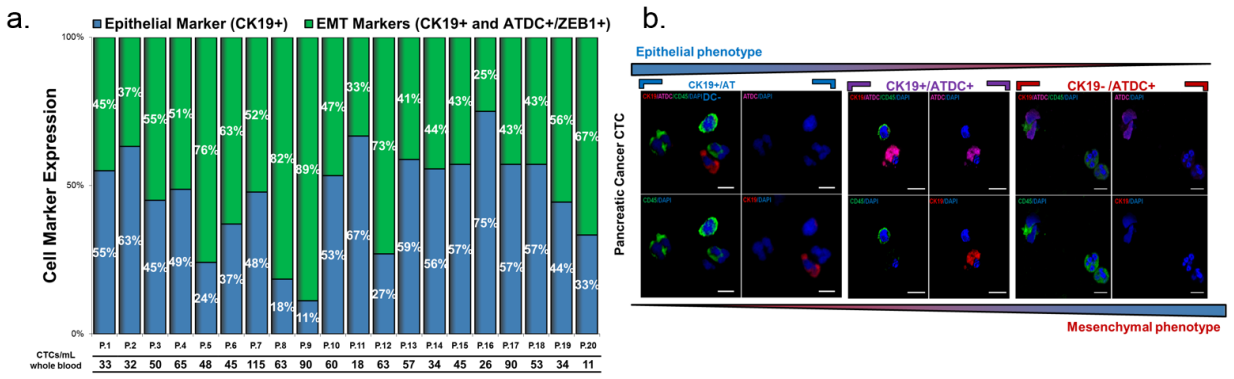

Figure 5.1 Results of pancreatic cancer patient samples using Labyrinth.
(A) Percentage of CTCs expressing both EMT and epithelial markers vs only epithelial markers. Column on the bottom indicates the total CTCs (CK+, CD45-, DAPI+) per mL of blood for each patient. (B) Immunocytochemistry analysis performed on a metastatic sample where both epithelial and EMT-like CTC subpopulations were found. Scale bar 10 µm.

5.4.2 Isolation of patient-derived pancreatic circulating tumor cells

9-10 ml of whole blood were obtained from 10 patients with locally advanced pancreatic cancer prior to the start of therapy and CTCs were isolated based on size using the continuous high throughput label free Labyrinth device (Figure 5.2A). The isolated CTCs were divided in order to: (1) enumerate CTCs (~15% of isolated CTCs) and (2) set up a CTC culture (~85% of isolated CTCs). Similar to previous studies [180], we observed a wide range of CTC numbers from different patients. CTC numbers ranged from 8 cells/ml in patient 4 to 83 cells/ml in patient 2 (Figure 5.2B).

Since the EMT is believed to be essential for the generation of metastatic cells, we examined the presence of EMT-like and epithelial cells in enriched CTC samples. (Figure 5.2C). The majority of patients (6/10) show both EMT- like and epithelial cells in the purified CTC samples. Nevertheless, EMT-like cells represent the majority of CTCs. Only EMT-like cells were observed in the remaining 4 patients.

We were able to obtain a second blood sample from three of the patients (patient 1, 2, 4). This sample was taken after the first round of chemotherapy. The epithelial CTC fraction was lost in all three patients in response to chemotherapy, suggesting that CTCs can be used to monitor treatment response (Figure 5.2D).

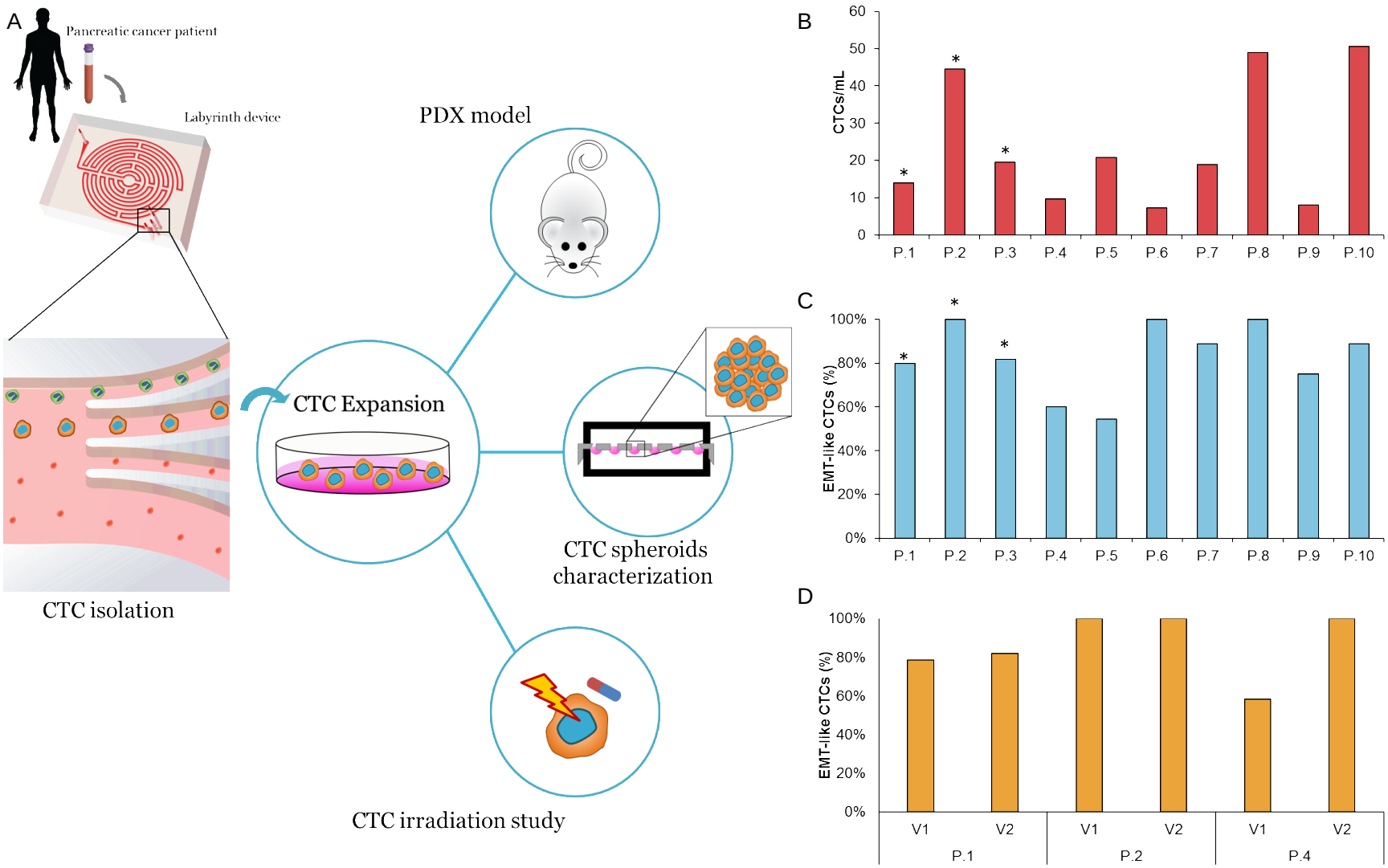

Figure 5.2 Characterizing patient-derived pancreatic CTCs
(A) Workflow of CTC extraction, culture and subsequent analysis. (B) CTC/mL enumeration for 10 PDAC patients. Asterisk marks the samples that were successfully expanded. (C) Co-expression percentage of cytokeratin and vimentin of CTCs isolated from 10 PDAC patients and (D) two consecutive visits of 3 patients prior to treatment and after the first course of chemotherapy.

5.4.3 Circulating tumor cell culture

Purified CTCs of all 10 patients were seeded onto fibronectin coated 24 well plates in order to generate CTC-derived cell lines. We were able to generate CTC-derived cell line from 3 individual patients (patient 1, 2 and 3). The majority of samples did not grow into stable CTC-derived cell lines. We observed an outgrowth of WBCs in one of the patients, while the remaining samples showed no growth or lost proliferation potential after the first passage.

The three CTC-derived cell lines display distinctly different morphologies in culture that are consistent with the morphology observed in pancreatic cancer cell lines (Figure 5.3A). We observed differences in growth rate that remain stable over a number of passages (Figure 5.3B). Similar to what we observed in the original CTC specimen, the cultures display a mixture of EMT-like and epithelial cells, which can be observed through differences in morphologies within cells of the same patient as well as staining for the respective markers (Figure 5.3A, C). Patient 3 showed no presence of epithelial cells in the original CTC specimen. The CTC-derived cell line from this patient, however, shows both epithelial and EMT-like cells (Figure 5.2C, 5.3C). This may be attributed to either a sampling related error due to low frequency in the original specimen or to a morphological drift that is related to the culture conditions.

Established CTC-derived cell lines were seeded on hanging drop array plates with 10cells/drop in order to evaluate their ability to form spheroids (Figure 5.4A). All cell lines formed spheroids within 14 days, although we observed difference in growth rates across the three sample, which was similar to that of observed in the adherent cultures (Figure 5.3B). H&E section of the spheroids show a patient-specific morphology that is consistent with the range of morphologies observed in pancreatic cancer (Figure 5.4B). Staining for the EMT maker vimentin and the

epithelial marker cytokeratin show a mix of both populations that is similar to what we observed in the adherent cell lines (Figure 5.4C).

In order to verify the identity of the CTC-derived cell lines, we used STR fingerprinting to compare WBC and with the corresponding CTC-derived cell line. Additionally, we also included WBC cell line that came up during a CTC culture attempt in one of the patients. The WBC cell line showed a perfect match (15/15 markers) when compared to WBC extracted from the buffy coats of the patients archived blood sample. The CTC-derived cell lines, however, show very little match with their corresponding WBCs (patient 1: 2/15, patient 2: 1/15, patient 3: 1/15). We do observe high similarities between CTC cell lines of different patients (8-13/15 markers), suggesting a selection towards a similar phenotype.

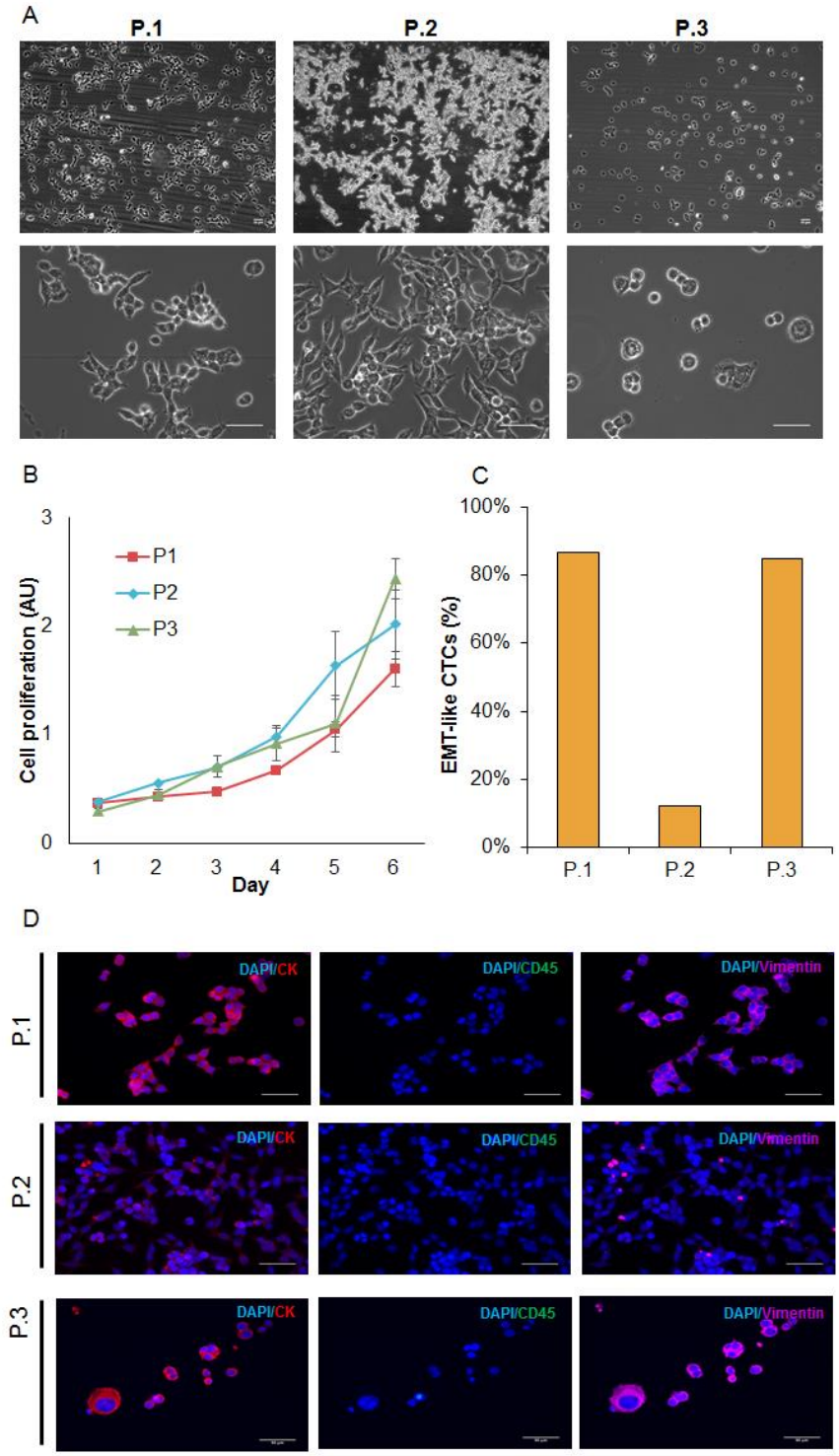

Figure 5.3 Characterizing CTC-derived cell lines
(A) Brightfield images (10x and 40x) of expanded CTC cultures. (B) Growth curve analysis of adherent CTC cultures (n=3). (C) Percentage of EMT-like CTC in adherent cultures. (D) Representative images of immunofluorescence staining using cytokeratin (red)/vimentin (magenta)/CD45 (green)/DAPI (blue)

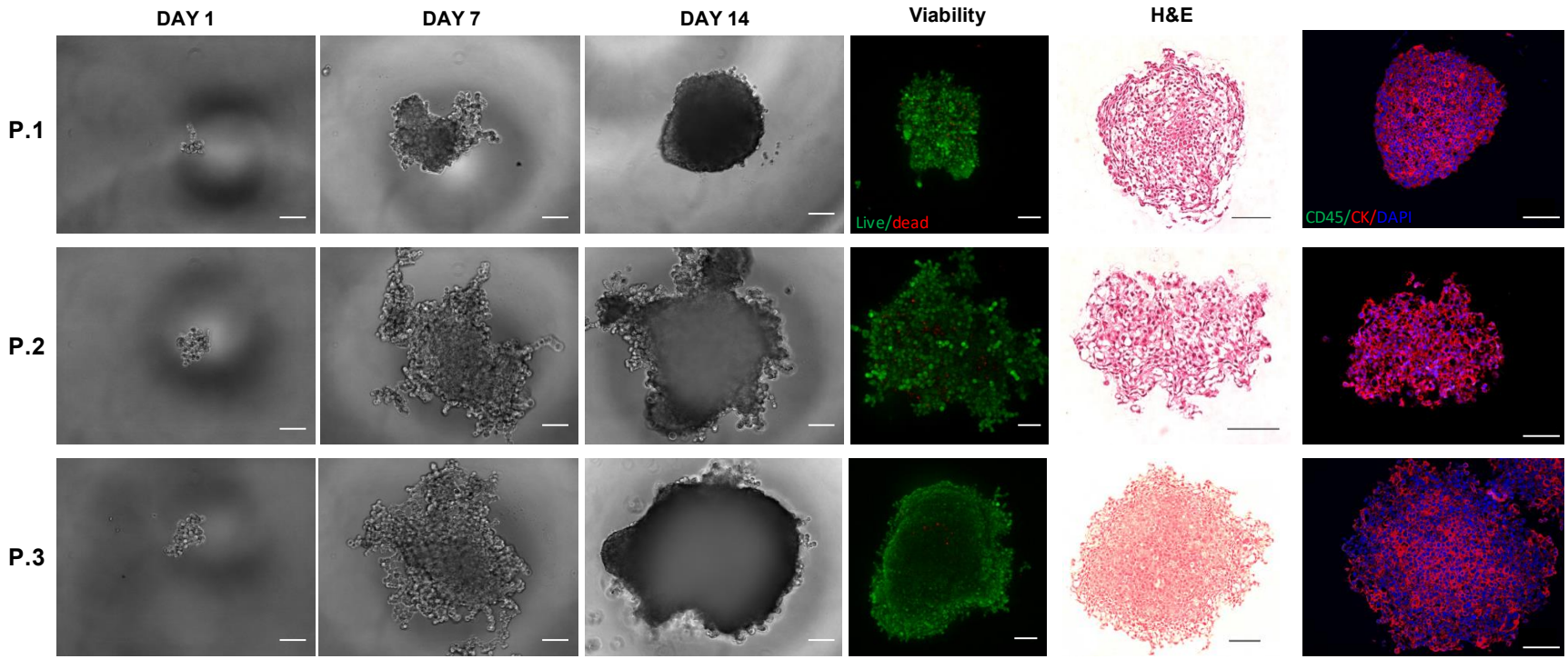

Figure 5.4 Characterization of the CTC-derived spheroid cultures

(A) Pancreatic CTCs were seeded on hanging drop array plates with 10 cells/drop. Alamarblue fluorescence was used to monitor viability/proliferation (expressed as a fold increase at Day 7 and Day 14, compared to Day 1). (B) Representative images of live/dead staining using calcein and ethidium homodimer at Day 14, indicate high viability within pancreatic CTC spheroids. (C) Representative images H&E of spheroids. (D) Immunoflourescence staining for cytokeratin (red), CD45 (green) and DAPI (blue) on spheroids. (Scale bar = 100μm)

5.4.4 Molecular Characterization of CTC PDX

In order to investigate whether the CTC cell lines maintained the ability to form tumor *in vivo* that preserved the morphological characteristics of pancreatic tumors, the CTC cell line derived from patient 3 was injected into the flanks of 4-5 week old NOD/SCID mice.

We observed the appearance of tumors in all injected mice 3-4 weeks after injection of 10^6 cells (Figure 5.5A). Tumors were harvested when the tumor size reached the humane end point. At that time, we observed wide spread metastasis from the subcutaneous injection site to a number of organs, including liver, peritoneum and pancreas, as well as the development of ascites (Figure 5.5A, B).

Pancreatic tumor masses were observed in 75% of the injected animals. Although some pancreatic tissue remained, the majority of the pancreas had been overtaken by tumors (Figure 5.5E). These tumors displayed large areas of tumor-associated stroma that are characteristic for the desmoplastic reaction typically observed in pancreatic cancer.

Smad 4 staining was observed throughout the subcutaneous tumors (Figure 5.5F). We did however observe a reduction in staining intensity in areas of pleural invasion. While Smad4 staining was lost in macro and micro metastases of the liver (Figure 5.5G), the expression was preserved in the pancreatic masses (Figure 5.5H). Similar to the subcutaneous tumors, staining intensity was reduced in areas of tissue invasion when compared to the tumor bulk.

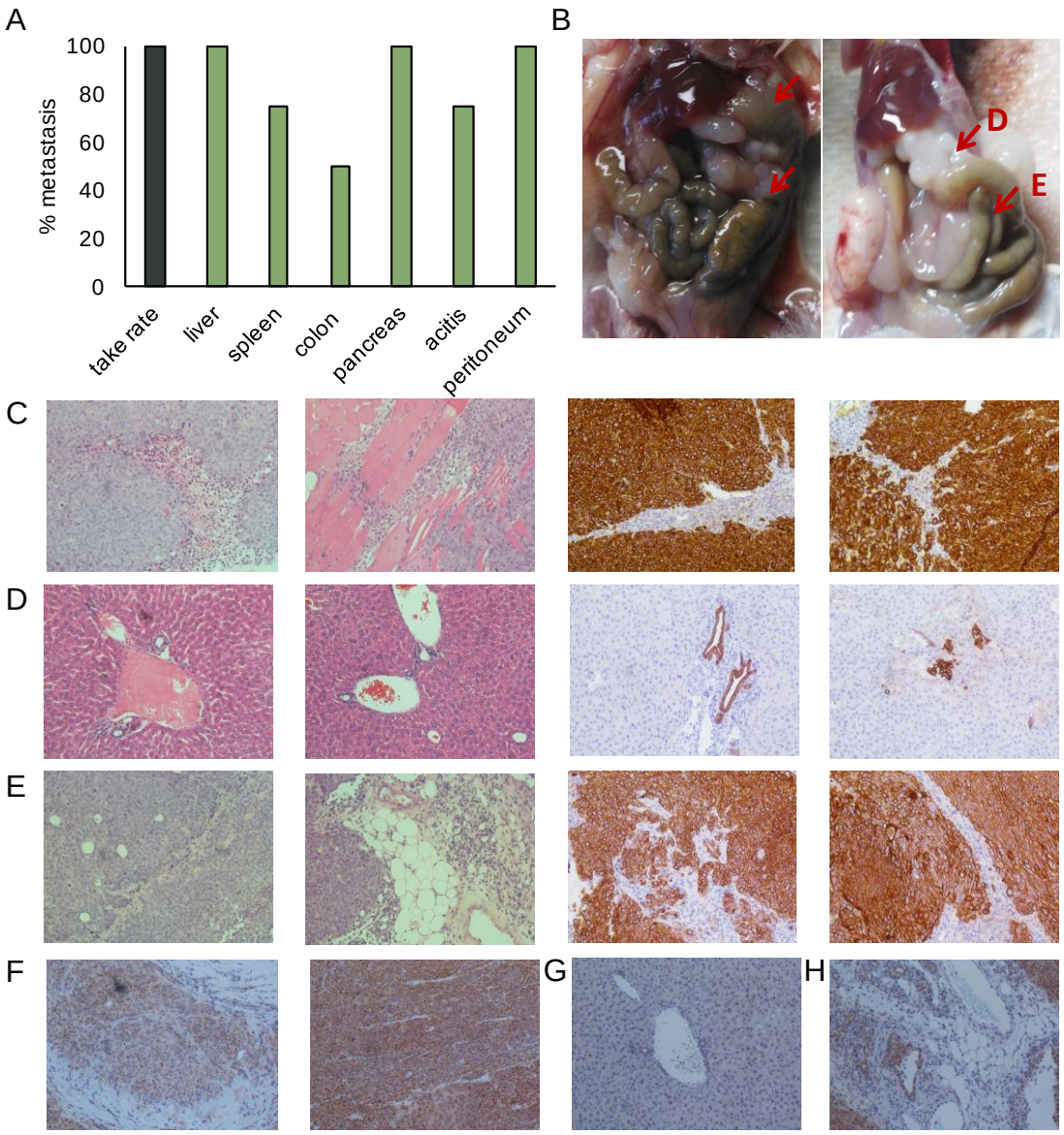

Figure 5.5 Characterization of the CTC PDX.
(A) Injection of the CTC cell line derived from patient 3 into the flanks of NOD/SCID mice resulted in the development of subcutaneous tumors in all injected mice. Additionally, we observed wide spread metastases and the development of ascites. (B) Representative images of mice showing metastases in the liver, peritoneum, colon and pancreas. Representative images of sections stained for cytokeratin and H&E of (C) subcutaneous tumors, (D) liver metastases and (E) pancreatic metastases. Representative images of sections stained for Smad4 of (F) subcutaneous tumors, (G) liver metastases and (H) pancreatic metastases.

5.5 Conclusion

Improvement in pancreatic cancer treatment represents an urgent medical goal that has been hampered by the lack of predictive and biomarkers. CTCs may be able to overcome this issue by allowing the monitoring of therapeutic response and tumor aggressiveness through *ex vivo* expansion. The successful expansion of CTCs is challenging due to low number in blood and the high contamination of blood cells. Here, we explored the utility of pancreatic CTC cultures as a preclinical model for treatment response. CTCs were isolated from ten locally advanced pancreatic cancer patients using the Labyrinth device and expanded three CTC samples in adherent and spheroid cultures. Proliferation and CTC phenotype were evaluated in culture and compared to the original patient specimen. Additionally, we evaluated take rate and metastatic potential *in vivo* and examined the utility of CTC lines for cytotoxicity assays. Our results demonstrate that CTC cultures are possible and provide a valuable resource for translational pancreatic cancer research while also providing meaningful insight into the development of treatment resistances and distant metastasis.

Despite decades of extensive preclinical and clinical research, survival rates of patients with advanced pancreatic cancer have not improved significantly. The development of novel treatment approaches has been mostly hampered by the lack of available biomarkers, which can be used to access aggressiveness and metastatic potential and predictive/pharmacological markers of treatment response. Obtaining serial tissue biopsies to evaluate treatment response is not feasible in pancreatic cancer patients due to the invasive nature and risks associated with a biopsy. This can be overcome with CTCs, which can be safely obtained at any time point over the course of the treatment as part of routine blood draws.

Systematic evaluation of CTC prior and during treatment will broaden our understanding of the biology of tumor aggression and metastasis, and ultimately improve treatment outcomes for

pancreatic cancer patients. Beyond CTC enumeration, an *ex vivo* expansion and functional studies with in addition to the ability of screening drugs and evaluating patient specific therapeutic targets, patient-derived CTCs will also help to elucidate the presence and functional differences of small CTC subpopulations within the CTC pool. This can address one of the critical challenges in treating pancreatic cancer; that is the ineffectiveness of drugs to treat the aggressive pancreatic cancer to eradicate cancer totally. Expanded CTCs will enable designing tailor-made treatments targeting all of the sub clones instead of basing decisions solely on the predominant clone. Due to low CTC frequency in pancreatic cancer patients, especially in early stages, expanding such cells becomes a dire need of any CTC functional study [192]. While CTC cultures have been reported in literature, including breast [187], colon [188] and lung [189],success rates are low. So far, no CTC cultures have been reported in pancreatic cancer. We have previously reported culture of lung cancer-derived CTCs using a microfluidic co-culture device, where 14 out of 19 samples were expanded [189]. However, this approach limits the use of the cultured CTC for downstream applications due to non-CTC cell contaminations. To overcome these limitations, the study presented here used a monoculture approach of patient-derived pancreatic CTC isolated through the label free approach Labyrinth.

Using the Labyrinth technology, we were able to isolate CTCs from 10 patients with locally advanced pancreatic cancer. The majority of the recovered cells were used to establish CTC cultures *in vitro*, while a small amount was used to evaluate and characterize the presence of epithelial- and EMT-like CTC sub populations.

We were able to isolate and evaluate CTC from all patients enrolled in this study; however, we were only able to establish CTC lines from 3 of the patients. We observed the presence of both epithelial- and EMT-like populations in two patient samples, and found that EMT-like cells were

significantly more abundant, pointing to the aggressive nature of pancreatic cancer. Similar ratios of EMT to epithelial cells were also observed in the 2D and 3D cultures, suggesting that our culture conditions maintained the heterogeneity of the patient CTC population. We are, however cognizant of the fact that extended *in vitro* culture will result in the enrichment of single clones. Hence, for our experimental studies using CTC cultures, we restricted the usage to CTCs expanded within a maximum of 10 passages, which allowed us to perform several functional studies. However, it is important to note that we are able to grow these cells with repeated thaws and freezes beyond 10 passages. In our expanded CTCs, we observed distinct morphological differences associated with different phenotypes, ranging from epithelial to mesenchymal types as well as significant differences in growth rate. Interestingly, we observed that CTC cell morphology was not predictive of molecular phenotype. For example, patient 2 exhibits mesenchymal-like cells with spindle like morphology (2D) and loosely packed spheroids (3D). However, the vimentin expression for this culture was substantially low compared to the other two CTC cultures. This highlights the importance of several functional studies to achieve a better understanding of CTCs rather than just few biomarkers by themselves.

In an effort to verify the identity of the three CTC-derived cell lines though STR fingerprinting, we observed a high similarity between CTC lines. Indeed, the similarity between cell lines was higher that between matched pairs of CTCs and WBCs. We hypothesize that the adaptation for survival in the blood stream enriches for cells with similar pheno- and genotypes. While this observation is certainly very interesting, due to the low sample number we are at this time unable to draw any conclusion with respect to the significance of this observation.

Previously, there are limited studies in other cancer for testing the tumor initiating ability of CTCs *in-vivo* [187, 188, 190] but none in pancreatic cancer. For the first time, we were able to

not only expand CTCs in pancreatic cancer, but also were able to demonstrate the tumor initiating ability of the expanded CTCs in a mouse model. Recently, a number of studies provided evidence for the role of CTCs in the formation of distant metastasis [194, 195]. While treatment of the primary tumor is a major concern in pancreatic cancer patients that do not qualify for surgery, most patients succumb to the disease because of the formation of metastasis in liver, lung, spleen and bowel. Consistent with the clinical phenotype of pancreatic cancer patients, the CTC-derived cell lines display rapid tumor growth *in vivo*. We observed wide spread metastasis in mice injected with CTC-derived cell lines that match the metastatic sides that are commonly found in patients, such as liver and bowel, as well as the formation of ascites. These results further support the importance of CTC models in enhancing our understanding of the metastatic process in pancreatic cancer.

Treatment options are very limited for pancreatic cancer patients and they typically receive treatment based on their tumor stage rather than using precision medicine approaches due to the lack of predictive markers of treatment response. We believe that CTC cultures may be able to fill this gap by allowing for preclinical testing of newly developed compounds or personalized treatment approaches in a clinical setting. We have evaluated the utility of two of the most commonly used methods for *in vitro* drug toxicity testing. Our CTC lines performed well in MTT cell toxicity assays and flow cytometry analysis of DNA damage and cell cycle progression, suggesting that these cultures can be used in range of cytotoxicity assays. These assays may be adapted to high throughput assays and used in personalized medicine approaches. Future studies will be necessary to evaluate the robustness of this system in a larger number of patient-derived CTC lines and evaluate the genetic and phenotypical stability of the cultures.

We had the opportunity to collect two consecutive samples from 3 patients. These samples were collected prior to the start of the therapy and after the first course of chemotherapy. While we were not able to establish CTC lines from consecutive visits, these samples enabled us to evaluate changes in the CTC phenotype in response to chemotherapy. Although both samples contained epithelial- and EMT-like populations of CTC, we observed a trend towards increased numbers of EMT-like cells in response to treatment with gemcitabine. The small patient population enrolled in this study was not sufficient to further address this observation or make conclusions on the general population. Future studies in a larger cohort will aim to collect multiple samples throughout the patients treatment cycle are currently in the planning/enrollment stage and will allow us to follow changes in the CTC phenotype in response to different treatment regimen. Once completed, these studies will shed further light on the importance of pancreatic CTCs in tumor metastasis and the impact of anti-cancer therapy on CTC populations.

CHAPTER 6 Conclusions

6.1 Summary of Research

6.1.1 Development of the High Throughput Label-Free Labyrinth Device

In an attempt to overcome the limitations in current CTC isolation approaches, we developed a high throughput, label-free, and inertial-based Labyrinth device (Chapter 1) for the size-based separation of CTCs. The cell separation in Labyrinth is based on the inertial focusing and Dean forces that focus and isolate sized cells into different streamlines. Cell line experiments were performed in order to understand the physics of cells in microfluidic environment, and to optimize the design for a separation of WBCs and CTCs. The finalized design of Labyrinth consists of 11 loops and 56 corners with 4 outlet at the end. The optimized flow condition is at 2.5 mL/min, in which over 95% of cancer cells are recovered and over 98% of WBCs are removed. Compared to other published label-free technologies, Labyrinth offers the highest throughput, equal or higher performance, the capability to preserve cell viability, and the potential for further downstream analysis.

6.1.2 Detection of Circulating Tumor Cells from Breast Cancer Patients using Labyrinth

The high throughput, label-free, and inertial-based Labyrinth device for the size-based separation of CTCs was optimized and applied in metastatic breast cancer patient samples (Chapter 2). The blood samples were collected in EDTA tubes and stored on ice to be processed within 4 hours from blood drawn to ensure the preservation of cell integrity, cell viability, and RNA stabilization. The optimized protocol involves a sample pre-processing step using Dextran to remove the majority of RBCs, and the application of double Labyrinth in series that were operated at 2.5 mL min^{-1}. The isolation results of CTCs from 56 metastatic breast cancer patient samples demonstrate the sensitivity and specificity of the Labyrinth platform. CTCs were found in 93% of the patient samples (52/56), with a low contamination of WBCs (663 ± 647 WBCs/mL). CTCs with different morphologies were also observed in the isolated samples, including typical single cells, multinucleated cells, and cluster of cells. Moreover, the immunostaining and quantification of enriched CTCs with epithelial marker EpCAM and the CSC and EMT marker CD44 further confirmed Labyrinth's capability of isolating the heterogeneous populations of CTCs that could have been missed by affinity based approaches.

6.1.3 Characterization of Circulating Cancer Stem Cells in Breast Cancer Patients at Single Cell Level

We developed a completely label-free and surface expression independent platform combining the previously introduced Labyrinth device and the commercially available C1™ system (Chapter 3). Multiplex gene expression analysis of seventy single cells recovered from patients identified different subpopulations of CTCs. Both inter- and intra-patient molecular heterogeneity at the single cell level were observed with cells expressing genes uniquely related

to epithelial, MET, and EMT phenotypes. The Labyrinth platform allows a thorough molecular understanding of the heterogeneity among CTCs. This platform also shows CTCs potential as a biomarker to non-invasively evaluate tumor progression and response to treatment in cancer patients.

6.1.4 Purification of Isolated Muscle Satellite Cells Using Labyrinth

Beyond CTC isolation, Labyrinth was applied in the study of skeletal muscle satellite cells in collaboration with Dr. Brian C. Syverud and Prof. Lisa M. Larkin. We utilized the size difference between satellite cells and fibroblasts, two primary cell types obtained from our skeletal muscle dissociation process, that allows for label-free, inertial separation in a Labyrinth microfluidic device and that these purified satellite cells could be used to engineer skeletal muscle. Throughout our engineered tissue fabrication process, Labyrinth purified cells were compared to unsorted controls to assess the efficiency of this novel sorting process and to examine potential improvements in myogenic proliferation, differentiation, and overall engineered tissue function. The results demonstrate the promise of microfluidic sorting in purifying isolated satellite cells and for tissue engineering. This unique technology could assist researchers in translating the regenerative potential of satellite cells to cell therapy and tissue engineering therapies.

6.1.5 Other Applications of Labyrinth in Transformative and Collaborative Projects for High Throughput Size-Based Cell Separation

The application of Labyrinth is not limited to the research in breast cancer, and is even further beyond the study of CTCs. Labyrinth is capable of isolating small cells or particles (7-12 μm) from larger ones, making it an efficient microfluidic approach for cell purification from different size classes. Labyrinth is widely adopted in Nagrath lab for the isolation of CTCs from

various types of cancers, including but not limited to adenoid cystic carcinoma (ACC), hepatocellular carcinoma (HCC), lung, and pancreatic cancers. Besides enumeration, the isolated CTCs were also used in a wide range of studies, such as *ex vivo* culture of live CTCs from pancreatic patients and generating xenograft tumor model in mice from expanded CTCs. CTCs were isolated from newly diagnostic and locally advanced pancreatic cancer patients disease using the Labyrinth device and expanded three CTC samples in adherent and spheroid cultures. Proliferation and CTC phenotype were evaluated in culture and compared to the original patient specimen. Additionally, we evaluated take rate and metastatic potential in vivo and examined the utility of CTC lines for cytotoxicity assays. Our results demonstrate that CTC cultures are possible and provide a valuable resource for translational pancreatic cancer research while also providing meaningful insight into the development of treatment resistances and distant metastasis.

6.2 Limitations and Future Directions

6.2.1 Automation of Labyrinth in Clinical Setting

Labyrinth has been proven to have high clinical utility for CTC isolation in various types of cancers. Running the device is a relatively simple procedure and does not require advanced technical skills. However, Labyrinth could benefit from a streamlined process where sample processing is completely automated. Such a system could consist of a blood injection into an apparatus that would automatically perform all of the pre- and post-processing steps, including CTC counts. Clinical staff would just have to load the blood to receive automated CTC counts within a few hours. To make this process possible, an automatic staining and scanning procedure must be developed and optimized. Roche© currently offers a system called the Discovery Ultra. This automated IHC/ISH research slide staining system could be optimized for the use of ICC

staining for isolated CTCs. The combination of this technology along with an automated CTC counter could streamline and automate the process of using the Labyrinth as a reliable CTC scanning procedure performed in a clinical setting.

6.2.2 Red Blood Cell Removal

Our work mainly focused on the separation of cancer cells from WBCs. However, the excessive amount of red blood cells (RBCs) remained at the end of Labyrinth process could obstruct the delicate process of single cell analysis. Labyrinth was designed to isolate cells above the size of 7 microns. The smaller size of RBCs (5-6 microns) and the biconcave disk shape of them resulted in a poor focusing in Labyrinth. In fact, RBCs are observed across all channels, as they are not focused in Labyrinth. For higher purification of CTCs, which is essential for single cell CTC analysis, we adopted the dextran density separation to the current sample processing protocol. Nonetheless, 10^6 order of RBCs contamination were still observed even with the Dextran step.

In the past, we have tested various microfluidic devices with simple geometry in an attempt to continuously and efficiently remove RBCs from nucleated cells as a pre- or post- step to Labyrinth. Straight microfluidic channel devices with various aspect ratios were fabricated and tested in combination of different flow rates and blood dilution ratios in order to observe the flow patterns of blood cells. We hypothesized that larger cells, i.e. WBCs and CTCs, can be forced away from the main stream, and that these cells can be directed to the outlets placed on the side walls while RBCs can be kept in the main channel. In cell line experiments, we did observe the separation of nucleated cells from the main stream in some of the settings. However the separation gap between nucleated cells and the main RBC stream was not huge enough for an efficient isolation.

Another device with opposite concept to the straight channel device was proposed by me recently (Figure 6.1). In the newly proposed device, non-processed blood was injected from side inlets, along with sheath buffer injected from the center inlet. We hypothesized that the nucleated cells (WBCs and CTCs) are focused at the center of channel through the serpentine focusing region based on the same effects adopted in Labyrinth, while the RBCs are kept at the side of the channel by the sheath buffer flow. A separation of nucleated cells from RBCs can be obtained at the outlet of the device. Multiple devices can be connected in series to achieve a high purity separation. The device is still in design and not tested yet.

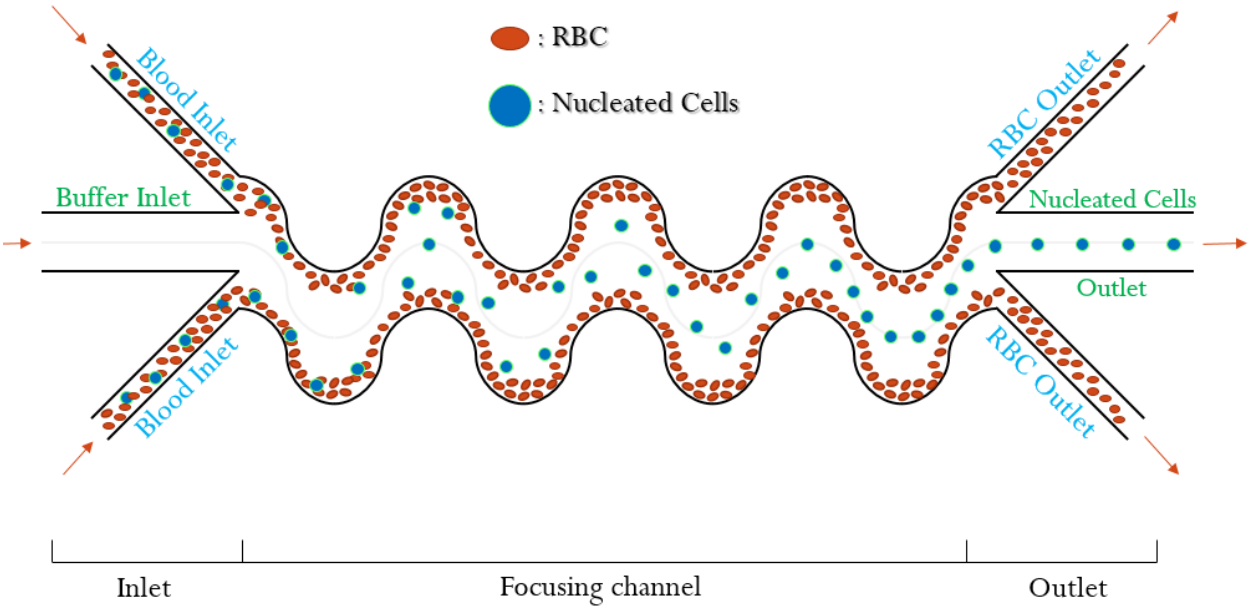

Figure 6.1 Concept of RBC separation device.
Blood is injected from side inlets, along with sheath buffer injected from the center inlet. The nucleated cells (WBCs and CTCs) are focused at the center of channel through the serpentine focusing region, while the RBCs are kept at the side of the channel by the sheath buffer flow. A separation of nucleated cells from RBCs can be obtained at the outlet of the device.

6.2.3 Next-gen single cell multiplex gene expression analysis

Hydro-Seq was applied as a next-gen platform for the single cell RNA sequencing of isolated CTCs from Labyrinth (Chapter 3), and was able to efficiently isolate single CTCs from

metastatic breast cancer patient into individual chambers. We achieved an extremely high sample purity containing no RBC contamination and 90% overall CTC purity, and a total processing time of four hours including Labyrinth to Hydro-Seq. A total of 4 cancer patient samples (2 breast and 2 pancreatic cancers) processed with Labyrinth and Hydro-Seq were sequenced by Sequencing Core (University of Michigan) to identify the mRNA expression on isolated single cells. Among the 68 CTCs identified, we observed the clustering of CTCs from the same patient in terms of gene expression on tSNE and PCA plots. The normalized heatmap presented over 1000 genes analyzed in these cells, demonstrating the potential of this approach in acquiring orders more data compared to gene panel applied in C1™.

A comprehensive interpretation of the single cell sequencing data is as crucial as the development of the isolation technology. There are three major fields under developed: i) the validation of sequencing data, ii) pathway analysis of the gene expression, and iii) the study of heterogeneity between single cell and primary tumor. To confirm the integrity and accuracy of the sequencing data, the RNA expression can be compared with protein expression from IF staining. The correlation between these expressions could provide insights of our sensitivity. To study the single cell at a bigger picture, pathway analysis could recreate an intricate network of interactions and help interpret the data in the context of biological processes. To translate the scientific finding from single cells to clinic, the study of heterogeneity between single cell and primary tumor could serve as a guidance of therapeutic decisions and could determine the alteration of targeted therapy.

6.3 Conclusion

In conclusion, Labyrinth device offers a microfluidic technology to address the need for efficient isolation of rare cells and enables downstream studies on the target cells. Future work will focus on developing the technology further to be able to translate the work into clinics.

Bibliography

1. Siegel, R.L., K.D. Miller, and A. Jemal, *Cancer Statistics, 2017.* CA Cancer J Clin, 2017. **67**(1): p. 7-30.
2. Bednarz-Knoll, N., C. Alix-Panabieres, and K. Pantel, *Plasticity of disseminating cancer cells in patients with epithelial malignancies.* Cancer Metastasis Rev, 2012. **31**(3-4): p. 673-87.
3. Marshall, E., *Public health. Brawling over mammography.* Science, 2010. **327**(5968): p. 936-8.
4. Ashworth, T.R., *A Case of Cancer in Which Cells Similar to Those in the Tumors Were Seen in the Blood after Death.* Aust Med J, 1869(14): p. 146-149.
5. Balic, M., et al., *Most early disseminated cancer cells detected in bone marrow of breast cancer patients have a putative breast cancer stem cell phenotype.* Clin Cancer Res, 2006. **12**(19): p. 5615-21.
6. Ignatiadis, M., V. Georgoulias, and D. Mavroudis, *Micrometastatic disease in breast cancer: clinical implications.* Eur J Cancer, 2008. **44**(18): p. 2726-36.
7. Xenidis, N., et al., *Predictive and prognostic value of peripheral blood cytokeratin-19 mRNA-positive cells detected by real-time polymerase chain reaction in node-negative breast cancer patients.* J Clin Oncol, 2006. **24**(23): p. 3756-62.
8. Cristofanilli, M., et al., *Circulating tumor cells, disease progression, and survival in metastatic breast cancer.* N Engl J Med, 2004. **351**(8): p. 781-91.
9. Hayes, D.F., et al., *Circulating tumor cells at each follow-up time point during therapy of metastatic breast cancer patients predict progression-free and overall survival.* Clin Cancer Res, 2006. **12**(14 Pt 1): p. 4218-24.
10. Racila, E., et al., *Detection and characterization of carcinoma cells in the blood.* Proc Natl Acad Sci U S A, 1998. **95**(8): p. 4589-94.
11. Kahn, H.J., et al., *Enumeration of circulating tumor cells in the blood of breast cancer patients after filtration enrichment: correlation with disease stage.* Breast Cancer Res Treat, 2004. **86**(3): p. 237-47.
12. Krivacic, R.T., et al., *A rare-cell detector for cancer.* Proc Natl Acad Sci U S A, 2004. **101**(29): p. 10501-4.
13. Rolle, A., et al., *Increase in number of circulating disseminated epithelial cells after surgery for non-small cell lung cancer monitored by MAINTRAC(R) is a predictor for relapse: A preliminary report.* World J Surg Oncol, 2005. **3**(1): p. 18.
14. Zieglschmid, V., C. Hollmann, and O. Bocher, *Detection of disseminated tumor cells in peripheral blood.* Crit Rev Clin Lab Sci, 2005. **42**(2): p. 155-96.
15. Jonathan, D., *Rapid translation of circulating tumor cell biomarkers into clinical practice: technology development, clinical needs and regulatory requirements.* Lab on a Chip, 2014. **14**(1): p. 24-31.
16. Yu, Z.T.F., K.M. Aw Yong, and J. Fu, *Microfluidic Blood Cell Sorting: Now and Beyond.* Small, 2014. **10**(9): p. 1687-1703.

17. Maheswaran, S., et al., *Detection of mutations in EGFR in circulating lung-cancer cells.* N Engl J Med, 2008. **359**(4): p. 366-77.
18. Nagrath, S., et al., *Isolation of rare circulating tumour cells in cancer patients by microchip technology.* Nature, 2007. **450**(7173): p. 1235-9.
19. Stott, S.L., et al., *Isolation of circulating tumor cells using a microvortex-generating herringbone-chip.* Proc Natl Acad Sci U S A, 2010. **107**(43): p. 18392-7.
20. Stott, S.L., et al., *Isolation and characterization of circulating tumor cells from patients with localized and metastatic prostate cancer.* Sci Transl Med, 2010. **2**(25): p. 25ra23.
21. Yu, M., et al., *Circulating breast tumor cells exhibit dynamic changes in epithelial and mesenchymal composition.* Science, 2013. **339**(6119): p. 580-4.
22. Adams, A.A., et al., *Highly efficient circulating tumor cell isolation from whole blood and label-free enumeration using polymer-based microfluidics with an integrated conductivity sensor.* J Am Chem Soc, 2008. **130**(27): p. 8633-41.
23. Wang, S., et al., *Highly efficient capture of circulating tumor cells by using nanostructured silicon substrates with integrated chaotic micromixers.* Angew Chem Int Ed Engl, 2011. **50**(13): p. 3084-8.
24. Liu, Z., et al., *High throughput capture of circulating tumor cells using an integrated microfluidic system.* Biosens Bioelectron, 2013. **47**: p. 113-9.
25. Gleghorn, J.P., et al., *Capture of circulating tumor cells from whole blood of prostate cancer patients using geometrically enhanced differential immunocapture (GEDI) and a prostate-specific antibody.* Lab Chip, 2010. **10**(1): p. 27-9.
26. Yu, M., et al., *Circulating tumor cells: approaches to isolation and characterization.* J Cell Biol, 2011. **192**(3): p. 373-82.
27. Kaiser, J., *Medicine. Cancer's circulation problem.* Science, 2010. **327**(5969): p. 1072-4.
28. Saliba, A.E., et al., *Microfluidic sorting and multimodal typing of cancer cells in self-assembled magnetic arrays.* Proc Natl Acad Sci U S A, 2010. **107**(33): p. 14524-9.
29. Ozkumur, E., et al., *Inertial focusing for tumor antigen-dependent and -independent sorting of rare circulating tumor cells.* Sci Transl Med, 2013. **5**(179): p. 179ra47.
30. Alix-Panabieres, C. and K. Pantel, *Circulating tumor cells: liquid biopsy of cancer.* Clin Chem, 2013. **59**(1): p. 110-8.
31. Wicha, M.S. and D.F. Hayes, *Circulating tumor cells: not all detected cells are bad and not all bad cells are detected.* J Clin Oncol, 2011. **29**(12): p. 1508-11.
32. Bhagat, A.A., et al., *Pinched flow coupled shear-modulated inertial microfluidics for high-throughput rare blood cell separation.* Lab Chip, 2011. **11**(11): p. 1870-8.
33. Gerges, N., J. Rak, and N. Jabado, *New technologies for the detection of circulating tumour cells.* Br Med Bull, 2010. **94**: p. 49-64.
34. McKenzie, S.B., J.L. Williams, and K. Landis-Piwowar, *Clinical Laboratory Hematology*. Third edition. ed. Pearson clinical laboratory science series. 2015, Boston: Pearson Education Limited. 1 online resource (1,033 pages).
35. Jin, C., et al., *Technologies for label-free separation of circulating tumor cells: from historical foundations to recent developments.* Lab Chip, 2014. **14**(1): p. 32-44.

36. Mohamed, H., et al., *Development of a rare cell fractionation device: application for cancer detection.* IEEE Trans Nanobioscience, 2004. **3**(4): p. 251-6.
37. Vona, G., et al., *Isolation by size of epithelial tumor cells : a new method for the immunomorphological and molecular characterization of circulatingtumor cells.* Am J Pathol, 2000. **156**(1): p. 57-63.
38. Lin, H.K., et al., *Portable filter-based microdevice for detection and characterization of circulating tumor cells.* Clin Cancer Res, 2010. **16**(20): p. 5011-8.
39. Gossett, D.R., et al., *Label-free cell separation and sorting in microfluidic systems.* Anal Bioanal Chem, 2010. **397**(8): p. 3249-67.
40. Gascoyne, P.R., et al., *Isolation of rare cells from cell mixtures by dielectrophoresis.* Electrophoresis, 2009. **30**(8): p. 1388-98.
41. Becker, F.F., et al., *Separation of human breast cancer cells from blood by differential dielectric affinity.* Proc Natl Acad Sci U S A, 1995. **92**(3): p. 860-4.
42. Shim, S., et al., *Antibody-independent isolation of circulating tumor cells by continuous-flow dielectrophoresis.* Biomicrofluidics, 2013. **7**(1): p. 11807.
43. Cima, I., et al., *Label-free isolation of circulating tumor cells in microfluidic devices: Current research and perspectives.* Biomicrofluidics, 2013. **7**(1): p. 11810.
44. Di Carlo, D., et al., *Continuous inertial focusing, ordering, and separation of particles in microchannels.* Proc Natl Acad Sci U S A, 2007. **104**(48): p. 18892-7.
45. Hur, S.C., A.J. Mach, and D. Di Carlo, *High-throughput size-based rare cell enrichment using microscale vortices.* Biomicrofluidics, 2011. **5**(2): p. 22206.
46. Russom, A., et al., *Differential inertial focusing of particles in curved low-aspect-ratio microchannels.* New J Phys, 2009. **11**: p. 75025.
47. Sun, J., et al., *Double spiral microchannel for label-free tumor cell separation and enrichment.* Lab Chip, 2012. **12**(20): p. 3952-60.
48. Warkiani, M.E., et al., *An ultra-high-throughput spiral microfluidic biochip for the enrichment of circulating tumor cells.* Analyst, 2014. **139**(13): p. 3245-55.
49. Segré, G. and A. Silberberg, *Behaviour of macroscopic rigid spheres in Poiseuille flow Part 2. Experimental results and interpretation.* Journal of Fluid Mechanics, 1962. **14**(1): p. 136-157.
50. Segre, G. and A. Silberberg, *Radial Particle Displacements in Poiseuille Flow of Suspensions.* Nature, 1961. **189**(4760): p. 209-210.
51. Asmolov, E.S., *The inertial lift on a spherical particle in a plane Poiseuille flow at large channel Reynolds number.* Journal of Fluid Mechanics, 1999. **381**: p. 63-87.
52. Jackson, J.M., et al., *Materials and microfluidics: enabling the efficient isolation and analysis of circulating tumour cells.* Chem Soc Rev, 2017. **46**(14): p. 4245-4280.
53. Sollier, E., et al., *Size-selective collection of circulating tumor cells using Vortex technology.* Lab Chip, 2014. **14**(1): p. 63-77.
54. Caine, G.J., et al., *The hypercoagulable state of malignancy: pathogenesis and current debate.* Neoplasia, 2002. **4**(6): p. 465-73.
55. Allard, W.J., et al., *Tumor cells circulate in the peripheral blood of all major carcinomas but not in healthy subjects or patients with nonmalignant diseases.* Clin Cancer Res, 2004. **10**(20): p. 6897-904.

56. Tan, S.J., et al., *Versatile label free biochip for the detection of circulating tumor cells from peripheral blood in cancer patients.* Biosens Bioelectron, 2010. **26**(4): p. 1701-5.
57. Hou, H.W., et al., *Isolation and retrieval of circulating tumor cells using centrifugal forces.* Sci Rep, 2013. **3**: p. 1259.
58. Warkiani, M.E., et al., *Slanted spiral microfluidics for the ultra-fast, label-free isolation of circulating tumor cells.* Lab Chip, 2014. **14**(1): p. 128-37.
59. Autebert, J., et al., *High purity microfluidic sorting and analysis of circulating tumor cells: towards routine mutation detection.* Lab Chip, 2015. **15**(9): p. 2090-101.
60. Xu, T., et al., *A cancer detection platform which measures telomerase activity from live circulating tumor cells captured on a microfilter.* Cancer Res, 2010. **70**(16): p. 6420-6.
61. Plouffe, B.D., S.K. Murthy, and L.H. Lewis, *Fundamentals and application of magnetic particles in cell isolation and enrichment: a review.* Rep Prog Phys, 2015. **78**(1): p. 016601.
62. Yang, L., et al., *Optimization of an enrichment process for circulating tumor cells from the blood of head and neck cancer patients through depletion of normal cells.* Biotechnol Bioeng, 2009. **102**(2): p. 521-34.
63. Ozkumur, E., et al., *Inertial Focusing for Tumor Antigen–Dependent and –Independent Sorting of Rare Circulating Tumor Cells.* Science Translational Medicine, 2013. **5**(179): p. 179ra47.
64. Khoja, L., et al., *A pilot study to explore circulating tumour cells in pancreatic cancer as a novel biomarker.* Br J Cancer, 2012. **106**(3): p. 508-16.
65. Vona, G., et al., *Impact of cytomorphological detection of circulating tumor cells in patients with liver cancer.* Hepatology, 2004. **39**(3): p. 792-7.
66. Pailler, E., et al., *Detection of circulating tumor cells harboring a unique ALK rearrangement in ALK-positive non-small-cell lung cancer.* J Clin Oncol, 2013. **31**(18): p. 2273-81.
67. Kim, T.H., et al., *Cascaded spiral microfluidic device for deterministic and high purity continuous separation of circulating tumor cells.* Biomicrofluidics, 2014. **8**(6): p. 064117.
68. Sun, J., et al., *Double spiral microchannel for label-free tumor cell separation and enrichment.* Lab on a Chip, 2012. **12**(20): p. 3952-3960.
69. Li, P., et al., *Acoustic separation of circulating tumor cells.* Proceedings of the National Academy of Sciences, 2015. **112**(16): p. 4970-4975.
70. Ding, X., et al., *Cell separation using tilted-angle standing surface acoustic waves.* Proc Natl Acad Sci U S A, 2014. **111**(36): p. 12992-7.
71. Hyun, K.A., et al., *Microfluidic flow fractionation device for label-free isolation of circulating tumor cells (CTCs) from breast cancer patients.* Biosens Bioelectron, 2013. **40**(1): p. 206-12.
72. Liu, Z., et al., *Rapid isolation of cancer cells using microfluidic deterministic lateral displacement structure.* Biomicrofluidics, 2013. **7**(1): p. 11801.
73. Pantel, K. and M.R. Speicher, *The biology of circulating tumor cells.* Oncogene, 2016. **35**(10): p. 1216-24.
74. Alix-Panabieres, C. and K. Pantel, *Liquid biopsy in cancer patients: advances in capturing viable CTCs for functional studies using the EPISPOT assay.* Expert Rev Mol Diagn, 2015. **15**(11): p. 1411-7.
75. Smerage, J.B., et al., *Circulating tumor cells and response to chemotherapy in metastatic breast cancer: SWOG S0500.* J Clin Oncol, 2014. **32**(31): p. 3483-9.

76. Wan, L., K. Pantel, and Y. Kang, *Tumor metastasis: moving new biological insights into the clinic.* Nat Med, 2013. **19**(11): p. 1450-64.
77. Alix-Panabieres, C. and K. Pantel, *Challenges in circulating tumour cell research.* Nat Rev Cancer, 2014. **14**(9): p. 623-31.
78. Zhang, Z., et al., *Expanded Circulating Tumor Cells from a Patient with ALK-Positive Lung Cancer Present with EML4-ALK Rearrangement Along with Resistance Mutation and Enable Drug Sensitivity Testing: A Case Study.* J Thorac Oncol, 2017. **12**(2): p. 397-402.
79. Jordan, N.V., et al., *HER2 expression identifies dynamic functional states within circulating breast cancer cells.* Nature, 2016. **537**(7618): p. 102-106.
80. Gorges, T.M., et al., *Accession of Tumor Heterogeneity by Multiplex Transcriptome Profiling of Single Circulating Tumor Cells.* Clin Chem, 2016. **62**(11): p. 1504-1515.
81. Kidess, E. and S.S. Jeffrey, *Circulating tumor cells versus tumor-derived cell-free DNA: rivals or partners in cancer care in the era of single-cell analysis?* Genome Med, 2013. **5**(8): p. 70.
82. Speicher, M.R., *Single-cell analysis: toward the clinic.* Genome Med, 2013. **5**(8): p. 74.
83. Krebs, M.G., et al., *Molecular analysis of circulating tumour cells-biology and biomarkers.* Nat Rev Clin Oncol, 2014. **11**(3): p. 129-44.
84. Dawson, S.J., et al., *Analysis of circulating tumor DNA to monitor metastatic breast cancer.* N Engl J Med, 2013. **368**(13): p. 1199-209.
85. Yu, M., et al., *RNA sequencing of pancreatic circulating tumour cells implicates WNT signalling in metastasis.* Nature, 2012. **487**(7408): p. 510-U130.
86. Peeters, D.J., et al., *Semiautomated isolation and molecular characterisation of single or highly purified tumour cells from CellSearch enriched blood samples using dielectrophoretic cell sorting.* Br J Cancer, 2013. **108**(6): p. 1358-67.
87. Ting, D.T., et al., *Single-cell RNA sequencing identifies extracellular matrix gene expression by pancreatic circulating tumor cells.* Cell Rep, 2014. **8**(6): p. 1905-18.
88. Schneck, H., et al., *EpCAM-Independent Enrichment of Circulating Tumor Cells in Metastatic Breast Cancer.* PLoS One, 2015. **10**(12): p. e0144535.
89. Liu, S., et al., *Breast cancer stem cells transition between epithelial and mesenchymal states reflective of their normal counterparts.* Stem Cell Reports, 2014. **2**(1): p. 78-91.
90. Al-Hajj, M., et al., *Prospective identification of tumorigenic breast cancer cells.* Proc Natl Acad Sci U S A, 2003. **100**(7): p. 3983-8.
91. Ginestier, C., et al., *ALDH1 is a marker of normal and malignant human mammary stem cells and a predictor of poor clinical outcome.* Cell Stem Cell, 2007. **1**(5): p. 555-67.
92. Perkins, G., et al., *Chapter Three - Droplet-Based Digital PCR: Application in Cancer Research*, in *Advances in Clinical Chemistry*, S.M. Gregory, Editor. 2017, Elsevier. p. 43-91.
93. Bingham, C., et al., *Mutational studies on single circulating tumor cells isolated from the blood of inflammatory breast cancer patients.* Breast Cancer Research and Treatment, 2017: p. 1-12.
94. Chen, K., Y.H. Huang, and J.L. Chen, *Understanding and targeting cancer stem cells: therapeutic implications and challenges.* Acta Pharmacol Sin, 2013. **34**(6): p. 732-40.
95. McDermott, S.P. and M.S. Wicha, *Targeting breast cancer stem cells.* Mol Oncol, 2010. **4**(5): p. 404-19.

96. Korkaya, H. and M.S. Wicha, *HER-2, notch, and breast cancer stem cells: targeting an axis of evil.* Clin Cancer Res, 2009. **15**(6): p. 1845-7.
97. Kakarala, M., et al., *Targeting breast stem cells with the cancer preventive compounds curcumin and piperine.* Breast Cancer Res Treat, 2010. **122**(3): p. 777-85.
98. Liu, S. and M.S. Wicha, *Targeting breast cancer stem cells.* J Clin Oncol, 2010. **28**(25): p. 4006-12.
99. Jarvinen, T.A., et al., *Muscle injuries: biology and treatment.* Am J Sports Med, 2005. **33**(5): p. 745-64.
100. Turner, N.J. and S.F. Badylak, *Regeneration of skeletal muscle.* Cell Tissue Res, 2012. **347**(3): p. 759-74.
101. Huard, J., Y. Li, and F.H. Fu, *Muscle injuries and repair: current trends in research.* J Bone Joint Surg Am, 2002. **84-A**(5): p. 822-32.
102. Shadrach, J.L. and A.J. Wagers, *Stem cells for skeletal muscle repair.* Philos Trans R Soc Lond B Biol Sci, 2011. **366**(1575): p. 2297-306.
103. Tedesco, F.S., et al., *Repairing skeletal muscle: regenerative potential of skeletal muscle stem cells.* J Clin Invest, 2010. **120**(1): p. 11-9.
104. Grogan, B.F., J.R. Hsu, and C. Skeletal Trauma Research, *Volumetric muscle loss.* J Am Acad Orthop Surg, 2011. **19 Suppl 1**: p. S35-7.
105. Menetrey, J., et al., *Suturing versus immobilization of a muscle laceration. A morphological and functional study in a mouse model.* Am J Sports Med, 1999. **27**(2): p. 222-9.
106. Mertens, J.P., et al., *Engineering muscle constructs for the creation of functional engineered musculoskeletal tissue.* Regen Med, 2014. **9**(1): p. 89-100.
107. Greene, T.L. and M.E. Beatty, *Soft tissue coverage for lower-extremity trauma: current practice and techniques. A review.* J Orthop Trauma, 1988. **2**(2): p. 158-73.
108. Lin, C.H., et al., *Free functioning muscle transfer for lower extremity posttraumatic composite structure and functional defect.* Plast Reconstr Surg, 2007. **119**(7): p. 2118-26.
109. Emery, A.E., *The muscular dystrophies.* Lancet, 2002. **359**(9307): p. 687-95.
110. Mercuri, E. and F. Muntoni, *Muscular dystrophies.* Lancet, 2013. **381**(9869): p. 845-60.
111. Wicklund, M.P., *The muscular dystrophies.* Continuum (Minneap Minn), 2013. **19**(6 Muscle Disease): p. 1535-70.
112. Bushby, K., et al., *Diagnosis and management of Duchenne muscular dystrophy, part 1: diagnosis, and pharmacological and psychosocial management.* Lancet Neurol, 2010. **9**(1): p. 77-93.
113. Cossu, G. and M. Sampaolesi, *New therapies for Duchenne muscular dystrophy: challenges, prospects and clinical trials.* Trends Mol Med, 2007. **13**(12): p. 520-6.
114. Deconinck, N. and B. Dan, *Pathophysiology of duchenne muscular dystrophy: current hypotheses.* Pediatr Neurol, 2007. **36**(1): p. 1-7.
115. Badylak, S.F., D. Taylor, and K. Uygun, *Whole-organ tissue engineering: decellularization and recellularization of three-dimensional matrix scaffolds.* Annu Rev Biomed Eng, 2011. **13**: p. 27-53.
116. Beattie, A.J., et al., *Chemoattraction of progenitor cells by remodeling extracellular matrix scaffolds.* Tissue Eng Part A, 2009. **15**(5): p. 1119-25.

117. Li, Q., et al., *Autografting satellite cells to repair damaged muscle induced by repeated compression: an animal model.* Foot Ankle Int, 2010. **31**(8): p. 706-11.
118. Rando, T.A. and H.M. Blau, *Primary mouse myoblast purification, characterization, and transplantation for cell-mediated gene therapy.* J Cell Biol, 1994. **125**(6): p. 1275-87.
119. Bach, A.D., et al., *Engineering of muscle tissue.* Clin Plast Surg, 2003. **30**(4): p. 589-99.
120. Corona, B.T., et al., *Further development of a tissue engineered muscle repair construct in vitro for enhanced functional recovery following implantation in vivo in a murine model of volumetric muscle loss injury.* Tissue Eng Part A, 2012. **18**(11-12): p. 1213-28.
121. Juhas, M., et al., *Biomimetic engineered muscle with capacity for vascular integration and functional maturation in vivo.* Proc Natl Acad Sci U S A, 2014. **111**(15): p. 5508-13.
122. Larkin, L.M., et al., *Structure and functional evaluation of tendon-skeletal muscle constructs engineered in vitro.* Tissue Eng, 2006. **12**(11): p. 3149-58.
123. Lee, P.H. and H.H. Vandenburgh, *Skeletal muscle atrophy in bioengineered skeletal muscle: a new model system.* Tissue Eng Part A, 2013. **19**(19-20): p. 2147-55.
124. Asakura, A., et al., *Myogenic specification of side population cells in skeletal muscle.* J Cell Biol, 2002. **159**(1): p. 123-34.
125. Sherwood, R.I., et al., *Isolation of adult mouse myogenic progenitors: functional heterogeneity of cells within and engrafting skeletal muscle.* Cell, 2004. **119**(4): p. 543-54.
126. Peault, B., et al., *Stem and progenitor cells in skeletal muscle development, maintenance, and therapy.* Mol Ther, 2007. **15**(5): p. 867-77.
127. Fishman, J.M., et al., *Skeletal muscle tissue engineering: which cell to use?* Tissue Eng Part B Rev, 2013. **19**(6): p. 503-15.
128. Mauro, A., *Satellite cell of skeletal muscle fibers.* J Biophys Biochem Cytol, 1961. **9**: p. 493-5.
129. Syverud, B.C., et al., *Isolation and Purification of Satellite Cells for Skeletal Muscle Tissue Engineering.* J Regen Med, 2014. **3**(2).
130. Allen, R.E., et al., *Skeletal muscle satellite cell cultures.* Methods Cell Biol, 1997. **52**: p. 155-76.
131. Danoviz, M.E. and Z. Yablonka-Reuveni, *Skeletal muscle satellite cells: background and methods for isolation and analysis in a primary culture system.* Methods Mol Biol, 2012. **798**: p. 21-52.
132. Bischoff, R., *Enzymatic liberation of myogenic cells from adult rat muscle.* Anat Rec, 1974. **180**(4): p. 645-61.
133. Bischoff, R., *Proliferation of muscle satellite cells on intact myofibers in culture.* Dev Biol, 1986. **115**(1): p. 129-39.
134. Rosenblatt, J.D., et al., *Culturing satellite cells from living single muscle fiber explants.* In Vitro Cell Dev Biol Anim, 1995. **31**(10): p. 773-9.
135. Conboy, M.J. and I.M. Conboy, *Preparation of adult muscle fiber-associated stem/precursor cells.* Methods Mol Biol, 2010. **621**: p. 149-63.
136. Richler, C. and D. Yaffe, *The in vitro cultivation and differentiation capacities of myogenic cell lines.* Dev Biol, 1970. **23**(1): p. 1-22.
137. Gharaibeh, B., et al., *Isolation of a slowly adhering cell fraction containing stem cells from murine skeletal muscle by the preplate technique.* Nat Protoc, 2008. **3**(9): p. 1501-9.
138. Montarras, D., et al., *Direct isolation of satellite cells for skeletal muscle regeneration.* Science, 2005. **309**(5743): p. 2064-7.

139. Bosnakovski, D., et al., *Prospective isolation of skeletal muscle stem cells with a Pax7 reporter.* Stem Cells, 2008. **26**(12): p. 3194-204.
140. Pasut, A., P. Oleynik, and M.A. Rudnicki, *Isolation of muscle stem cells by fluorescence activated cell sorting cytometry.* Methods Mol Biol, 2012. **798**: p. 53-64.
141. Chapman, M.R., et al., *Sorting single satellite cells from individual myofibers reveals heterogeneity in cell-surface markers and myogenic capacity.* Integr Biol (Camb), 2013. **5**(4): p. 692-702.
142. Jankowski, R.J., et al., *Flow cytometric characterization of myogenic cell populations obtained via the preplate technique: potential for rapid isolation of muscle-derived stem cells.* Hum Gene Ther, 2001. **12**(6): p. 619-28.
143. Beliakova-Bethell, N., et al., *The effect of cell subset isolation method on gene expression in leukocytes.* Cytometry A, 2014. **85**(1): p. 94-104.
144. Blanco-Bose, W.E., et al., *Purification of mouse primary myoblasts based on alpha 7 integrin expression.* Exp Cell Res, 2001. **265**(2): p. 212-20.
145. Park, Y.G., J.H. Moon, and J. Kim, *A comparative study of magnetic-activated cell sorting, cytotoxicity and preplating for the purification of human myoblasts.* Yonsei Med J, 2006. **47**(2): p. 179-83.
146. Carbonaro, A., et al., *Cell characterization using a protein-functionalized pore.* Lab Chip, 2008. **8**(9): p. 1478-85.
147. Lee, D.J., et al., *Multiplex particle focusing via hydrodynamic force in viscoelastic fluids.* Sci Rep, 2013. **3**: p. 3258.
148. Akhoondi, M., et al., *Membrane hydraulic permeability changes during cooling of mammalian cells.* Biochim Biophys Acta, 2011. **1808**(3): p. 642-8.
149. Jester, J.V., et al., *Myofibroblast differentiation modulates keratocyte crystallin protein expression, concentration, and cellular light scattering.* Invest Ophthalmol Vis Sci, 2012. **53**(2): p. 770-8.
150. Weist, M.R., et al., *TGF-beta1 enhances contractility in engineered skeletal muscle.* J Tissue Eng Regen Med, 2013. **7**(7): p. 562-71.
151. Williams, M.L., et al., *Effect of implantation on engineered skeletal muscle constructs.* J Tissue Eng Regen Med, 2013. **7**(6): p. 434-42.
152. VanDusen, K.W., et al., *Engineered skeletal muscle units for repair of volumetric muscle loss in the tibialis anterior muscle of a rat.* Tissue Eng Part A, 2014. **20**(21-22): p. 2920-30.
153. National Research Council (U.S.). Committee for the Update of the Guide for the Care and Use of Laboratory Animals., Institute for Laboratory Animal Research (U.S.), and National Academies Press (U.S.), *Guide for the care and use of laboratory animals*. 8th ed. 2011, Washington, D.C.: National Academies Press. xxv, 220 p.
154. Syverud, B.C., K.W. VanDusen, and L.M. Larkin, *Effects of Dexamethasone on Satellite Cells and Tissue Engineered Skeletal Muscle Units.* Tissue Eng Part A, 2016. **22**(5-6): p. 480-9.
155. Costa, M.L. and #xed, *Cytoskeleton and Adhesion in Myogenesis.* ISRN Developmental Biology, 2014. **2014**: p. 15.

156. Mills, M., et al., *Differential expression of the actin-binding proteins, alpha-actinin-2 and -3, in different species: implications for the evolution of functional redundancy.* Hum Mol Genet, 2001. **10**(13): p. 1335-46.
157. van der Ven, P.F., et al., *Differentiation of human skeletal muscle cells in culture: maturation as indicated by titin and desmin striation.* Cell Tissue Res, 1992. **270**(1): p. 189-98.
158. Kosnik, P.E., J.A. Faulkner, and R.G. Dennis, *Functional development of engineered skeletal muscle from adult and neonatal rats.* Tissue Eng, 2001. **7**(5): p. 573-84.
159. Siegel, R.L., K.D. Miller, and A. Jemal, *Cancer statistics, 2016.* CA Cancer J Clin, 2016. **66**(1): p. 7-30.
160. American Cancer, S., *Cancer Facts & Figures 2014.* 2014.
161. Lockhart, A.C., M.L. Rothenberg, and J.D. Berlin, *Treatment for pancreatic cancer: current therapy and continued progress.* Gastroenterology, 2005. **128**(6): p. 1642-1654.
162. Sawicka, E., et al., *Chemoradiotherapy for locally advanced pancreatic cancer patients: is it still an open question?* Contemporary Oncology, 2016. **20**(2): p. 102.
163. Herreros-Villanueva, M. and L. Bujanda, *Non-invasive biomarkers in pancreatic cancer diagnosis: what we need versus what we have.* Annals of translational medicine, 2016. **4**(7).
164. Riethdorf, S. and K. Pantel, *Advancing personalized cancer therapy by detection and characterization of circulating carcinoma cells.* Ann N Y Acad Sci, 2010. **1210**: p. 66-77.
165. de Bono, J.S., et al., *Circulating tumor cells predict survival benefit from treatment in metastatic castration-resistant prostate cancer.* Clin Cancer Res, 2008. **14**(19): p. 6302-9.
166. Moreno, J.G., et al., *Circulating tumor cells predict survival in patients with metastatic prostate cancer.* Urology, 2005. **65**(4): p. 713-8.
167. Cohen, S.J., et al., *Prognostic significance of circulating tumor cells in patients with metastatic colorectal cancer.* Ann Oncol, 2009. **20**(7): p. 1223-9.
168. Yu, M., et al., *Circulating tumor cells: approaches to isolation and characterization.* The Journal of cell biology, 2011. **192**(3): p. 373-382.
169. Hayes, D.F., et al., *Circulating tumor cells at each follow-up time point during therapy of metastatic breast cancer patients predict progression-free and overall survival.* Clinical cancer research : an official journal of the American Association for Cancer Research, 2006. **12**(14 Pt 1): p. 4218-4224.
170. Bidard, F.C., et al., *Circulating tumor cells in locally advanced pancreatic adenocarcinoma: the ancillary CirCe 07 study to the LAP 07 trial.* Annals of Oncology : Official Journal of the European Society for Medical Oncology / ESMO, 2013. **24**(8): p. 2057-2061.
171. Riethdorf, S., et al., *Detection of circulating tumor cells in peripheral blood of patients with metastatic breast cancer: a validation study of the CellSearch system.* Clinical cancer research : an official journal of the American Association for Cancer Research, 2007. **13**(3): p. 920-928.
172. Miller, M.C., G.V. Doyle, and L.W. Terstappen, *Significance of Circulating Tumor Cells Detected by the CellSearch System in Patients with Metastatic Breast Colorectal and Prostate Cancer.* Journal of oncology, 2010. **2010**: p. 617421.
173. Sieuwerts, A.M., et al., *Anti-epithelial cell adhesion molecule antibodies and the detection of circulating normal-like breast tumor cells.* Journal of the National Cancer Institute, 2009. **101**(1): p. 61-66.

174. Armstrong, A.J., et al., *Circulating tumor cells from patients with advanced prostate and breast cancer display both epithelial and mesenchymal markers.* Molecular cancer research : MCR, 2011. **9**(8): p. 997-1007.
175. Königsberg, R., et al., *Detection of EpCAM positive and negative circulating tumor cells in metastatic breast cancer patients.* Acta Oncologica, 2011. **50**(5): p. 700-710.
176. Mikolajczyk, S.D., et al., *Detection of EpCAM-Negative and Cytokeratin-Negative Circulating Tumor Cells in Peripheral Blood.* J Oncol, 2011. **2011**: p. 252361.
177. Murlidhar, V., L. Rivera-Baez, and S. Nagrath, *Affinity Versus Label-Free Isolation of Circulating Tumor Cells: Who Wins?* Small, 2016. **12**(33): p. 4450-63.
178. Paterlini-Brechot, P. and N.L. Benali, *Circulating tumor cells (CTC) detection: clinical impact and future directions.* Cancer letters, 2007. **253**(2): p. 180-204.
179. Hyun, K.-A. and H.-I. Jung, *Advances and critical concerns with the microfluidic enrichments of circulating tumor cells.* Lab on a Chip, 2014. **14**(1): p. 45-56.
180. Nagrath, S., et al., *Opportunities and Challenges for Pancreatic Circulating Tumor Cells.* Gastroenterology, 2016. **151**(3): p. 412-426.
181. Kulemann, B., et al., *Circulating tumor cells found in patients with localized and advanced pancreatic cancer.* Pancreas, 2015. **44**(4): p. 547-550.
182. Catenacci, D.V., et al., *Acquisition of portal venous circulating tumor cells from patients with pancreaticobiliary cancers by endoscopic ultrasound.* Gastroenterology, 2015. **149**(7): p. 1794-1803. e4.
183. Bobek, V., et al., *Circulating tumor cells in pancreatic cancer patients: enrichment and cultivation.* World Journal of Gastroenterology: WJG, 2014. **20**(45): p. 17163.
184. Gao, Y., et al., *Clinical significance of pancreatic circulating tumor cells using combined negative enrichment and immunostaining-fluorescence in situ hybridization.* Journal of Experimental & Clinical Cancer Research, 2016. **35**(1): p. 66.
185. Kulemann, B., et al., *KRAS mutations in pancreatic circulating tumor cells: a pilot study.* Tumor Biology, 2016. **37**(6): p. 7547-7554.
186. Cappelletti, V., et al., *Circulating Biomarkers for Prediction of Treatment.* J Natl Cancer Inst Monogr, 2015. **2015**: p. 51.
187. Yu, M., et al., *Ex vivo culture of circulating breast tumor cells for individualized testing of drug susceptibility.* Science, 2014. **345**(6193): p. 216-220.
188. Cayrefourcq, L., et al., *Establishment and characterization of a cell line from human circulating colon cancer cells.* Cancer Res, 2015. **75**(5): p. 892-901.
189. Zhang, Z., et al., *Expansion of CTCs from early stage lung cancer patients using a microfluidic co-culture model.* Oncotarget, 2014. **5**(23): p. 12383-97.
190. Hodgkinson, C.L., et al., *Tumorigenicity and genetic profiling of circulating tumor cells in small-cell lung cancer.* Nat Med, 2014. **20**(8): p. 897-903.
191. Kalluri, R. and R.A. Weinberg, *The basics of epithelial-mesenchymal transition.* The Journal of clinical investigation, 2009. **119**(6): p. 1420-1428.
192. Rhim, A.D., et al., *EMT and dissemination precede pancreatic tumor formation.* Cell, 2012. **148**(1-2): p. 349-61.

193. Karamitopoulou, E., *Role of epithelial-mesenchymal transition in pancreatic ductal adenocarcinoma: is tumor budding the missing link?* Front Oncol, 2013. **3**: p. 221.
194. Maheswaran, S. and D.A. Haber, *Circulating tumor cells: a window into cancer biology and metastasis.* Current opinion in genetics & development, 2010. **20**(1): p. 96-99.
195. Aceto, N., et al., *En Route to Metastasis: Circulating Tumor Cell Clusters and Epithelial-to-Mesenchymal Transition.* Trends in Cancer, 2015. **1**(1): p. 44-52.